# Investigation of Ship Target Recognition Using Neural Networks in Conjunction with the Fourier Mellin Transform

Hyram Serretta

A dissertation submitted to the Department of Electrical Engineering, University of Cape Town, in fulfillment of the requirements for the degree of Master of Science in Engineering.

Cape Town, February 1998

# Declaration

I declare that this dissertation is my own, unaided work. It is being submitted for the degree of Master of Science in Engineering in the University of Cape Town. It has not been submitted before for any degree or examination in any other university.

Signature of Author .....

Cape Town
6 March 1998

# Abstract

The purpose of this dissertation is to investigate the feasibility of using neural networks in conjunction with the Fourier Modified Direct Mellin Transform (FMDMT) for the recognition of ship targets. The FMDMT is a modification of the Direct Mellin Transform for digital implementations, and is applied to the magnitudes of the Discrete Fourier Transforms (DFT) of range profiles of ships. Necessity for the use of the FMDMT is corroborated by the fact that features can be extracted from the range profiles of targets, regardless of target aspect angle. Variation in aspect angle results in variation of the independent variable. Feature extraction is made possible by the scale invariant properties of the Mellin Transform.

Substantial emphasis was placed on preprocessing techniques applied in the implementation of the FMDMT on simulated range profiles and in particular, real ship profiles. The FMDMT was thus examined extensively and utilised as it was developed and demonstrated in [20]. At the completion of this examination, the recognition procedures and methods were applied on simulated data with the aid of a radar simulator developed and adapted for this dissertation. Results of the recognition of simulated ship targets were scrutinized closely and recorded. Employment of this procedure afforded the ability to compare the recognition results for real ship data with those of simulated ship data at a later stage.

Acquisition of a large database of ship profiles was made successful by a ship target data capture plan implemented at the Institute for Maritime Technology (IMT) in Simon's Town. The database included the radar range profile data for the SAS Protea and the Outeniqua, which carried out several successful full

circular manoeuvres in the line of sight of the search radar utilised (Raytheon). The relevant ships performed these circular manoeuvres in order that the acquired data incorporate radar range profiles of the relevant ships at most aspect angles from 0 degrees to 360 degrees. Extensive and thorough testing of the performance of the FMDMT would thus be possible since every possible aspect angle would be scrutinized. Preprocessing of data and recognition of targets was implemented in exactly the same manner and order as was the case with the simulated ship data.

Extensive examination of the FMDMT revealed that the MDMT should only be applied to one side of a real and even Fourier Transform of a ship target. Literature on the FMDMT had failed to elaborate on this point.

Comparison of the recognition results for real and simulated data, indicates a great similarity in success, thus validating the methods and procedures described theoretically and adopted practically for preprocessing of the radar range profiles and recognition of the targets.

In order to demonstrate the feasibility of ship target recognition using the procedures and methods incorporated in the dissertation, real ship data for an entire range of different ships should be acquired in the same manner as indicated above.

# Acknowledgements

I would like to thank my supervisor, Professor Michael Inggs, for his constant support, guidance and assistance throughout the dissertation. Some members of the UCT Radar Remote Sensing Group are due thanks for their assistance and advice, especially Richard Lord for his assistance with the dissertation write-up, Rolf Lengenfelder for his contribution to the radar simulations and theory and Andrew Wilkenson for theoretical advice. Thanks must go to Dr. Morrison for assistance in signal processing, to Dr. Richard Young and Mr. Gerhard Kruger for utilisation of their company resources and to IMT for use of the search radar.

Final thanks must go to my parents for their encouraging support.

# Contents

**Declaration** i

**Abstract** ii

**Acknowledgements** iv

**Contents** v

**List of Figures** ix

**List of Tables** xiv

**List of Symbols** xviii

**Nomenclature** xix

**1 Introduction** 1

**2 The Mellin Transform Theory** 8

2.1 Introduction . . . . . 8

2.2 The Mellin Transform and its Significance . . . . . 9

2.3 A Mathematical Explanation of the Mellin Transform . . . . . 10

2.3.1 The Mellin Transform in the Continuous Domain . . . . . 10

2.3.2 The Mellin Transform in the Discrete Domain . . . . . 11

2.3.3 The Fourier-Mellin alternative . . . . . 12

2.3.4 The Direct and Modified Direct Mellin Transform . . . . . 13

2.4 A Geometrical Explanation of the Mellin Transform . . . . . 16

2.4.1 Feature Migration of a Single Feature . . . . . 16
2.4.2 Scaling of a Function with Multiple Features . . . . . 21
2.4.3 Non-Linear Scaling of a Function with Multiple Features . 27
2.4.4 The Mellin Transform of a Two-sided Fourier Transform . 27
2.5 The Effect of Thermal Noise and Clutter . . . . . 27

**3 Ship Target Simulations** **29**
3.1 Theoretical Review of Sea Clutter . . . . . 30
3.2 Theoretical Review of Thermal Noise . . . . . 32
3.3 Theoretical Review of Scintillation . . . . . 32
3.4 Implementation of Clutter, Thermal Noise and Scintillation in Simulations . . . . . 35
3.4.1 Sea Clutter and Thermal Noise . . . . . 35
3.4.2 Scintillation . . . . . 38
3.5 The Matched-Filter Concept . . . . . 40
3.6 Review of the Simulator . . . . . 41
3.6.1 Summary . . . . . 43
3.7 Background to the Neural Network - Self-Organizing Map . . . . 43
3.7.1 Attributes of the Neural Network . . . . . 43
3.7.2 Description of the Self-Organizing Map . . . . . 44
3.7.3 Competitive/Unsupervised Learning . . . . . 45
3.7.4 The Significance of the Neural Network in Conjunction with the MDMT Algorithm . . . . . 45

**4 Performance of Classification Methods on Simulated Data** **48**
4.1 Introduction to the Simulator . . . . . 49
4.1.1 Simulator Parameters . . . . . 49
4.1.2 Motion of Simulated Vessels . . . . . 50
4.1.3 Implementation of Radar Signal Processing and Data Processing . . . . . 51
4.2 Performance Analysis of the Mellin Transform in Conjunction with the Neural Network . . . . . 52
4.2.1 Discussion of Significant Test Scenarios . . . . . 53

4.2.2 Simulation of Appropriate Data . . . . . 53
4.2.3 Performance Test Cases for Simulations . . . . . 56

**5 Recognition Results of Tests on Real Data** **89**
5.1 The Acquisition of Radar Range Profiles . . . . . 89
5.2 Extraction of Clean Profiles . . . . . 90
5.2.1 Method 1 : Compound Identification . . . . . 91
5.2.2 Method 2 : Successive Elimination . . . . . 92
5.3 Preparation of Acquired Data . . . . . 92
5.4 Data Processing of Acquired Data . . . . . 94
5.5 Training and Testing with the LVQ Neural Network . . . . . 94
5.5.1 Test Case One . . . . . 95
5.5.2 Test Case Two . . . . . 100

**6 Conclusions and Recommendations** **109**
6.1 Specifics of the Mellin Transform . . . . . 110
6.2 Simulator Characteristics . . . . . 110
6.3 Simulations and Recognition . . . . . 111
6.4 Real Data . . . . . 112
6.5 Data Extraction Tools . . . . . 112
6.6 Real Data and Recognition . . . . . 113
6.7 Formulated Regions of Recognition . . . . . 113
6.8 Recommendations . . . . . 115
6.8.1 Software . . . . . 115
6.8.2 Mellin Transform . . . . . 115
6.8.3 Authentic Ship Data . . . . . 116

**Bibliography** **116**

**A Mathcad Simulations** **119**
A.1 Non-Linear Scaling of a Function with Multiple Features . . . . . 126
A.2 The Mellin Transform of a Two-sided Fourier Transform . . . . . 128
A.3 The Effect of Thermal Noise and Clutter . . . . . 133

**B Learning Vector Quantization Algorithms** **138**
B.1 Learning Vector Quantization . . . . . 138
B.2 The Algorithms Encompassing LVQ Methods . . . . . 139
B.2.1 Learning Vector Quantization One (LVQ1) . . . . . 139
B.2.2 Learning Vector Quantization Two (LVQ2) . . . . . 140
B.2.3 Learning Vector Quantization Three (LVQ3) . . . . . 141

# List of Figures


1.1 Downrange Radar Profile of Ship Target. . . . . 3

1.2 Scaling of Range Profile due to Rotation of Target. . . . . 4

2.1 Difference between FMT and FMDMT Implementations. . . . . 15

2.2 Position of a Ship at Two Aspect Angles with Respect to the Radar. . . . . 17

2.3 Profiles of a ship at Two Different Aspect Angles. . . . . 18

2.4 Representation of a Single Feature in the Discrete Domain. . . . . 18

2.5 Linear Expansion of $g_k$ to Form $h_k$ in Discrete Domain. . . . . 19

2.6 Polar Plot of Vectors of FMDMT of $g_k$. . . . . 19

2.7 Polar Plot of Vectors of FMDMT of $h_k$. . . . . 20

3.1 A Radar Return Signal of a Real Ship (Outeniqua) Disguised by Interference. . . . . 31

3.2 Polar Plot of Two Return Vectors from Two Different Point Sources on a Radar Target. . . . . 34

3.3 Polar Plot of Same Two Return Vectors from Same Two Point Sources on a Radar Target at Different Orientations. . . . . 34

3.4 Addition of Noise Components to Signal Components Illustrated in the Polar Co-ordinate System. . . . . 36

3.5 Implementation of 40 % Scintillation on Radar Return Vector. . . 39

3.6 Gaussian Representation of Scintillation Indicating the 40% Cut-off Point. . . . . 40

3.7 Specialization of the Spacial Representation of Codebook Vectors $m_i(t)$ for the Function $x(t)$. . . . . 46

4.1 Illustration of how a Ship was Modelled by the Simulator, Indicating the Direction of Motion of the Ship's Axis. . . . . 50

4.2 Illustration of how a Ship was Modelled by the Simulator. . . . . 51

4.3 Magnitude of Downrange Profile of Simulated Tanker. . . . . 52

4.4 Sixteen Range Profiles for the Simulated Tanker at 16 Aspect Angles in the Range of 0 to 30 Degrees. . . . . 54

4.5 Illustration of Different Positions Taken up by the Ship in Relation to the Radar. . . . . 55

4.6 Profiles Constituting Tanker Training Set in the Aspect Angle Range of 0 to 30 Degrees. SNR = $\infty$. . . . . 59

4.7 FMDMTs Constituting Tanker Training Set in the Aspect Angle Range of 0 to 30 Degrees. SNR = $\infty$. . . . . 60

4.8 Profiles Constituting Tanker Training Set in the Aspect Angle Range of 0 to 30 Degrees. SNR = $0dB$. . . . . 63

4.9 FMDMTs Constituting Tanker Training Set in the Aspect Angle Range of 0 to 30 Degrees. SNR = $0dB$. . . . . 64

4.10 Profiles Constituting Tanker Training Set in the Aspect Angle Range of 0 to 30 Degrees. Aspect Angle Interval = 4°. . . . . 70

4.11 Profiles Constituting Tanker Training Set in the Aspect Angle Range of 0 to 30 Degrees. Aspect Angle Interval = 8°. . . . . 70

4.12 Profiles Constituting Tanker Training Set in the Aspect Angle Range of 0 to 30 Degrees. Aspect Angle Interval = 16°. . . . . 71

4.13 FMDMTs Constituting Tanker Training Set in the Aspect Angle Range of 0 to 30 Degrees. Aspect Angle Interval = 4°. . . . . 71

4.14 FMDMTs Constituting Tanker Training Set in the Aspect Angle Range of 0 to 30 Degrees. Aspect Angle Interval = 8°. . . . . 72

4.15 FMDMTs Constituting Tanker Training Set in the Aspect Angle Range of 0 to 30 Degrees. Aspect Angle Interval = 16°. . . . . 72

4.16 Profiles Constituting Tanker Training Set in the Aspect Angle Range of 0 to 90 Degrees. . . . . 79

4.17 Profiles Constituting Tanker Training Set in the Aspect Angle Range of 180 to 210 Degrees. . . . . 79

4.18 FMDMTs Constituting Tanker Training Set in the Aspect Angle Range of 0 to 90 Degrees. . . . . 80

4.19 FMDMTs Constituting Tanker Training Set in the Aspect Angle Range of 180 to 210 Degrees. . . . . 80

4.20 Profiles Constituting Tanker Training Set in the Aspect Angle Range of 0 to 30 Degrees. Scintillation = 10%. . . . . 83

4.21 Profiles Constituting Tanker Training Set in the Aspect Angle Range of 0 to 30 Degrees. Scintillation = 100%. . . . . 83

4.22 FMDMTs Constituting Tanker Training Set in the Aspect Angle Range of 0 to 30 Degrees. Scintillation = 10%. . . . . 84

4.23 FMDMTs Constituting Tanker Training Set in the Aspect Angle Range of 0 to 30 Degrees. Scintillation = 100%. . . . . 84

5.1 Illustration of Method of Compound Identification. . . . . 91

5.2 Radar Range Profiles for SAS Protea in Aspect Angle Range 0 to 30 Degrees. Sampling Frequency = 2 x Outeniqua Sampling Frequency. . . . . 96

5.3 Radar Range Profiles for Outeniqua in Aspect Angle Range 0 to 30 Degrees. . . . . 96

5.4 FMDMTs for SAS Protea in Aspect Angle Range 0 to 30 Degrees. 97

5.5 FMDMTs for Outeniqua in Aspect Angle Range 0 to 30 Degrees. 97

5.6 Normalized FMDMTs for SAS Protea in Aspect Angle Range 0 to 30 Degrees. . . . . 98

5.7 Normalized FMDMTs for Outeniqua in Aspect Angle Range 0 to 30 Degrees. . . . . 98

5.8 Radar Range Profiles for SAS Protea in Aspect Angle Range 180 to 240 Degrees. Sampling Frequency = 2 x Outeniqua Sampling Frequency. . . . . 102

5.9 Radar Range Profiles for Outeniqua in Aspect Angle Range 180 to 240 Degrees. . . . . 102

5.10 FMDMTs for SAS Protea in Aspect Angle Range 180 to 240 Degrees. 103

5.11 FMDMTs for Outeniqua in Aspect Angle Range 180 to 240 Degrees. 103

5.12 Normalized FMDMTs for SAS Protea in Aspect Angle Range 180 to 240 Degrees. . . . . 104

5.13 Normalized FMDMTs for Outeniqua in Aspect Angle Range 180 to 240 Degrees. . . . . 104

6.1 Recognition Zones. . . . . 114

A.1 Non-Linear Range Migration of Function $g_k$. . . . . 127

A.2 Magnitude Plot of FFT of Real and Positive Function $f(nT)$. (True Representation). . . . . 129

A.3 Magnitude Plot of FFT of Real and Positive Function $f(nT)$. (Common Representation). . . . . 129

A.4 Magnitude Plot of FFT of Real and Positive Function $f(nT)$. (True Representation of Linearly Scaled FFT). . . . . 130

A.5 Linear Scaling of Double-Sided FFT. . . . . 131

B.1 Window Referred to in the LVQ3 Algorithm. . . . . 142

# List of Tables


4.1 Twelve Batches of Range Profiles . . . . . 56

4.2 Recognition Percentages. Aspect Angle Range of Training Set is 0 to 30 Degrees. . . . . 61

4.3 Recognition Percentages. Aspect Angle Range of Training Set is 0 to 52 Degrees. . . . . 61

4.4 Recognition Percentages. Aspect Angle Range of Training Set is 0 to 60 Degrees. . . . . 62

4.5 Recognition Percentages in the Presence of Noise. Aspect Angle Range of Training Set is 0 to 30 Degrees. Aspect Angle Range of Test Set is 1 to 31 Degrees. . . . . 64

4.6 Recognition Percentages in the Presence of Noise. Aspect Angle Range of Training Set is 0 to 30 Degrees. Aspect Angle Range of Test Set is 1 to 53 Degrees. . . . . 65

4.7 Recognition Percentages in the Presence of Noise. Aspect Angle Range of Training Set is 0 to 30 Degrees. Aspect Angle Range of Test Set is 1 to 61 Degrees. . . . . 65

4.8 Recognition Percentages in the Presence of Noise. Aspect Angle Range of Training Set is 0 to 52 Degrees. Aspect Angle Range of Test Set is 1 to 53 Degrees. . . . . 66

4.9 Recognition Percentages in the Presence of Noise. Aspect Angle Range of Training Set is 0 to 52 Degrees. Aspect Angle Range of Test Set is 1 to 61 Degrees. . . . . 66

4.10 Recognition Percentages in the Presence of Noise. Aspect Angle Range of Training Set is 0 to 60 Degrees. Aspect Angle Range of Test Set is 1 to 61 Degrees. . . . . 67

4.11 Recognition Percentages for Profiles Representing an Aspect Angle of 0 Degrees. . . . . 68

4.12 Recognition Percentages for Profiles Representing an Aspect Angle of 16 Degrees. . . . . 68

4.13 Recognition Percentages for Profiles Representing an Aspect Angle of 30 Degrees. . . . . 68

4.14 Statistics for the Three Groups of Tests . . . . . 73

4.15 Recognition Percentages for Aspect Angle Interval = 4 deg. for Training Set. . . . . 74

4.16 Recognition Percentages for Aspect Angle Interval = 8 deg. for Training Set. . . . . 75

4.17 Recognition Percentages for Aspect Angle Interval = 16 deg. for Training Set. . . . . 75

4.18 Recognition Percentages. . . . . 81

4.19 Recognition Percentages for a Test Set of 1 to 31 degrees and a Training Set of 0 to 30 degrees . . . . . 85

4.20 Recognition Percentages for a Test Set of 1 to 53 degrees and a Training Set of 0 to 30 degrees . . . . . 85

4.21 Recognition Percentages for a Test Set of 1 to 61 degrees and a Training Set of 0 to 30 degrees . . . . . 86

4.22 Recognition Percentages for a Test Set of 1 to 53 degrees and a Training Set of 0 to 52 degrees . . . . . 86

4.23 Recognition Percentages for a Test Set of 1 to 61 degrees and a Training Set of 0 to 52 degrees . . . . . 86

4.24 Recognition Percentages for a Test Set of 1 to 61 degrees and a Training Set of 0 to 60 degrees . . . . . 87

4.25 Recognition Percentages for a Test Profile at 0 degrees and a Training Set of 0 to 30 degrees . . . . . 87

4.26 Recognition Percentages for a Test Profile at 16 degrees and a Training Set of 0 to 30 degrees . . . . . 87

4.27 Recognition Percentages for a Test Profile at 30 degrees and a Training Set of 0 to 30 degrees . . . . . 88

5.1 Format of Captured Radar Data of Ship Profiles . . . . . 90

5.2 Recognition Percentages. Aspect Angle Range of Training Set is 0 to 30 Degrees. . . . . 99

5.3 Recognition Percentages. Aspect Angle Range of Training Set is 0 to 60 Degrees. . . . . 99

5.4 Recognition Percentages. Aspect Angle Range of Training Set is 0 to 80 Degrees. . . . . 99

5.5 Recognition Percentages. Aspect Angle Range of Training Set is 0 to 60 Degrees. Aspect Angle Interval = 9.6 Degrees. . . . . 105

5.6 Recognition Percentages. Aspect Angle Range of Training Set is 0 to 60 Degrees. Aspect Angle Interval = 19.2 Degrees. . . . . 105

5.7 Recognition Percentages. Aspect Angle Range of Training Set is 0 to 60 Degrees. Aspect Angle Interval = 28.8 Degrees. . . . . 105

5.8 Recognition Percentages. Aspect Angle Range of Training Set is 0 to 80 Degrees. Aspect Angle Interval = 9.6 Degrees. . . . . 106

5.9 Recognition Percentages. Aspect Angle Range of Training Set is 0 to 80 Degrees. Aspect Angle Interval = 19.2 Degrees. . . . . 106

5.10 Recognition Percentages. Aspect Angle Range of Training Set is 0 to 80 Degrees. Aspect Angle Interval = 28.8 Degrees. . . . . 106

5.11 Recognition Percentages. Aspect Angle Range of Training Set is 0 to 90 Degrees. Aspect Angle Interval = 9.6 Degrees. . . . . 106

5.12 Recognition Percentages. Aspect Angle Range of Training Set is 0 to 90 Degrees. Aspect Angle Interval = 19.2 Degrees. . . . . 107

5.13 Recognition Percentages. Aspect Angle Range of Training Set is 0 to 90 Degrees. Aspect Angle Interval = 28.8 Degrees. . . . . 107

5.14 Recognition Percentages. Aspect Angle Range of Training Set is 0 to 60 Degrees. Aspect Angle Interval = 4.8 Degrees. . . . . 107

# List of Symbols

**SNR**—Signal-to-Noise Ratio

**PRF**—Pulse Repetition Frequency

**c**—Speed of light

**BW**—band width of a pulse

**PRI**—Pulse Repetition Interval

**N**—Noise power

**T**—Radar receiver temperature

**F**—Noise Figure

**I**—In-phase

**Q**—Quadrature

$n_I$—In-phase noise

$n_Q$—Out of phase or quadrature noise

$S_v$—Signal voltage

$N_v$—Noise voltage

$E_{\max}$—Maximum received energy from a point scatterer

# Nomenclature

**Aspect Angle**—Angle with respect to the perpendicular line of sight of the radar.

**Azimuth**—Angle in a horizontal plane, relative to a fixed reference, usually north or the longitudinal reference axis of the aircraft or satellite.

**Beamwidth**—The angular width of a slice through the mainlobe of the radiation pattern of an antenna in the horizontal, vertical or other plane.

**DFT**—Discrete Fourier Transform.

**DMT**—Direct Mellin Transform.

**FFT**—Fast Fourier Transform.

**FMDMT**—Fourier Modified Direct Mellin Transform.

**FMT**—Fourier Mellin Transform.

**IMT**—Institute for Maritime Technology.

**LVQ**—Learning Vector Quantization.

**LVQ1**—Learning Vector Quantization One.

**LVQ2**—Learning Vector Quantization Two.

**LVQ3**—Learning Vector Quantization Three.

**MSc**—Master of Science.

**PRI**—Pulse repetition interval.

**Range**—The radial distance from a radar to a target.

**SAS**—South African Ship.

**SOM**—Self-Organizing Map.

**UCT**—University of Cape Town.

# Chapter 1

# Introduction

Ship Target recognition is applicable in the realms of sea rescue, coast-guard control, harbour control and naval warfare. The significance of utilising radar for classification is clear in these instances. Radar can detect relatively small targets at great distances. The range to the target can also be calculated accurately in most weather conditions, as opposed to the inadequacy of optical techniques. The process of ship target detection is taken a step further into the domain of recognition of the detected targets. The output and product of detection by radar is a one-dimensional radar range profile as shown in Figure 1.1. Owing to the large length-to-width ratio of ships, these vessels can be regarded as a linear array of reflectors, the relative ranges of which will change as the ships rotate. The principal downfall in faultless recognition of ship targets is the scaling of the radar range profiles, due to rotation of the target. The variation in relative range of reflectors results in non-linear scaling of the independent variable of a range profile. The independent variable is time or range. This is illustrated in Figure 1.2. The range profile has its greatest length when the radar signal and the target length axis are aligned as in the zero degree aspect angle case depicted by Figure 1.1. The rotation of the ship target results in non-linear scaling, such that the radar range profile decreases in dimension. The signatures or radar images of the target are characterised by distinct differences due to scaling. This is the prime shortcoming in any recognition of the same class or

individual which naturally relies on similarity. This dissertation deals specifically with this problem by making use of the Mellin Transform. Chapter 2 explains this transform in more detail.

The subject matter of this study necessitates the explanation of two apparently similar terms, these being *recognition* and *classification*. *Classification* refers to recognition down to a class level. Examples of these classes, as far as ship classification is concerned, are tankers, patrol boats and trawlers. *Recognition* would entail individual identification. Examples of these individuals for ship recognition are the SAS Protea and the Outeniqua. Due to the fact that very specific types of ships could not be modelled with a simulator, *classification* would be the applicable term in this instance. Identification of real ship targets in the dissertation is thus referred to as *recognition*. Since the study culminates in the examination of real data for identification purposes and the simulations are used as a tool, reference in ensuing chapters will be made to *recognition* only.

This dissertation also investigates the use of neural networks in conjunction with the Mellin Transform, for the classification of ship targets. Some papers concentrate on the use of the Mellin Transform for ship recognition and emphasize the aspect of feature extraction as a product of the Mellin Transform [20]. This study, on the other hand, delegates the role of feature extraction to the neural network as was the case in a study by M.R. Inggs and A.R. Robinson [4], with the exception that greater emphasis is placed on the use of these techniques with real data. The independent variable of a range profile varies with aspect angle, as explained before, making the radar range profiles very sensitive to variations in aspect angle. This independent variable is made invariant by use of the Modified Direct Mellin Transform [20]. Classification is then feasible since all range profiles for a class of target will be similar, the only differences involved being magnitude fluctuations due to speckle and scintillation. The scale-invariance of the Mellin Transform utilised for the data pre-processing is also examined in greater detail in Chapter 2. Neural networks are significant in the classification instance since the Mellin Transform of a target at one aspect angle will possess similar features to the Mellin Transform of the same target at a different aspect angle. The recognition of these similar features or signatures is the basis of all

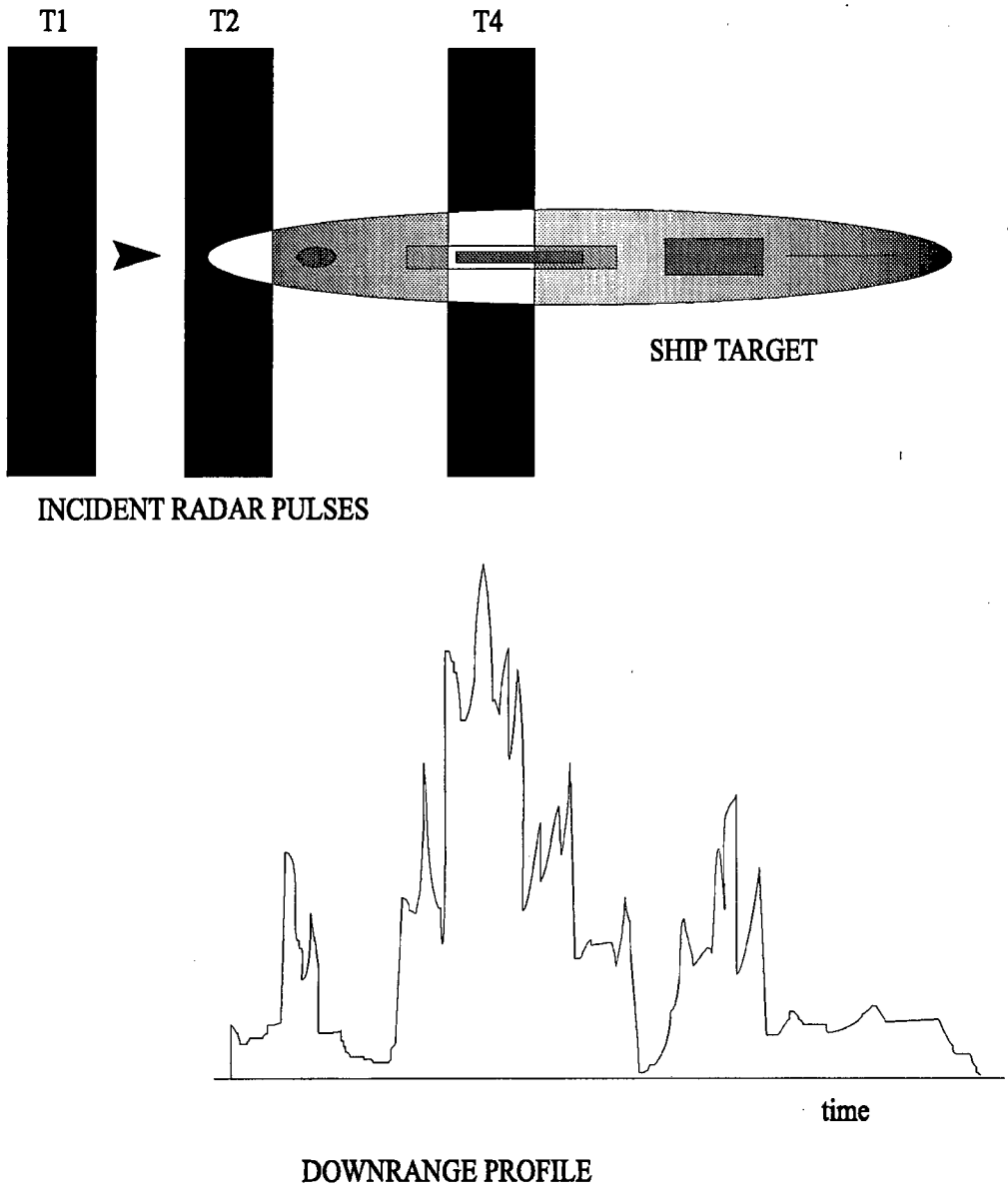


Figure 1.1: Downrange Radar Profile of Ship Target.

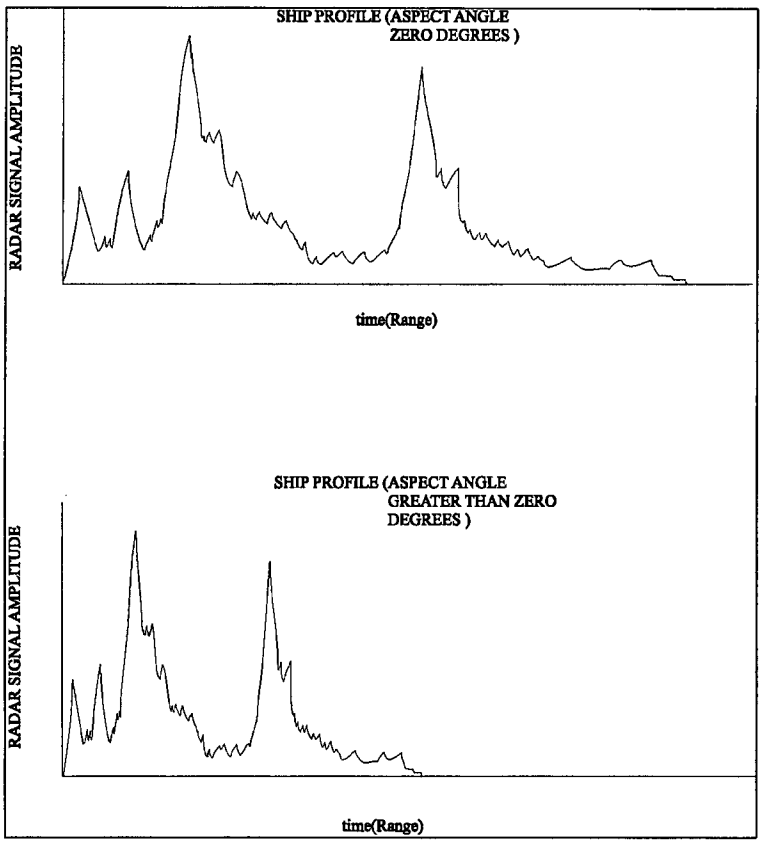


Figure 1.2: Scaling of Range Profile due to Rotation of Target.

natural classification techniques implemented by neural networks.

This study is a continuation of a project by Anthony Robinson, a University of Cape Town (UCT) Master of Science in Engineering (MSc) graduate from the Radar Remote Sensing group [12]. The paper regarding this study can also be referenced [4]. Robinson investigated the feasibility of utilising neural networks for ship recognition instead of classical recognition techniques such as nearest neighbour classifiers and parameter range matching. Robinson places emphasis on the different neural architectures and their advantage and significance as far as recognition of radar range profiles is concerned.

Robinson's work was limited to a theoretical study [12]. Real data available at the time was very limited. The current dissertation places a greater emphasis on the significance of pre-processing for recognition purposes by investigating the Mellin Transform more closely. In this study, problems overlooked by previous studies are overcome. These problems include the simulations and methods utilised for pre-processing of real and simulated data. The aim of the dissertation is to focus attention on the results of classification of real data, illustrating the operation of the Mellin Transform in real applications. This was made possible by the acquisition of a database of ship profiles through a successful implementation of a ship target data capture plan set out by Professor Michael Inggs of UCT. The Institute for Maritime Technology (IMT) assisted in the capturing of data relating to profiles of the SAS Protea and Outeniqua, while each ship undertook a full circular manoeuvre in the line of sight of the radar. At least every fourth aspect angle from zero degrees to three hundred and sixty degrees was characterised by valid data.

The feasibility of using neural networks for recognition has been confirmed by previous work as far as a theoretical study and simulations are concerned. Previous work can be referenced in [12] and [20]. This dissertation concentrates on acquiring a good set of real data and corroborating the feasibility of utilising neural networks for classification. In this way, the study adopts a more practical approach, while rigorously keeping track with the theoretical studies and implications of the methods for pre-processing and recognition by neural networks.

In the light of the above, the prime goal of the research presented in this dissertation is to corroborate the assertion that it is indeed feasible to implement effective classification of radar range profiles of ship targets using neural networks. This is achieved by a number of project objectives:

- To investigate the scale and translation invariant properties of a modified version of the Direct Mellin Transform. This modification of the Mellin Transform pertains to the digital implementation thereof, and will be explained in Chapter 2.
- To relate these properties to results of simulations of previous studies, thereby focussing on the errors encountered. More specific information regarding these simulations can be referenced in a previous study by Anthony Robinson [12].
- To uncover the problems and shortcomings of previous work by developing and utilising a new simulator for low-resolution down-range radar profiles of ship targets. The new simulator incorporates thermal noise, clutter, scintillation and the matched filter effect.
- To investigate the neural networks which are utilised in this dissertation and to acquire a sound knowledge thereof.
- To simulate and investigate the effect of noise and scintillation as far as successful classification is concerned.
- To develop tools for extracting clean radar range profiles from scans of real targets which have been corrupted by radar interference and clutter.
- To evaluate the entire classification method with a good and suitable data set, thus uncovering problems in previous work due to limited real data.

Chapter 2 details the theory of the Mellin Transform and its derivatives. The Modified Direct Mellin Transform is mathematically derived from the Direct Mellin Transform and the scale-invariance thereof, demonstrated with the aid of simulations. The mathematical operations are made clear in these simulations.

Chapter 3 discusses the simulator used in this study. The chapter clarifies the operations performed by the Mellin Transform and uncovers the problems and errors encountered with the previous simulations in this regard. These previous simulations can be referenced in [12]. The new simulations incorporate clutter, thermal noise and scintillation. This chapter provides comprehensive details on the theory of clutter and scintillation and how these were simulated. This section finally describes how the targets were modelled in the new simulator. The matched filter effect was also incorporated in conjunction with the noise and scintillation in order to simulate real radar range profiles as closely as possible. The dissertation then discusses the need for data pre-processing as far as neural networks is concerned. The neural networks used are explained in greater detail. The transforms used, the order of execution of the transforms and reasons therefore are mentioned, again with regard to classification by neural networks. These transforms include the Fourier Transform and the Mellin Transform. The results of classification are then outlined in Chapter 4.

The next chapter is concerned with extraction of real data, pre-processing and classification. Examination of sinograms of real data indicate that some of the profiles in each scan are polluted with sea clutter and radar interference from other radars. Tools were developed to deal with this problem and to select good profiles for pre-processing and classification. These tools were developed in Matlab. The two methods developed for data processing aimed at eliminating the above-mentioned problem concerning clutter, one being '*Compound Identification*' and the other being '*Successive Elimination*', are explained in this section of the dissertation. The second method involves a process of elimination of bad profiles. The results of classification are finally summarised in this chapter.

In the final chapter, conclusions are drawn as to the efficiency and usability of these methods used for classification as far as simulations and particularly real data, are concerned. Shortcomings of the research are also discussed, while recommendations for future research are also made.

# Chapter 2

# The Mellin Transform Theory

This particular dissertation was inspired by an undergraduate thesis at the University of Cape Town by Anthony Robinson [12] and a paper on neural approaches to ship target recognition [4]. Robinson's project concentrates specifically on neural approaches to the recognition of ship targets and produces convincing results. This chapter however, lays the foundation for future emphasis placed on the significance of the Mellin Transform for ship target recognition and provides a thorough understanding of the Mellin Transform and its implementation.

## 2.1 Introduction

Initially, the necessity for the Mellin Transform is outlined. This chapter then provides a mathematical explanation of the Mellin Transform and its modifications [20]. These modifications to the Mellin Transform will ensure retention of its scale-invariant properties but removal of implementation and conceptual problems. The Mellin Transform is investigated then demonstrated in the form of simulations in Appendix A. Next, an examination of the situations where the Modified Direct Mellin Transform will not work and thus an explanation of how it should be used. These thorough explanations of the Modified Direct Mellin Transform by means of simulations are presented in Appendix A while introduc-

tions to the subjects are presented in sections 2.4.3, 2.4.4 and 2.5. The operations of the Mellin Transform are then investigated in a situation where the range profile is polluted with thermal noise and clutter. Corresponding demonstrations are also presented in Appendix A.

## 2.2 The Mellin Transform and its Significance

The ship target recognition problem is centered around the fact that ships are slow-moving but able to alter their course rapidly. The difficulty arises in the determination of target orientation at the desired period of recognition. Recognition should therefore be entirely independent of target orientation or aspect angle. Non-linear scaling of the independent variable of a range profile is the result of a change in the aspect angle of a target with respect to the radar line of sight. Ship targets are usually much greater in length than width. This simply means that a change in aspect angle will lead to the radar range profile becoming compressed or stretched as is demonstrated by Figure 1.2 in Chapter 1. The range profile possesses its greatest dimension when the line of sight of the radar is facing the ship head-on in a zero degree aspect angle position as in Figure 1.1 of Chapter 1.

The distinctive property of the Mellin Transform that sanctions its use in this particular project, is that the magnitude is invariant to scaling of the independent variable. This transform is utilised for pre-processing of radar range profiles of ships in order to eliminate scaling of the target image as far as the independent variable is concerned.

## 2.3 A Mathematical Explanation of the Mellin Transform

### 2.3.1 The Mellin Transform in the Continuous Domain

The Mellin Transform is best understood by relating it to the Fourier Transform as is done in [20]. Assume a given function is $g(t)$ with the independent variable being $t$. This particular explanation introduces an exponential distortion of the independent variable $t$, by letting $t = Te^x$. This is done with the purpose of relating the Mellin Transform to the Fourier Transform for explanation. The new function in $x$ is characterised by an independent variable increasing linearly in $x$ while $t$ in the function $g(t)$, increases exponentially.

The Mellin Transform of a function, $g(t)$ is [20]:

$$g^*(s) = M[g(t); s] = \int_0^\infty g(t)t^{s-1}dt \tag{2.1}$$

Exponential distortion of the independent variable as explained above, indicates that the Mellin Transform can now be implemented by the Fourier Transform :

$$g^*(s) = T^s \int_{-\infty}^{\infty} g(Te^x)e^{xs}dx \tag{2.2}$$

It is now evident that the magnitude of $T^s$ is unity, if $s$ is replaced with $-j\omega$. Equation 2.2 is now the Fourier transform of an exponentially distorted function. This relation to the Fourier transform will now be used to demonstrate the scale invariance of the Mellin transform as follows : let $h(t) = g(kt)$ and,

$$h^*(s) = T^s \int_{-\infty}^{\infty} g(kTe^x)e^{xs}dx \tag{2.3}$$

$$= T^s \int_{-\infty}^{\infty} g(Te^{x+\ln k})e^{xs}dx \tag{2.4}$$

If $y = x + \ln k$, for explanatory purposes, then :

$$\begin{aligned} h^*(s) &= T^s \int_{-\infty}^{\infty} g(Te^{y-\ln k+\ln k}) e^{(y-\ln k)s} d(y - \ln k) \\ &= T^s \int_{-\infty}^{\infty} g(Te^y) e^{sy}.e^{-s\ln k}(dy - d\ln k) \end{aligned} \tag{2.5}$$

$$h^*(s) = k^{-s} g^*(s) \tag{2.6}$$

Considering magnitude only of both sides of equation 2.6 produces the following equation :

$$|h^*(s)| = |g^*(s)| \tag{2.7}$$

The scale factor $k$ is simply reduced to a phase component in the Fourier transform. The magnitude of the Mellin Transform is thus invariant to the scale factor. Equation 2.7 indicates the reason for only considering the magnitude of the Mellin Transform for purposes of acquiring scale invariance for recognition. The phase shift term is disregarded in this instance.

### 2.3.2 The Mellin Transform in the Discrete Domain

It must be noted that in the preceding explanation of the Mellin transform, a function $g(t)$ was exponentially distorted in the domain of the independent variable, and then the Fourier transform was taken of the new function. In the discrete domain, this means sampling the given function $g(t)$ exponentially. If $g(t)$ is given as:

$$g(t), t = 0, T, 2T, ....., NT \tag{2.8}$$

in the discrete domain, this function must be sampled exponentially. With reference to Equation 2.2 the resulting function must consist of samples at equal

intervals of $x$ where $t$ increases exponentially. If samples of $g(t)$ at some $x$ occur at locations on the $t$ axis due to uniform $\Delta x$ sampling, they must be interpolated. The Fast Fourier Transform is now taken of the new function. This is the Fast Mellin Transform. Interpolation however, introduces extraneous frequency components which are undesired. The Mellin Transform is translation invariant and exponential sampling must thus be synchronized with the leading edge of the profile. The profile to which the Mellin Transform is applied is the function in the discrete domain. This could be a very difficult task especially in low signal-to-noise ratio conditions.

### 2.3.3 The Fourier-Mellin alternative

The alternative to attempting to synchronize exponential sampling with the leading edge of the profile, is to take a Fast Fourier Transform of the profile. The magnitude of the Discrete Fourier Transform is centered at the origin in the frequency domain and the problem of translation invariance or phase invariance is overcome. Exponential sampling is now performed on the normalised magnitude of the Discrete Fourier Transform of the profile. The magnitude of the Discrete Fourier Transform must always be normalised due to the reciprocal-scaling property of the Fourier Transform [8] :

$$g(\alpha t) \Longleftrightarrow \frac{1}{|\alpha|} G(\frac{\omega}{\alpha}) \tag{2.9}$$

which scales the magnitude in the frequency domain if scaling occurs of the independent variable in the time domain.

Due to exponential sampling of the Discrete Fourier Transform of the profile, lower frequency components are accentuated. The low-pass filtering effect smooths out all the DFTs which is undesirable, since the Mellin transform of different classes of ship profiles will be very similar if smoothed out.

### 2.3.4 The Direct and Modified Direct Mellin Transform

The alternative to all these setbacks is to implement Equation 2.1 directly in the discrete time domain, thus avoiding any necessity to perform exponential sampling. This form of the Mellin Transform is the Direct Mellin Transform (DMT) which should be performed on the profile. The DMT is however performed on the Fourier Transform of the profile since the Fourier Transform is invariant. The unknown origin or time-zero of the profile is thus circumvented. The discussion that follows, is based on the assumption that the DMT is performed directly on the profile given by $g(t)$. This discussion is a derivation of the DMT using $g(t)$. $T$, in the following equations, is the sample interval in time (t) for the function $g(t)$.

If the profile is a sampled version of $g(t)$ then equation 2.1 is viewed as follows :

$$g^*(s) = \int_0^T g(t)t^{s-1}dt + \int_T^{2T} g(t)t^{s-1}dt + .... \tag{2.10}$$

Integration is now carried out on each sample, assuming each sample is constant in the interval $T$. Equation 2.10 reduces to :

$$sg^*(s) = g(0)t^s|_0^T + g(T)t^s|_T^{2T} + ..... \tag{2.11}$$

where $g(0) = g_1$ and $g(T) = g_2$ and $g((k-1)T) = g_k$ When the integration is carried out, the scaling factor comes into the equation in the form of $k$ since this actually relates to the position of each sample in the profile. If linear compression or stretching of the profile occurs, $k$ moves according to the scale factor. The equation then produced is :

$$\begin{aligned} sg^*(s) &= \sum_{k=1}^{N-1} k^s \Delta_k \\ &= \sum_{k=1}^{N-1} e^{\ln k^s} \Delta_k \end{aligned} \tag{2.12}$$

$$= \sum_{k=1}^{N-1} e^{s \ln k} \Delta_k$$

where $N$ is the number of samples in the profile and $\Delta_k = (g_k - g_{k+1})$. Replacing $s$ by $-j\omega$, we get :

$$-j\omega g^*(-j\omega) = \sum_{k=1}^{N-1} e^{-j\omega \ln k} \Delta_k \tag{2.13}$$

$$g^*(j\omega) = \frac{1}{-j\omega} \sum_{k=1}^{N-1} e^{-j\omega \ln k} \Delta_k$$

The $\frac{1}{j\omega}$ term is removed due to the low-pass filtering effect which is an undesired effect as described before. The Modified Direct Mellin Transform is thus :

$$g^*(\omega) = \sum_{k=1}^{N-1} (\cos(\omega \ln k) - j \sin(\omega \ln k)) \Delta_k \tag{2.14}$$

Since Equation 2.14 is implemented on the Fourier Transform of the profile, the resulting transform is the Fourier Modified Direct Mellin Transform (FMDMT). It is obvious from Equation 2.14 that if the points on the Fourier Transform of the down-range profile at each $k$ migrate linearly in range, then this migration factor is multiplied by $k$ in equation 2.14, and simply reduced to a phase/translation term which rotates the magnitudes of the components of the equation ($|\Delta_k|$) by the same angle. The same magnitude components will be produced each time where a $\Delta_k$ occurs. $\Delta_k$ is the differencing action between consecutive samples of the Fourier Transform of the target's down-range profile. The FMDMT is thus very dependent on the samples or prominent features of the function it is executed on, since it incorporates a differencing action on the sampled data. Figure 2.1 is a flow diagram which can also be found in [20], illustrating the difference between the implementations of the Fourier Mellin Transform (FMT) and the FMDMT.

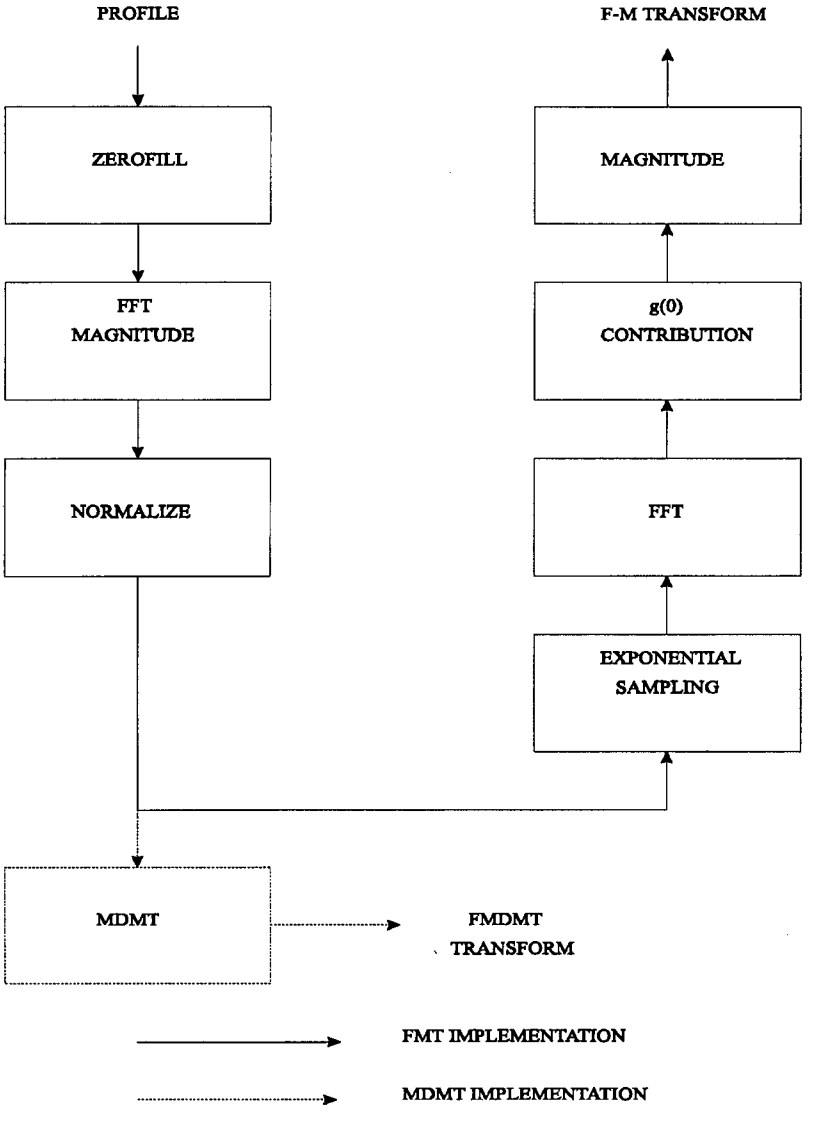


Figure 2.1: Difference between FMT and FMDMT Implementations.

## 2.4 A Geometrical Explanation of the Mellin Transform

This particular section demonstrates the geometrical operation of the FMDMT. In the cases discussed in the ensuing sections, features have been created in the simulations and diagrams which can be regarded as geometrical features of any Discrete Fourier Transform on which the Mellin Transform is applied. The following explanations provide a visual perspective of the operation of the Mellin Transform on sampled data, so as to provide an understanding of the transform and highlight its underlying significance in eliminating the effect of non-linear scaling of target profiles. Scaling refers to the movement of features to the left or right of the profile across range bins and thus with reference to the independent variable of the profile. Scaling in the time domain causes scaling in the frequency domain. Figure 2.2 illustrates the position of a ship at two aspect angles, $\phi_1$ and $\phi_2$. Two profiles of this ship for these aspect angles, are presented in Figure 2.3 which illustrates scaling. The profile for aspect angle $\phi_1$ has been scaled to that for $\phi_2$.

Amplitudes of the features (the dependent variable) in simulations and diagrams are all kept constant since the aim of the section is to demonstrate the scale invariance of the Mellin Transform geometrically, as far as the independent variable of functions is concerned. In this section, *features* refers to the features of a discrete Fourier Transform undergoing scaling.

### 2.4.1 Feature Migration of a Single Feature

The single feature in this explanation is described by the function $g_k$ and is illustrated in Figure 2.4. The function described by $h_k$ in Figure 2.5 is the product of every point or component of $g_k$ having undergone feature migration by a factor of $\alpha$ in this instance. The simulation of these two functions and the FMDMT thereof is presented in the first simulation in Appendix A.

The function $g_k$ then undergoes scaling. The feature will migrate with reference

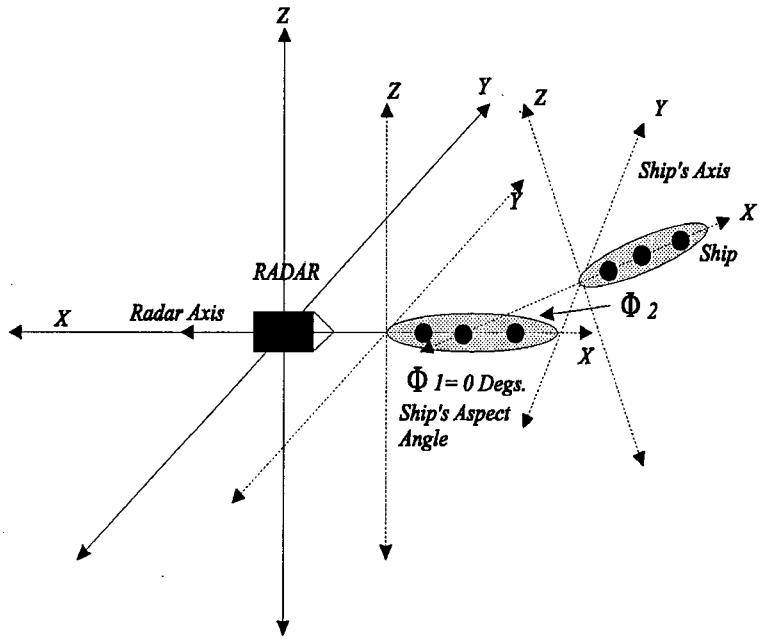


Figure 2.2: Position of a Ship at Two Aspect Angles with Respect to the Radar.

to the independent variable ($k$ or discrete frequency). Scaling of a Fourier Transform of a profile would occur if the time-domain profile is scaled as is evident in Equation 2.9, where the independent variables in the time and frequency domains are affected by the scale factor $\alpha$. Bearing in mind that $\Delta_k = g_k - g_{k+1}$ as in Equation 2.14, it is evident in Figure 2.5 that $\Delta_3$ and $\Delta_4$ in Figure 2.4 have both moved right by two due to every point of the feature being scaled by a factor of two. In this instance $\Delta_3 = \Delta_6$ and $\Delta_4 = \Delta_8$. Only two $\Delta'_k s$ exist for each function i.e. $\Delta_3$ and $\Delta_4$ in the one instance and $\Delta_6$ and $\Delta_8$ in the other. $\Delta_7 = 0$ for $h_k$. Equation 2.14 is demonstrated geometrically in Figure 2.6 and in Figure 2.7. In the figures, $v_1 = \Delta_3 = \Delta_6$ and $v_2 = \Delta_4 = \Delta_8$.

If the Mellin Transform is implemented on $g_k$ the following is true :

$$g^*(s) = \sum_{k=1}^{N-1} e^{-j\omega \ln k} \Delta_k \tag{2.15}$$

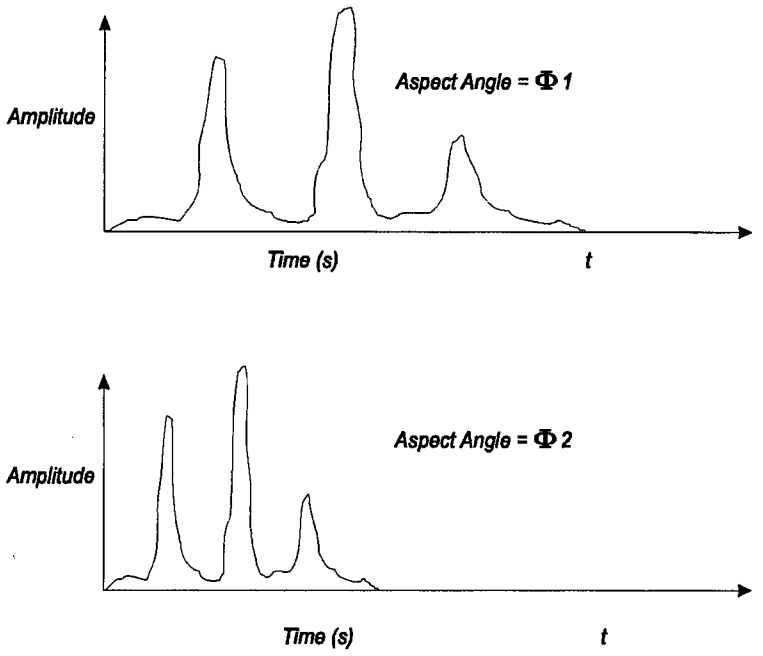


Figure 2.3: Profiles of a ship at Two Different Aspect Angles.

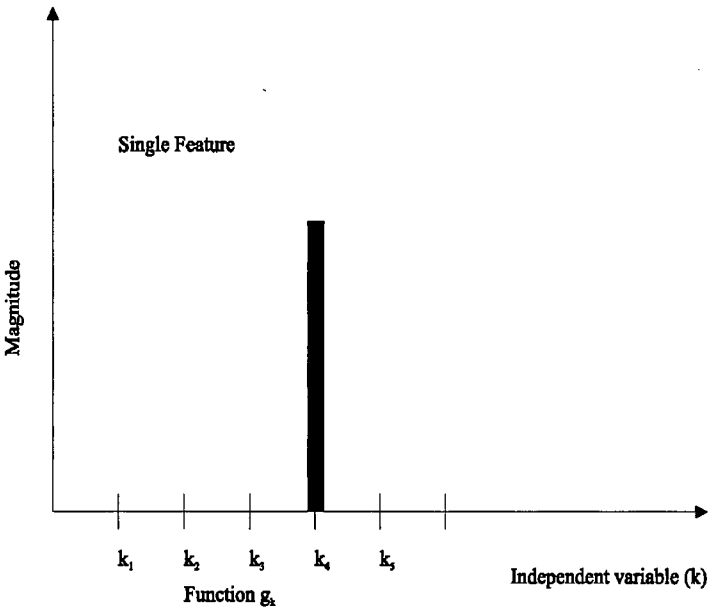


Figure 2.4: Representation of a Single Feature in the Discrete Domain.

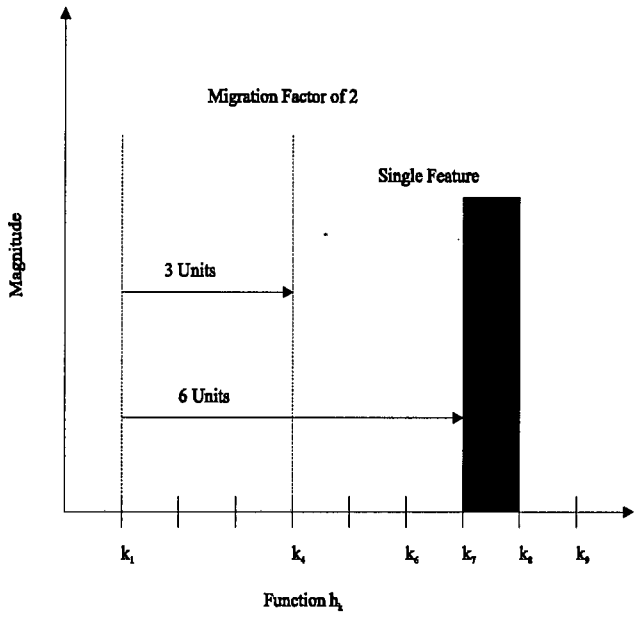


Figure 2.5: Linear Expansion of $g_k$ to Form $h_k$ in Discrete Domain.

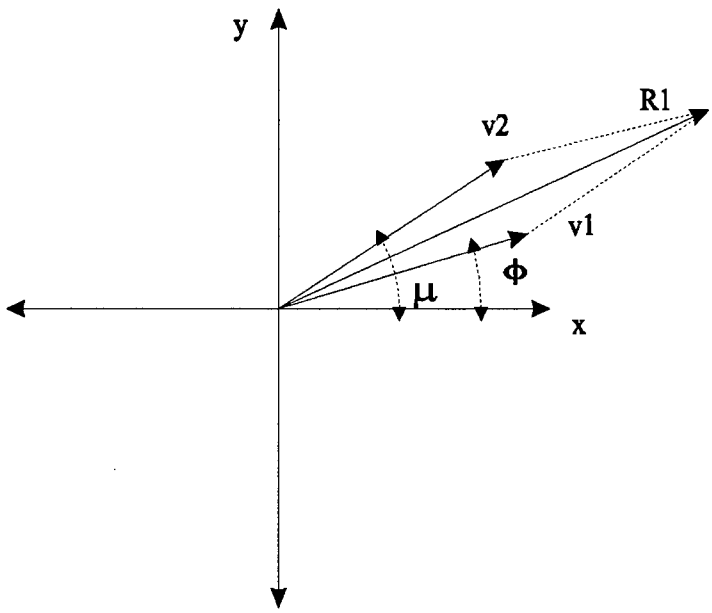


Figure 2.6: Polar Plot of Vectors of FMDMT of $g_k$.

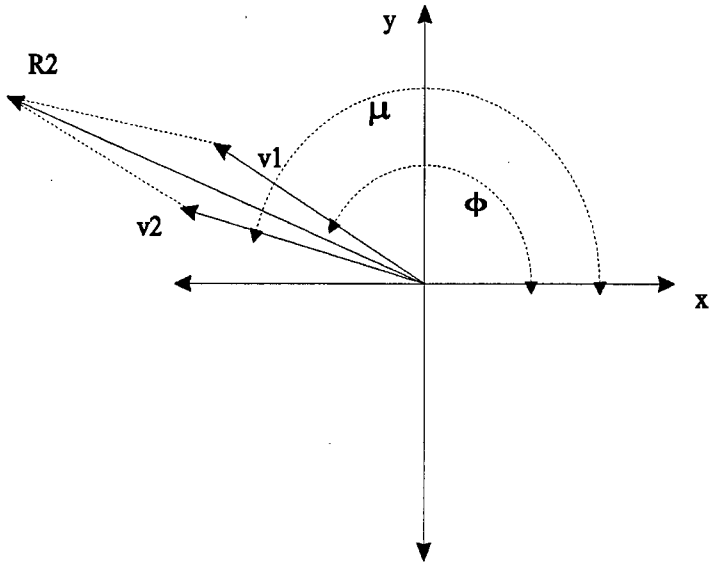


Figure 2.7: Polar Plot of Vectors of FMDMT of $h_k$.

which signifies the addition of vectors $\Delta_3$ and $\Delta_4$ in Figure 2.6 to produce resultant $R1$. The phases of these vectors are $\phi = \omega \ln 3$ and $\mu = \omega \ln 4$ respectively. If scaling occurs by a factor of $\alpha = 2$ , the following applies :

$$\begin{aligned} h^*(s) &= \sum_{k=1}^{N-1} e^{-j\omega \ln \alpha k} \Delta_k \\ &= \sum_{k=1}^{N-1} e^{-j\omega(\ln \alpha + \ln k)} \Delta_k \\ &= \sum_{k=1}^{N-1} (e^{-j\omega \ln \alpha} * e^{-j\omega \ln k}) \Delta_k \\ &= e^{-j\omega \ln \alpha} \sum_{k=1}^{N-1} e^{-j\omega \ln k} \Delta_k \end{aligned} \tag{2.16}$$

Equation 2.16 indicates that the vectors in Figure 2.6 are all just shifted by $\omega \ln \alpha$, thus shifting the resultant $R1$ by the same angle, producing resultant $R2$ in Figure 2.7. In Figure 2.7 $\phi = \omega(\ln(3 * \alpha))$ and $\mu = \omega(\ln(4 * \alpha))$. The

magnitudes of the resultants $R1$ and $R2$ are equal, i.e. the magnitudes of the two Mellin Transforms are equal.

The objective of using the Mellin Transform for scale invariance is clearly evident in the demonstration above.

### 2.4.2 Scaling of a Function with Multiple Features

The following explanation emphasizes the fact that all points in a range profile should migrate in the event of scaling due to rotation of the target i.e. *every single* discretely sampled point. This scenario is a requisite if the desired effect of the Mellin Transform is to be attained. Although feature migration is the outcome of rotation of a radar target in reality, it is simply pointed out in this case, that simulations must take this into account if implementation of the Mellin Transform is to be successful. In this simulation below, the function $FUNC1$ is comprised of a set of Rect functions, all of which are of the same width. The Rect function is also referred to as the *rectangular function* (width $\tau$) for which the definition in Equation 2.17 exists.

$$\begin{aligned} \mathrm{Re}ct(\frac{t}{\tau}) &\equiv 1, |t| < \frac{\tau}{2} \\ \mathrm{Re}ct(\frac{t}{\tau}) &\equiv 1, |t| > \frac{\tau}{2} \end{aligned} \tag{2.17}$$

The formal definition of this function can be referenced in [8].

$FUNC2$ is a compression of $FUNC1$ by a factor of $\alpha = \sqrt{2}$. Each Rect function is scaled accordingly i.e. every single point in the function is scaled by the same factor. Equation 2.15 applies to the Mellin Transform of $FUNC1$ while Equation 2.16 applies to the Mellin Transform of $FUNC2$ where $\alpha = \sqrt{2}$ .

In this case, the scaling factor of $\sqrt{2}$ can be removed since every sampled point has been shifted to the left i.e. $FUNC1$ has been compressed to produce the function $FUNC2$. The magnitude of the two Mellin Transforms, $P(s)$ and $Q(s)$,

of the functions $FUNC1$ and $FUNC2$ consecutively, are equal. The mentioned Mathcad demonstration is presented as follows:

## DEMONSTRATION OF MELLIN TRANSFORMS ON FOURIER TRANSFORMS

The functions created here, FUNC1 and FUNC2, are modelled to look like two profiles of two ships at two different aspect angles. FUNC1 represents a profile for a 4-featured ship at 0 degrees aspect angle. The return (pulse) from each feature in this case, possesses the same amplitude for the sole purpose of demonstrating the scale-invariant properties of the Mellin Transform. FUNC2 is representative of a profile of a ship at 45 degrees aspect angle. The profile was compressed. The Mellin Transform should be the same for the compressed profile as it is for the uncompressed profile. Normally the Mellin Transform would be performed on the Fourier Transform of a profile since the Fourier Transform is phase-invariant. In this case, the Mellin Transform was performed on the actual profile in order to demonstrate scale invariance. In this case the profile has been compressed, but in the case of the Fourier Transform, the Transform would expand instead and be shift-invariant. Phase is not a problem in this case, since the ship is not moving. This means that the Mellin Transform would operate in the same manner with the profiles as it would with the Fourier Transforms. In fact, the two profiles could be viewed as two Fourier Transforms.

$t := 0..2550$

$A_t := 0$

$blk1 := 0..30$

$A_{blk1} := 10$

$blk2 := 200..230$

$A_{blk2} := 10$

$blk3 := 400..430$

$A_{blk3} := 10$

$blk4 := 600..630$

$A_{blk4} := 10$

Profile for 0 degrees

$me := \overrightarrow{|rnorm(2551,0,0.00000001)|}$

$FUNC1 := A + me$

$B_t := 0$

$alk1 := 0..21$

$B_{alk1} := 10$

$alk2 := 141..163$

$B_{alk2} := 10$

$alk3 := 283..304$

$B_{alk3} := 10$

$alk4 := 424..445$

$B_{alk4} := 10$

Profile for 45 degrees

$you := \overrightarrow{|rnorm(2551,0,0.00000001)|}$

$FUNC2 := B + you$

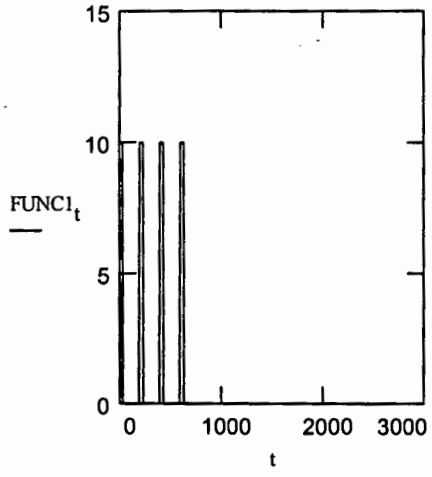


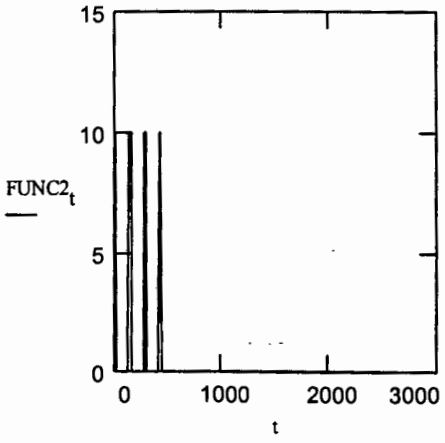


$c := 0..2550$

$W_{c+1} := A_c$

$a := 2552$

$W_a := 0$

$m := 1..2551$

$\Delta_m := W_m - W_{m+1}$

$N := 2552$

$j := \sqrt{-1}$

$$P(s) := \sum_{m=1}^{N-1} (\cos(s \cdot (\ln(m))) - j \cdot \sin(s \cdot (\ln(m)))) \cdot \Delta_m$$

$$Q(s) := \sum_{n=1}^{N-1} (\cos(s \cdot (\ln(n))) - j \cdot \sin(s \cdot (\ln(n)))) \cdot \Gamma_n$$

$d := 0..2550$

$X_{d+1} := B_d$

$b := 2552$

$X_b := 0$

$n := 1..2551$

$\Gamma_n := X_n - X_{n+1}$

$N := 2552$

$s := 120 .. 160$

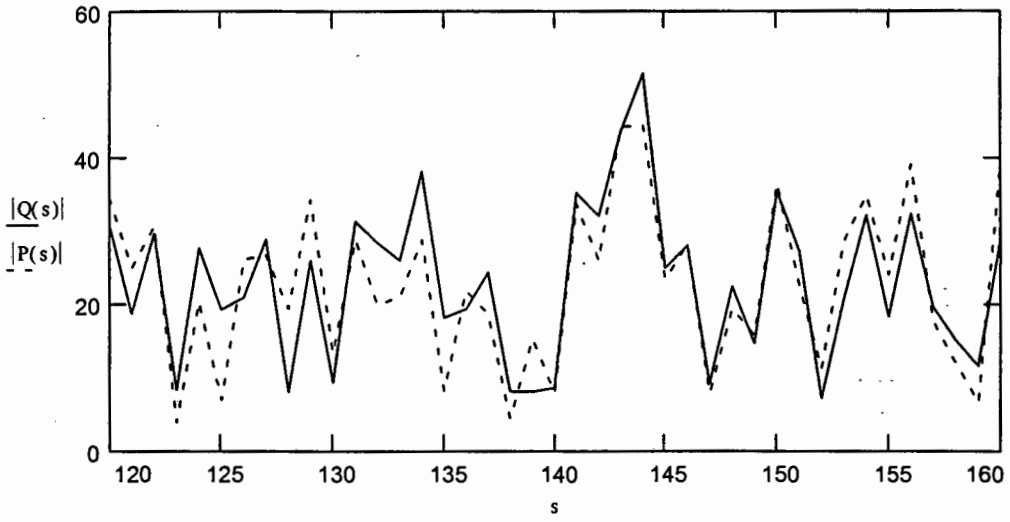


$r := 120 .. 160$

$K_r := |P(r)|$

$p := mean(K)$

$MELLK := \frac{K}{p}$

$J_r := |Q(r)|$

$q := mean(J)$

$MELLJ := \frac{J}{q}$

The Mellin transforms are divided their means below:

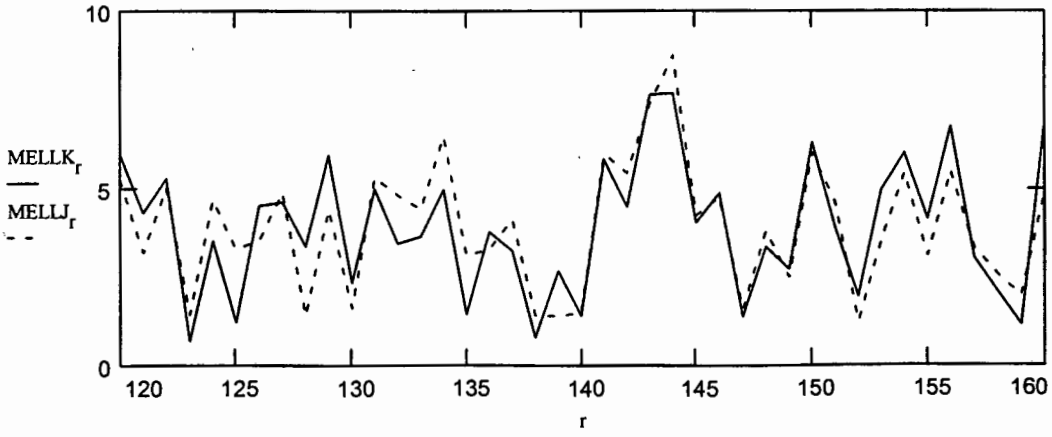

## RESULTS

The Mellin Tranform of the two profiles are very similar for Mellin components in this case of 120 to 160 i.e. from $\omega$=120 to $\omega$=160 in steps of one ($\omega$ is the Mellin component). They are not exact due to the fact that the sampling frequency of the samples is not high enough and the return pulses are possibly not placed in the correct range bins.

### 2.4.3 Non-Linear Scaling of a Function with Multiple Features

Results of non-linear scaling of multiple features are demonstrated in Appendix A. This particular subject is examined in detail since it must be seriously considered in the development of simulations pertaining to ship target recognition with the Mellin Transform.

### 2.4.4 The Mellin Transform of a Two-sided Fourier Transform

This section details the manner in which the Mellin Transform should be applied. The difference between a single and double-sided Fourier Transform will be indicated, as far as implementation of the Mellin Transform is concerned. Appendix A contains a detailed explanation related to taking the Mellin Transform of a double-sided Fourier Transform.

## 2.5 The Effect of Thermal Noise and Clutter

Evaluation of the Mellin Transform's performance in the presence of thermal noise and clutter is performed in this particular section. Should a radar range profile of a ship target be polluted or corrupted in some way with any considerable amount of noise or interference, the Fourier Transform thereof is represented by a noisy function with a zero frequency value considerably greater in amplitude than the rest of the Fourier Transform. The DC value occurs at the origin and is known as the *unit impulse* $\delta(t)$. This impulse is described in Equations 2.18 and 2.19.

$$\delta(t) = 0, t \neq 0 \tag{2.18}$$

$$\int_{-\infty}^{\infty} \delta(t)dt = 1 \tag{2.19}$$

The presence of the DC value is due to the fact that the radar range profile of a target is positive and real and the average value is the DC component of the function in the Fourier domain.

A simulated Fourier Transform of a noise-polluted function can be referenced in Appendix A. Evaluation of the Mellin Transform under these conditions is also presented in Appendix A on page 148.

# Chapter 3

# Ship Target Simulations

This Chapter evaluates the radar simulator developed for and utilised in this dissertation and details the errors and problems encountered with previous simulations as far as the implementation of the Mellin Transform is concerned [12]. The simulator was developed by Rolf Lengenfelder of the Remote Radar Sensing Group and modified and adapted appropriately by the author for this dissertation. The development of certain key characteristic features of the simulator was deemed necessary due to errors encountered in previous simulations with regard to the study documented in this dissertation. The previous simulations referred to, are presented in [12].

An analysis of the findings due to taking the Mellin Transform of a double-sided Fourier Transform and a single-sided Fourier Transform are presented and comparisons are drawn. These findings emphasize the significance of only considering one side of the Fourier Transform of a radar range profile (see Chapter 2, section 2.4.4). Evaluation of these findings was implemented with the radar simulator used for this study.

The radar signal in reality is subject to a number of hindrances and obstacles on its journey to the target and back to the transmitter. These include land surface reflections and in the context of this dissertation, sea surface reflections. The latter effect is clutter. Thermal noise, scintillation and clutter are reviewed in this

section with the purpose of providing background theory to these concepts. Next, an explanation of the methods of modelling and implementation of these concepts and a mathematical consideration thereof. A theoretical study and significance of the radar matched-filter concept is presented since it is incorporated in the simulations. The final section is dedicated to the basic theory and operations of the simulator and the modelling of the radar ship targets with respect to creating radar range profiles for the purpose of pre-processing and classification.

## 3.1 Theoretical Review of Sea Clutter

The radar system illuminates the earth's surface or ocean in the case of this dissertation, and in doing so, causes a portion of radar energy to be scattered back towards the radar system being utilised. These echoes are radar clutter echoes, and constitute echoes from reflectors other than those of the target, and thus obscuring the signals from targets that are of interest. Radar clutter owes its presence to the sea, weather, chaff, mountains and other radars operating within the same frequency band and in the same area of surveillance. Sea clutter owes its characteristics to the presence of random returns from features like cusps, waves, foam, turbulence and even spray. An example of interference is illustrated in Figure 3.1. An in-depth explanation of clutter is presented in [14, page 470].

A useful description of clutter is required in order to model clutter in simulations producing downrange profiles of ships. If sea clutter is considered in this dissertation, the ships are located in the region of clutter from the perspective of the radar system. The clutter region is composed of small independent broadband point scatterers for which the size and location of such scatterers is a random variable. These individual scattering elements are spaced closer than the effective waveform resolution capability at the matched-filter output. The composite clutter signal in a specific range cell thus has the characteristic of random noise as a result of the overlap of many signals that are present and will resemble a stationary Gaussian random process. When the statistical characteristics of a sampled function does not change with time, the random process is said to be

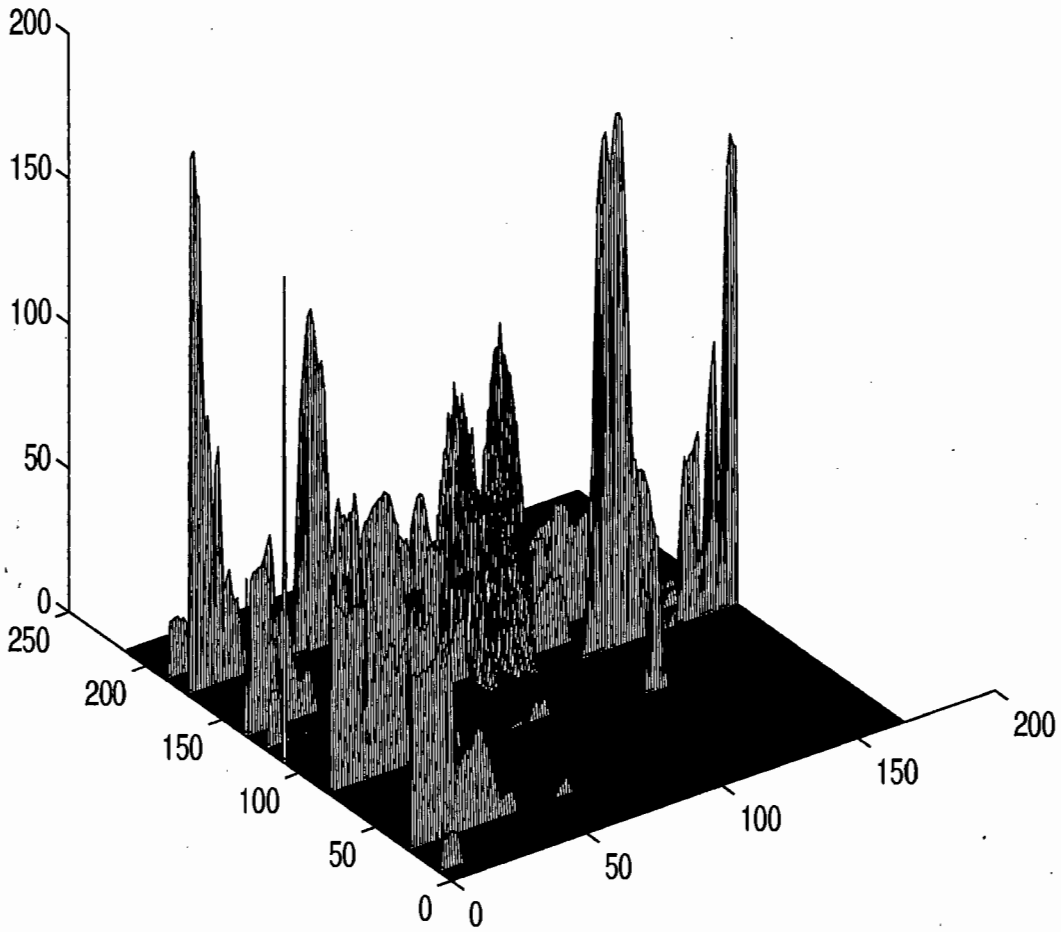


Figure 3.1: A Radar Return Signal of a Real Ship (Outeniqua) Disguised by Interference.

stationary.

## 3.2 Theoretical Review of Thermal Noise

Thermal noise is also recognised as receiver noise or system noise. The sources of this noise lie within the radar itself or in the environment external to the radar system. Thermal noise generated within the receiver can be attributed to the thermal agitation of electrons in the receiver i.e. the random motion of free electrons in a conducting medium like the receiver antenna. It is safe to assume that thermal noise is white. The thermal noise in the receiver is dependent on the noise temperature of the receiver in degrees kelvin and the bandwidth of the receiver, thus producing the relation [17] :

$$N = kT_eB \tag{3.1}$$

where $N$ is thermal noise in the receiver and $T_e$ is the effective temperature of a white thermal noise source at the input that would be required to produce the same noise power at the output of an equivalent noiseless system. $B$ is the bandwidth of the transceiver system. The thermal noise has therefore been limited according to the specified receiver bandwidth. In order to model thermal noise correctly, a good description of the system noise is required in terms of its distribution and characteristics. An adequate explanation and description of system noise is provided in [17, page 482].

## 3.3 Theoretical Review of Scintillation

This section provides one with a comprehensive insight to the theory concerning target scintillation in order to understand why it was implemented in the simulations in this dissertation and how it was implemented.

In order to acquire an understanding of the concept of scintillation, one must be

introduced to *radar target cross-section.* This term defines the equivalent area producing the same amount of energy returned to the radar as would be produced by a scatterer intercepting the energy transmitted from the radar along the boresight axis of the antenna. Factors such as the size, shape and discontinuities of the target affect its radar cross-section. As far as the transmitter is concerned, wavelength and aspect angle of the transmitted signal also affect the radar cross-section of the target. The radar cross-section of a target fluctuates as a function of time. This is due to the motion of scattering points of a target viewed by the radar.

Target scintillation can be of two general types. Scintillation can occur between pulses which have been transmitted. This is pulse-to-pulse scintillation. The radar cross-section can also vary between scans thus producing scan-to-scan scintillation. As far as high frequency pulsed modern radars are concerned, scan-to-scan scintillation is more representative of actual radar-target dynamic conditions. In this dissertation, scan-to-scan scintillation is modelled in the simulations of radar range profiles. Scintillation is described as follows, while referring to Figures 3.2 and 3.3.

Assume that the target is composed of two point sources which are close together. The radar return signal is represented as a vector. If the target is illuminated by the radar, the two signals returning to the receiver will interfere and the resulting return vector as seen in Figure 3.2 will be the sum of the two vectors. If the orientation of the target changes slightly then the relative distance of the two points representing the target, will change. the two return vectors or signals from the two points will therefore interfere again but with a different phase difference thus producing a smaller resultant signal as in Figure 3.3. The sum may thus vary greatly from one moment to the next. Recognizing that appreciable returns will be reflected from different parts of the target, it is possible to see why a target's echoes or radar cross-section scintillates.

The resultant depicted in Figures 3.2 and 3.3 can scintillate due to the phase changes of its component vectors. Another method of simulation, would be to scintillate the resultant by scintillating the actual values of its components

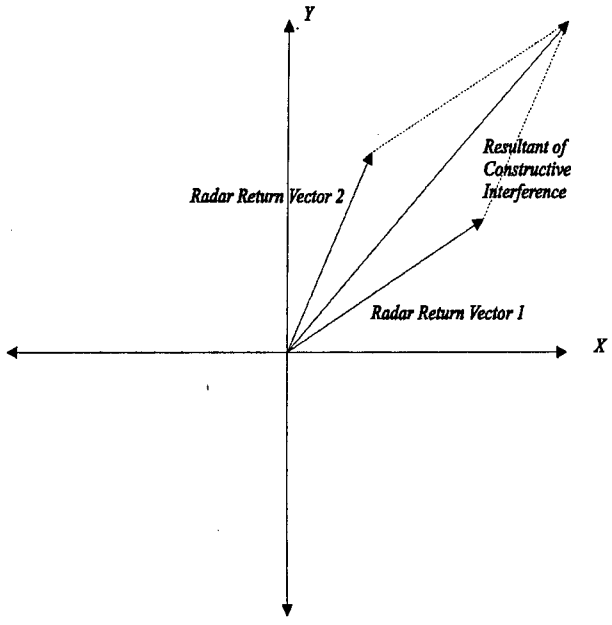


Figure 3.2: Polar Plot of Two Return Vectors from Two Different Point Sources on a Radar Target.

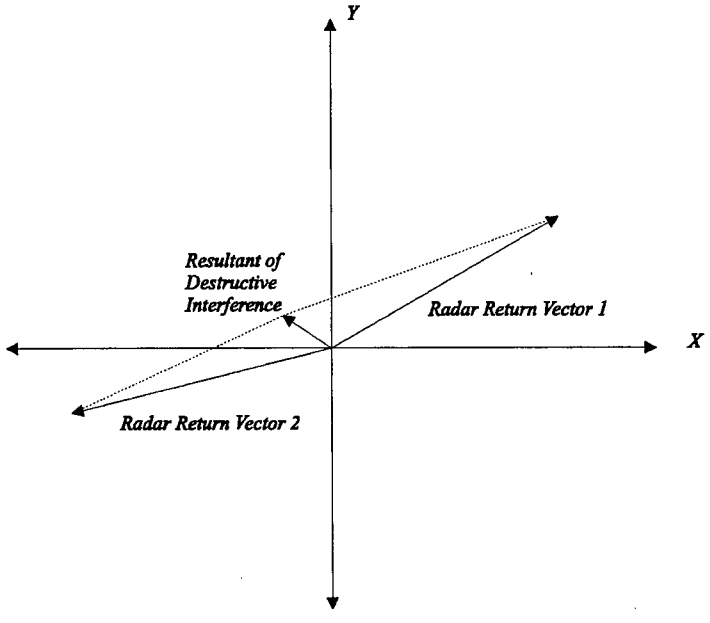


Figure 3.3: Polar Plot of Same Two Return Vectors from Same Two Point Sources on a Radar Target at Different Orientations.

between scans.

## 3.4 Implementation of Clutter, Thermal Noise and Scintillation in Simulations

This section outlines the models utilised in simulating the concepts of radar clutter, thermal noise and scintillation. Methods for simulation of the above-mentioned concepts reflect on the theory provided for these factors which lead to degradation of radar performance.

### 3.4.1 Sea Clutter and Thermal Noise

Thermal noise is a Gaussian-distributed quantity as can be assumed by the *central limit theorem [17],* while sea clutter is assumed to possess a Weibull distribution [14, page 13.8]. It was decided to approximate both effects as Gaussian-distributed white noise due to the fact that the generation of accurate clutter distributions is tedious.

Each signal transmitted by the radar system can be viewed as a phasor with a magnitude and phase i.e. a signal comprising of a quadrature and in-phase component. For each resolution cell of the radar, the return is the vector sum of the transmitted signals. Equation 3.2 indicates that the total energy returned from a target is the vector sum of all return vectors for a particular resolution cell of the radar.

$$E_r = \sum_i \left(e_{ri} e^{\phi_i}\right) \tag{3.2}$$

where $E_r$ is the total energy returned and $e_{ri}$ is the magnitude of the energy returned by the $i_{th}$ reflector. $\phi_i$ Is the phase of the return vector from each $i_{th}$ reflector. The noise vector is then added to $E_r$ as in Equation 3.3.

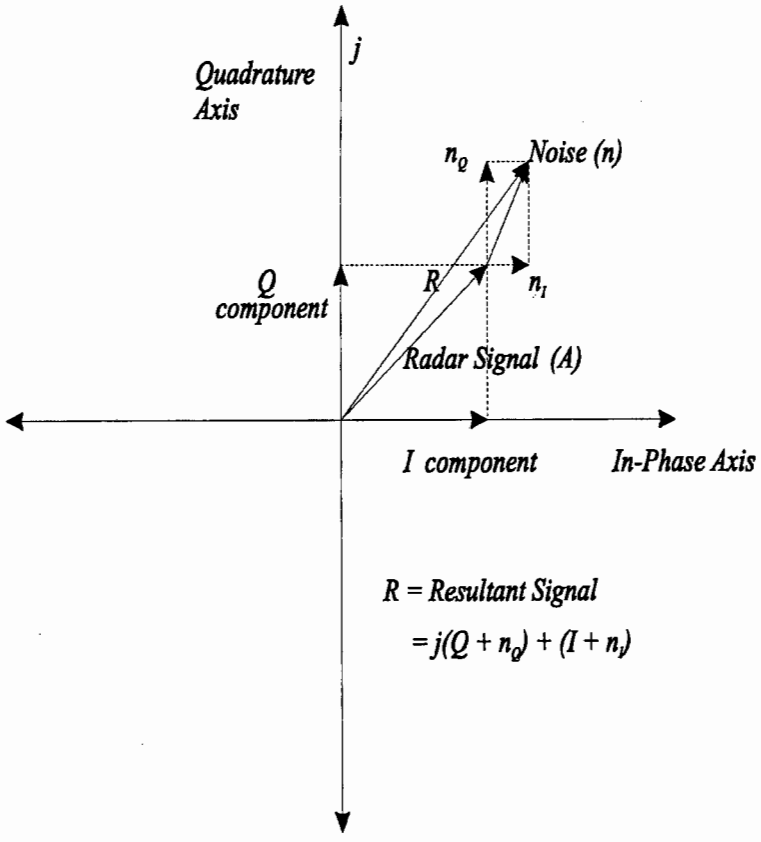


Figure 3.4: Addition of Noise Components to Signal Components Illustrated in the Polar Co-ordinate System.

$$E_r = \sum \left(e_{ri} e^{\phi_i}\right) + e_n e^{\psi} \tag{3.3}$$

where $e_n$ is the magnitude of a noise vector whose in-phase and quadrature components are equal i.e. its $x$ and $y$ components are equal. $\psi$ Is the phase of the noise vector. Figure 3.4 illustrates the addition of the noise vector to that of the sum of all return vectors for a radar resolution cell.

In order to simulate a specific signal-to-noise ratio, a quantitative measure of the amount of noise applied is important. For the simulations, it was important to examine the results of all recognition tests under certain noise levels. These noise levels are pre-determined according to the power of the return signal. The

entire range profile consists of range bins with return vectors or phasors. The return power within a particular downrange profile was calculated by Equation 3.4.

$$P_r \alpha \frac{1}{T} \int_{t_1}^{t_2} A(t)^2 dt \tag{3.4}$$

where $T = t_2 - t_1$ and is the distance over which the ship extends and not over which the measured profile extends i.e. the number of range bins occupied by the ship and not by the entire range profile. $A$ is the magnitude of the sum of all return vectors for a resolution cell, as indicated in 3.4. This was done in order to obtain a more realistic impression of the real power in the profile which is only significant in the area where a valid return signal is evident. Once this figure is known and the desired signal-to-noise ratio for the simulation is known, one can calculate the noise power required for the simulation. Equation 3.5 was used to calculate the total required noise power for a profile.

$$SNR = 10 \log \left( \frac{S}{N} \right) \tag{3.5}$$

where $S$ is signal power and $N$ is noise power. The noise power is given by Equation 3.6.

$$N = \frac{1}{T} \int_{t_1}^{t_2} n^2 dt \tag{3.6}$$

where $n$ is the magnitude of the noise vector added to the return vector of a radar signal in a resolution cell. This noise power is also the variance($\sigma^2$) of the noise, since white noise is Gaussian with zero mean [17].

For the simulation, a set of random complex numbers needed to be generated for the noise vectors. Each random complex number would consist of a real and imaginary part of equal magnitude, constituting the noise vector for each resolution cell. Let the imaginary part of this vector be $n_Q$ and the real part be $n_I$ and $n$ be the magnitude of the noise vector as in Equation 3.7.

$$n = \sqrt{n_I^2 + n_Q^2} \tag{3.7}$$

Since $n_I$ and $n_Q$ are equal let each equal $x$. Equation 3.7 is now represented by Equation 3.8.

$$\begin{aligned} n &= \sqrt{2x^2} \\ \frac{n}{\sqrt{2}} &= x \end{aligned} \tag{3.8}$$

If the variance of $n$ is $N$, then the variance of $x$ is $\frac{N}{\sqrt{2}}$. Random numbers for the real and imaginary parts of the noise vectors were generated with zero mean and a variance of $\frac{N}{\sqrt{2}}$.

### 3.4.2 Scintillation

The following discussion refers to the implementation of scintillation in the simulator used for this study [6]. Based on the methods used to simulate the ships, as indicated in Chapter 4, the radar return vectors from each point scatterer on a ship add vectorially. This addition causes constructive and destructive interference and thus scintillation, by virtue of the explanation provided in section 3.3. It was found in the simulations that this modelling caused scintillation such that the magnitude of each return vector in a resolution cell changed by at least 40% of the mean value with a variance of about 6.79% of the mean value, due to target rotation. This means that each feature scintillates just due to rotation.

Additional functionality of the simulator also makes provision for extra scintillation apart from that just discussed, for the purpose of more rigorous recognition tests. This section describes how this scintillation was implemented. It must be noted that this scintillation was performed after the scintillation discussed in the previous paragraph, which was due to constructive and destructive interference of the addition of return vectors in each resolution cell.

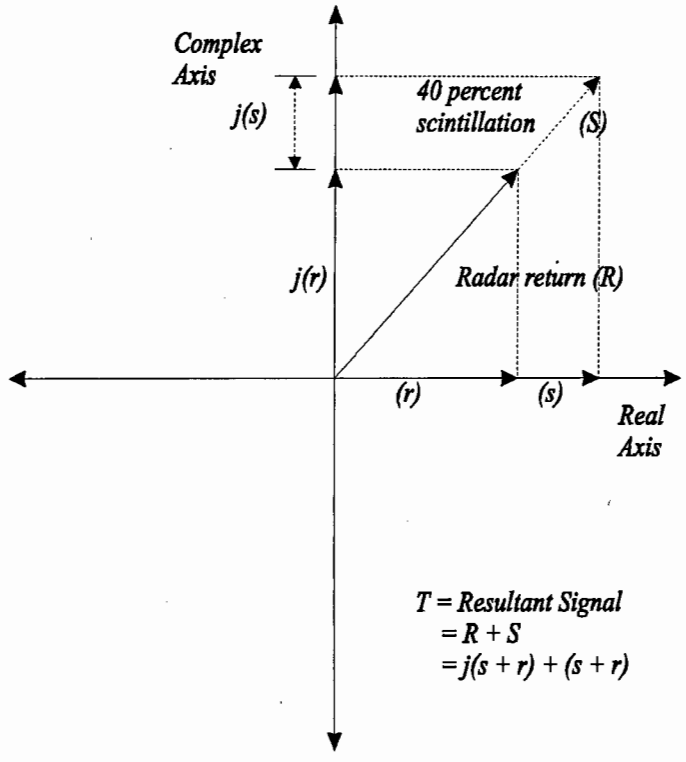


Figure 3.5: Implementation of 40 % Scintillation on Radar Return Vector.

As pointed out in paragraph 3.3, the extra scintillation was implemented on a scan-to-scan basis. Each range profile of a ship at a different aspect angle possesses different values. Again, it was necessary to acquire some quantitative measure of the amount of scintillation to be incorporated into the simulations. The method implemented for the purposes of scintillation is the method mentioned in paragraph 3.3, whereby each return vector's component is scintillated equally by a certain percentage in a single range bin. The signal referred to is the resultant addition of all complex return signals in that particular range bin after scintillation due to the ships' rotation and constructive and destructive interference as discussed in the paragraph above. This signal is $R$ in Figure 3.5. The particular percentage of scintillation incorporated depends entirely on the predetermined percentage which the simulation requires at the time. Figure 3.5 and Figure 3.6 indicate how scintillation was performed in the simulations.

Each range bin comprises a return vector($R$) as in Figure 3.5. The absolute

value of a complex, normal-distributed random number with equal quadrature and in-phase parts, is then added to the resultant return vector. The mean of this random number distribution is the resultant magnitude of the return vector for that range bin, while the standard deviation is the percentage of that return vector as illustrated in Figure 3.6. Scintillation in the dissertation was quantized as a percentage of the return vector (scintillation percentage).

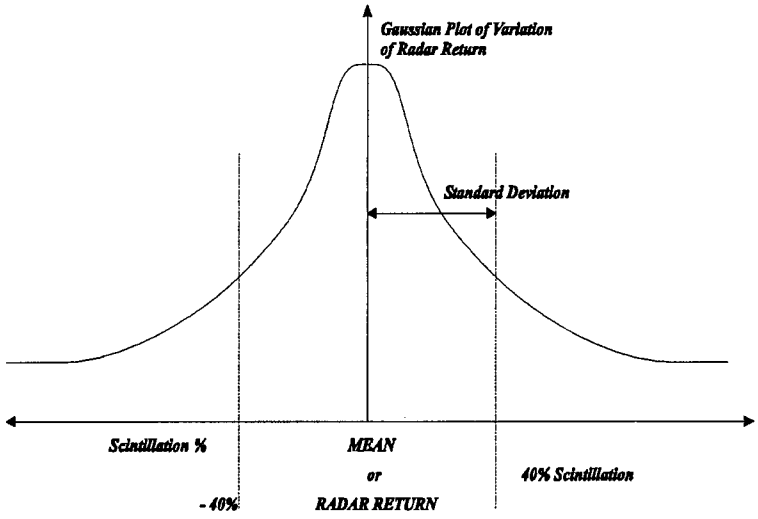


Figure 3.6: Gaussian Representation of Scintillation Indicating the 40% Cut-off Point.

## 3.5 The Matched-Filter Concept

The return signal of a radar is usually enhanced for detection, by applying a matched filter to the received signal. Filter characteristics matching those of the transmitted radar signal are created in the receiver. The enhancement of the radar return signal is such that the signal-to-noise ratio is at a peak at

some point. The matched filter is used for the recognition of the signal in the presence of white noise. It must be noted that the fidelity of the signal is not restored. Detailed information concerning the matched-filter effect is available in Stremler's text [17].

## 3.6 Review of the Simulator

This section provides a brief explanation of the model for the simulation of radar signatures of ship targets. As mentioned before, the simulator was developed by Rolf Lengenfelder of the Radar Remote Sensing Group [6] and adapted by the author of this dissertation for the study at hand. The simulator provides a controlled environment in which thermal noise, clutter and scintillation can also be included in order to examine the effects thereof on the process of ship recognition. Clutter, thermal noise and scintillation is the author's contribution to the simulator. A brief rundown of all other extra features is also provided. The simulator was written in Mathcad initially. In order to attain greater speeds of computation, the simulator can be written more appropriately in C or C++.

The simulator attempts to simulate reality as close as possible. According to specifications provided by the Institute for Maritime Technology, the pulse duration for their non-coherent radar is 80ns, providing a maximum resolution of 12m. Sampling is non-coherent (magnitude only), at a variable sampling frequency. This particular pulse-width is specified within the simulator in the section providing the radar parameters. The pulse repetition interval (PRI) is 3.6kHz. The carrier frequency is 9.6GHz. These specifications are also set in the simulator. According to user requirements, other specifications are also set. These include the beam shape, elevation beam-width, azimuth beam-width, elevation angle, azimuth angle and power output of the radar antenna. As far as thermal noise, clutter and scintillation are concerned, scintillation percentages and signal-to-noise ratios are also specified within the simulator [6]. The antenna beam shape is isotropic and not sinusoidal, therefore producing a constant antenna gain of one for the purpose of simulation.

Each target is comprised of a number of point scatterers. The radar illuminates the targets with small bursts of electromagnetic energy in the form of a pulse. The backscatter power is then recorded as a function of time. The result is a range profile that is a one-dimensional projection of the spatial distribution of the radar reflectivity. The backscattered power received at any given time consists of the sum of scatter from all point scatterers in that corresponding range bin. The received signal energy from a point scatterer is specified as in Equation 3.9 :

$$S = \sum \frac{PG^2\sigma_i\lambda^2}{(4\pi)^3 R^4 L} \tag{3.9}$$

where :

$P$ = *transmitter power*

$G$ = *antenna gain*

$\sigma_i$ = *radar cross section of* $i_{th}$ *reflector*

$\lambda$ = *wavelength of carrier frequency*

$R$ = *range to target*

$L$ = *total losses*

$S$ = *received signal energy*

These returns are passed through a matched filter and non-coherent sampling then implemented, thus producing the final range profile. The matched filter utilised for this particular simulator [6] was multiplied by a window function called the Bartlett window. Details concerning the Bartlett window is presented in [11].

Apart from all the standard signal processing applied, the Fourier Transform and MDMT were incorporated in the simulations, and the corresponding outputs plotted. Plots of the downrange radar profiles of the simulated sea vessels were also generated.

### 3.6.1 Summary

Implementation of thermal noise, clutter and scintillation was successful. Profiles resembled those of real range profiles of such ships and theory described above and applied to the simulator produced expected results as far as the simulations were concerned. Real data sets acquired for ensuing tests on real data were not large enough. In order to perform adequate tests on large amounts of data, a good simulator was required with the capacity to correctly simulate scintillation and clutter. The profiles produced, were very realistic and possessed very similar characteristics to those of real data, especially when considering clutter and scintillation.

## 3.7 Background to the Neural Network - Self-Organizing Map

The neural network implemented in this particular study is the Self-Organizing Map (SOM) [5]. which incorporates Learning Vector Quantization (LVQ) [5].

This section provides an overview of the neural network and some of the algorithms used on the simulated data. Specifics of the algorithms can be referenced in Appendix B and was acquired from [5]. The aim of this section is to justify the choice of neural networks for ship target recognition and to provide a high-level understanding of the implications thereof in this dissertation.

### 3.7.1 Attributes of the Neural Network

The choice of the neural network or Self-Organizing Map as opposed to traditional feedforward or backpropagation methods are attributed to the following factors [12] :

- The Feedforward network is superior since the decision boundaries are capable of being non-linear.

- The neural network would seem to be more efficient. Convergence for learning periods are however very lengthy.

- The probability density function of the features of each class or ship in this particular matter, is Gaussian [12, page 31]. These features are the amplitudes of the range profiles of the ships which depend on scintillation. This implies that features of the Mellin Transform of the same sea vessel for different aspect angles, possess very similar characteristics. Non-linear decision boundaries are thus not a requisite for the classification of ship targets.

- The convergence times for Self-Organizing Maps are small compared to those of other traditional neural networks.

### 3.7.2 Description of the Self-Organizing Map

The prominent and principal characteristic of this neural network, is the ability to spatially arrange representations of features of input signals [5]. These representations are distinct and often eminent due to the almost linear decision boundaries attributed to the SOM.

The SOM is an unsupervised neural network in that the individual cells are specifically tuned in order to identify different classes of functions, by means of this so-called unsupervised learning process [5]. The co-ordinates of a cell or group of cells fall within the domain of a group of similar input patterns or functions to the neural network. One could interpret this concept as one such explanation applied to the human brain where certain regions of the topographical map of the brain are dedicated to specific and distinguishable tasks. This particular description is very applicable in the realms of ship target recognition, since the Mellin Transforms of a single vessel at different aspect angles, constitutes this set of similar input signals or functions.

### 3.7.3 Competitive/Unsupervised Learning

The Learning Vector Quantization algorithms have the capacity to produce approximations to Gaussian distributions as far as the vectorial inputs to the neural network are concerned.

A set of randomly-selected reference vectors are represented as $\{m_i(t) : m_i \in \Re^n, i = 1, 2, ..., k\}$

For $t = 1$, the best-matching $m_i(t)$ is chosen to match $x(t)$ at $t = 1$ more closely. This means the closest $m_i(1)$ will be minimized. One should bear in mind that all $m_i(t)$ initially occupy random positions in their spacial representation in Figure 3.7.b. While $m_i(1)$ is manipulated, all other $m_i(t)$ are left intact. The so-called cells or reference vectors $(m_i(t))$, in this manner become specifically tuned to the different domains of $x$. This means that for every different $t$ each $x(t)$ domain will be closer to a different and more specific $m_i(t)$ for that $t$. The representation for the particular class of functions into which Figure 3.7 falls, will vary in its random spacial form to a definite spacial representation presented in Figure 3.7.b.

This representation will become more specific and specialised towards a specific class of functions, the more the neural network is trained with vectorial inputs of that specific class. This particular discussion leads to the introduction and explanation of the Learning Vector Quantization algorithms implemented in the current dissertation.

### 3.7.4 The Significance of the Neural Network in Conjunction with the MDMT Algorithm

The role of the Modified Direct Mellin Transform (MDMT) is that of extracting common features which are insensitive to any aspect angle variations of the radar or ship targets. According to theoretical explanations of Chapter 2 in paragraph 2.2, the Modified Direct Mellin Transform algorithm ameliorates scaling or migration of features of the down-range profile of a ship target with respect to the independent variable. The implication is that the MDMT of range profiles of the

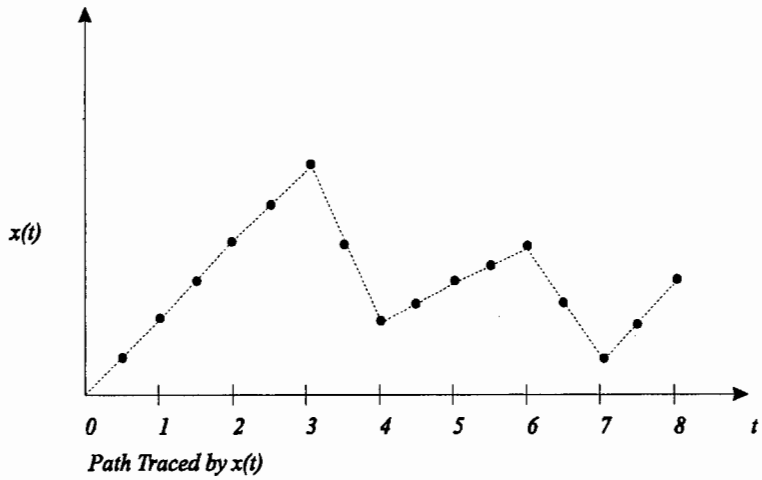


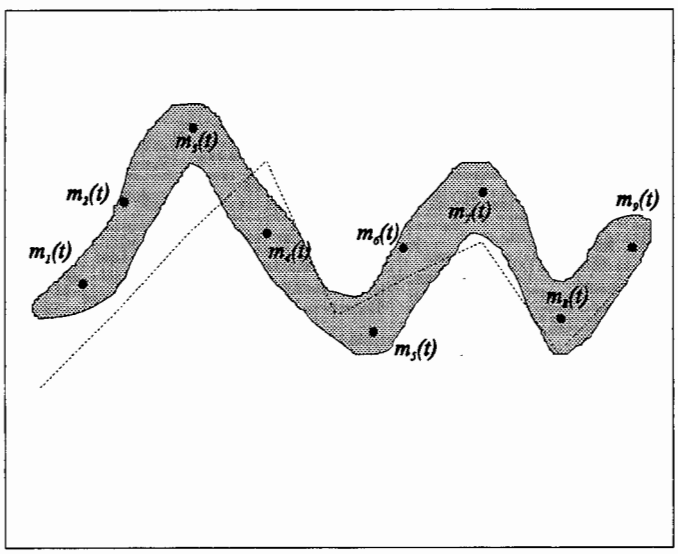


*Comparison of Spacial Representation of x(t) by 9 Codebook Vectors of $m_i(t)$ and Actual Path Traced by x(t).*

Figure 3.7: Specialization of the Spacial Representation of Codebook Vectors $m_i(t)$ for the Function $x(t)$.

same target at different aspect angles, possess very similar characteristics and prominent features. Learning Vector Quantization algorithms ensure that the neural network becomes feature-sensitive such that a class of vessels are classifiable or recognizable by means of their characteristic features in terms of the output produced by preprocessing of the radar range profiles. As discussed in Chapter 2, paragraph 2.3.4, preprocessing involves the application of the Fourier Transform on the profile of a ship target and implementation of the MDMT theorem.

The vectorial inputs ($x(t)$) employed to make the preceding discussions more comprehensive, is replaceable by the sampled data ($x_k$) of the ship targets. This includes sampled data for simulations and genuine ship targets in this dissertation. Theoretical applications in this chapter apply accordingly to this data in the endeavour to eventually recognize the targets by successful extraction of common features from the FMDMTs by the neural network.

# Chapter 4

# Performance of Classification Methods on Simulated Data

This chapter sets out to verify the theoretical explanations of the Mellin Transform in the classification of ship targets. This is achieved by the simulation of downrange radar profiles of ship targets and the application of preprocessing on the data. The classification results were then analysed in detail under various conditions discussed in Chapter 3 and mentioned below.

An attempt is made to emphasize the varied success in classification when different conditions in nature and imperfections pertaining to the radar system are simulated. These conditions include, amongst others, sea clutter and scintillation of the target reflectors. Imperfections of the radar receiver include the generation of thermal noise. In this way, the dissertation attempts to massage the classification techniques so as to acquire better results when real ship data is used in the classification process. Comparison of the results of classification and methods incorporated as far as real and simulated data is concerned, will indicate a great degree of similarity in success of target recognition.

## 4.1 Introduction to the Simulator

The simulator utilised in the dissertation modelled each feature of a ship as a large number of closely-spaced point targets or reflectors. Radar return vectors associated with these point targets would add in a complex manner, producing constructive and destructive interference.

### 4.1.1 Simulator Parameters

This dissertation aims at providing realistic simulations. Simulations incorporating the use of the Mellin Transform for recognition, are meant to corroborate the theory and functionality of the Mellin Transform as far as ship target recognition is concerned. The results of implementing the Mellin Transform on real data will corroborate those results attained in conditions of controlled simulation. Parameters selected for the simulator were identical to those which were characteristic of the radar utilized at the Institute for Maritime Technology (IMT) in Simon's Town.

The following characteristics are inherent in both the simulated radar and authentic radar used at IMT :

1. Pulse repetition interval (PRI) of 3.6 kHz.
2. Pulse width of 80 ns, offering a radar resolution of $\frac{c\tau}{2}$ ( 12m ).
3. Beam shape was isotropic for the simulator.
4. Power output of the radar was 10 kW for the purpose of simulation.

Principal features of the simulator include the capability to produce thermal noise and scintillation for each simulation, so as to determine the effect on ship target recognition.

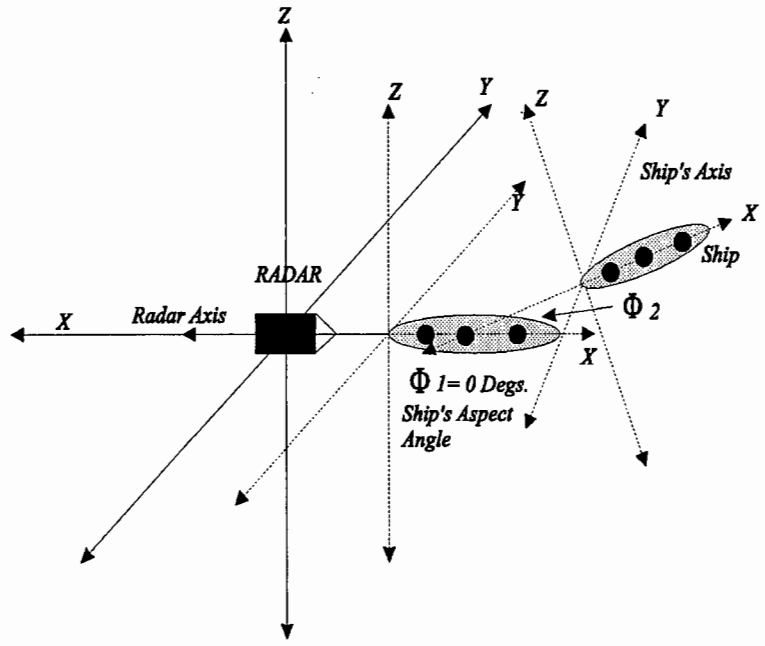


Figure 4.1: Illustration of how a Ship was Modelled by the Simulator, Indicating the Direction of Motion of the Ship's Axis.

### 4.1.2 Motion of Simulated Vessels

Insight is provided in the following section as to how the vessels were positioned so as to simulate variations in aspect angle from the direct line of sight of the radar.

The radar was placed on a global three-dimensional axis, with the line of sight aimed along the $x$-axis. Each vessel was positioned on its own axis platform to which a path of motion was attributed. As the vessel's position moved slowly along that path, a rotation vector multiplied by the ship's matrix representation, would rotate the vessel such that a particular aspect angle was attained. This can be seen in Figure 4.1. The matrix representation is the ship's mathematical representation with reference to its own axis platform. The matrix representation is 3-dimensional.

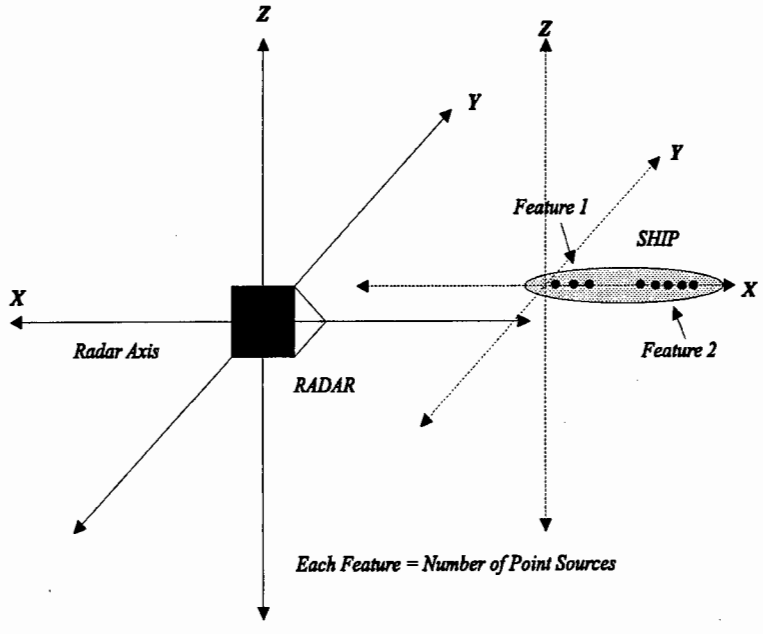


Figure 4.2: Illustration of how a Ship was Modelled by the Simulator.

Figure 4.1 indicates two possible aspect angles characteristic to the ship's position $(\phi_1, \phi_2)$, while Figure 4.2, for example, provides a geometrical explanation as to how a tanker was simulated.

### 4.1.3 Implementation of Radar Signal Processing and Data Processing

Portions of the radar simulator constituting signal processing, include those that use the matched-filter-effect to reject undesired signals and noise. Data processing in the form of the Mellin Transform occurs after detection of the target is successful. Success in ship target recognition is attained by means of the Mellin Transform which was adapted and modified for discrete implementations. Chapter 2 emphasizes and explains the modification of the Mellin Transform in section 2.3.4, thus yielding the MDMT. The code for the implementation of the thermal noise, clutter, scintillation and the MDMT is presented in [13]. The output of

the radar simulator after signal processing and before data processing (Fourier Transforms and Mellin Transforms), is a downrange profile of a ship target, an example of which can be viewed in Figure 4.3. This profile is totally dilute.

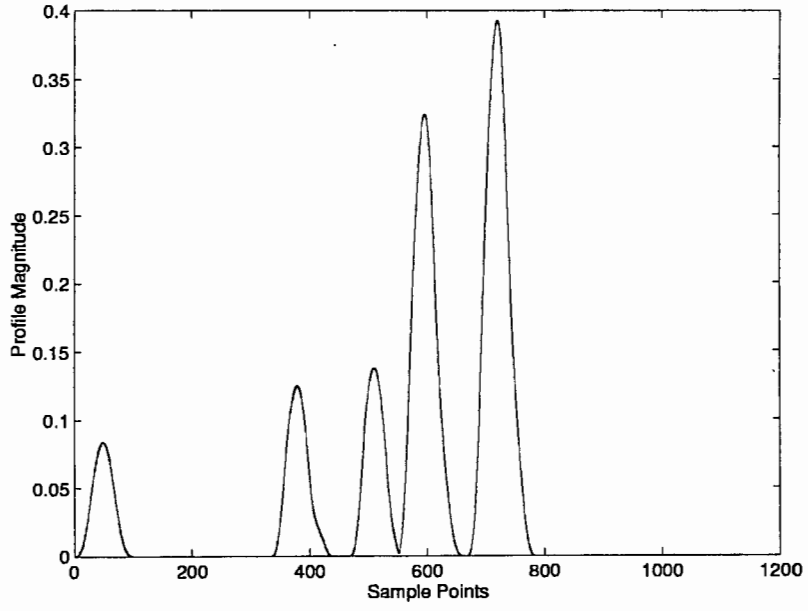


Figure 4.3: Magnitude of Downrange Profile of Simulated Tanker.

## 4.2 Performance Analysis of the Mellin Transform in Conjunction with the Neural Network

A series of test cases were implemented. These test cases are related to the goals of this study which attempts to ascertain that it is feasible to implement effective classification of radar range profiles of ship targets.

### 4.2.1 Discussion of Significant Test Scenarios

As the section above reveals, the test cases will be presented together with their purpose, significance in relation to using the Modified Direct Mellin Transform and the neural network with LVQ algorithms.

Four vessels were simulated,

- Tanker - $215m$
- Trawler - $159m$
- Patrol Boat - $95m$
- Tug - $39.5m$

### 4.2.2 Simulation of Appropriate Data

The design of the simulator and its features discussed in Section 4.1.2, afforded the simulation of range profiles at any desired aspect angle. Range profiles for the tanker at thirty aspect angles are provided in a single plot in Figure 4.4. These aspect angles range from zero to thirty degrees at one degree intervals.

In order to have been able to implement the tests pertaining to the different test cases mentioned in Section 4.2, one batch of profiles for each ship was required for teaching the neural network. This batch of profiles would constitute the profiles of each ship at $n$ different aspect angles at an interval of two degrees. The FMDMTs of these profiles would be used to train the LVQ neural network. Next, for testing and recognition purposes, another batch of profiles was required for each ship. This batch of profiles would also consist of $n$ different profiles at $n$ different aspect angles, two degrees apart. As far as angles are concerned, the profiles of the first batch for learning, would lie between those of the second batch used for testing. Explanation of this procedure is provided in Figure 4.5, with each line representing the position of the ship with respect to the radar.

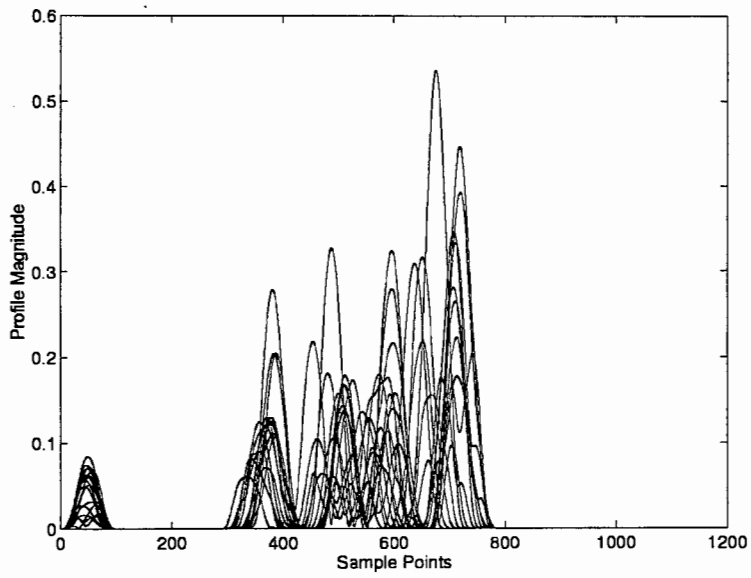


Figure 4.4: Sixteen Range Profiles for the Simulated Tanker at 16 Aspect Angles in the Range of 0 to 30 Degrees.

Radar range profiles were produced for each position assumed by the vessel in Figure 4.5.

In recent studies, recognition success was poor for aspect angles close to 90 degrees. The maximum range used for evaluation in the majority of tests mentioned in 4.2, was 0 to 90 degrees as indicated in Figure 4.5.

Twelve batches of range profiles were produced for each ship for training and testing of the neural network. One must bear in mind that each profile in the test sets are representative of the ship at angles between those created for training sets. This concept is portrayed in Figure 4.5. The batches are characterized as in Table 4.1.

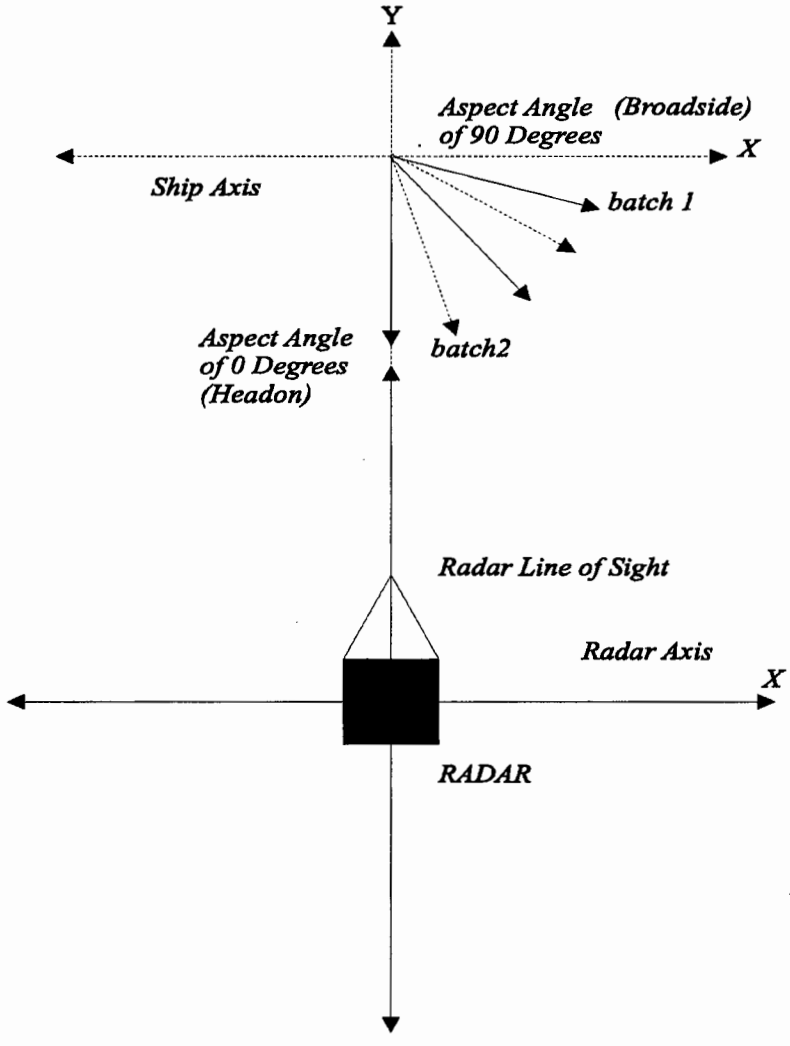


Figure 4.5: Illustration of Different Positions Taken up by the Ship in Relation to the Radar.

| Aspect ∠ Range · | Aspect ∠ Interval | Number of Profiles | Training or Test Set |
|---|---|---|---|
| 0-30° | 2° | 15 | Training |
| 0-30° | 2° | 15 | Test |
| 0-52° | 2° | 26 | Training |
| 0-52° | 2° | 26 | Test |
| 0-60° | 2° | 30 | Training |
| 0-60° | 2° | 30 | Test |
| 0-70° | 2° | 35 | Training |
| 0-70° | 2° | 35 | Test |
| 0-80° | 2° | 40 | Training |
| 0-80° | 2° | 40 | Test |
| 0-90° | 2° | 45 | Training |
| 0-90° | 2° | 45 | Test |

Table 4.1: Twelve Batches of Range Profiles

### 4.2.3 Performance Test Cases for Simulations

Procedural steps followed to assess the performance of the Mellin Transform in conjunction with neural networks for ship target recognition, are laid out in this section. The standards and objectives of the research which will form the backdrop against which test results can be displayed, are presented in the following test cases.

This section then addresses the Mellin Transform, the principal mechanism used for the purpose of recognition in this dissertation. Implementation of the Fourier Modified Direct Mellin Transform (FMDMT) on the profiles of the tanker have produced outputs which will also be shown graphically for the tanker in [13]. The various test cases referred to previously, are included in the mentioned appendices with corresponding profiles and FMDMTs thereof. This section provides several examples of profiles and FMDMTs for the tanker for different test cases.

As far as the training and testing of the neural network is concerned, each training

set of input functions corresponds to a discrete set of patterns for the decision process. An example of a training set would be the FMDMTs of the range profiles of a ship in the aspect angle range of 0 to 30 degrees at one degree intervals. Codebook vectors of the LVQ network form a map which approximates the probability density function of the input vectors. Several codebook vectors represent a particular set of input functions and are localised in the input space in order to minimize recognition errors. At completion of the training process, the orientation of the codebook vectors in this input space, defines clear decision boundaries between the different classes of input functions pertaining to the different classes of ships.

Training the neural network included the implementation of the LVQ1 algorithms mentioned in Appendix B, section B.2.1.for the initial structuring of the class boundaries between the different classes of input vectors. Input vectors comprise the FMDMTs of range profiles of the different classes of vessels. at different aspect angles. Tuning of the neural network was accomplished by means of the LVQ3 algorithms described in Appendix B, paragraph B.2.3. Progressive desizing of the *window* was carried out for each training iteration of LVQ3. Obviously, the number of codebook vectors was minimized in order to prevent the class boundaries from becoming too specific with respect to the different classes. Ability of the neural network to generalise for test data, would be minimized by specific tuning to different classes. Based on research carried out on Anthony Robinson's thesis [12], the following parameters were used for the classifier used in this instance :

1. Codebook Vectors = 9

Initializing Options (Balance Algorithm) = 1

OLVQ1 Training Cycles = 1500

1. LVQ3 Training Cycles = 500 (First Run)

Initial Alpha = 0.03

Window Width = 0.3

Epsilon = 0.1

1. LVQ3 Training Cycles = 600 (Second Run)

Initial Alpha = 0.02

Window Width = 0.1

Epsilon = 0.1

1. LVQ3 Training Cycles = 190 (Third Run)

Initial Alpha = 0.01

Window Width = 0.05

Epsilon = 0.1

Conclusions will drawn from the analysis of the results acquired for recognition of simulated ships in the mentioned test cases.

**Test Case One**

The objective of the first test case is to examine degradation of the performance of the Mellin Transform as the aspect angle of the radar target varies, excluding all other external effects like clutter etc. The signal-to-noise ratio was infinite. Training set aspect angle ranges in degrees were :

- 0 to 30
- 0 to 52
- 0 to 60

Test set aspect angle ranges in degrees were :

- 0 to 30
- 0 to 52
- 0 to 60

**Profiles and FMDMTs** Radar range profiles for the first scenario's training set for the neural network is presented in Figure 4.6 for aspect angle range of 0 to 30 degrees. The FMDMTs of these profiles are presented in Figure 4.7 for the tanker.

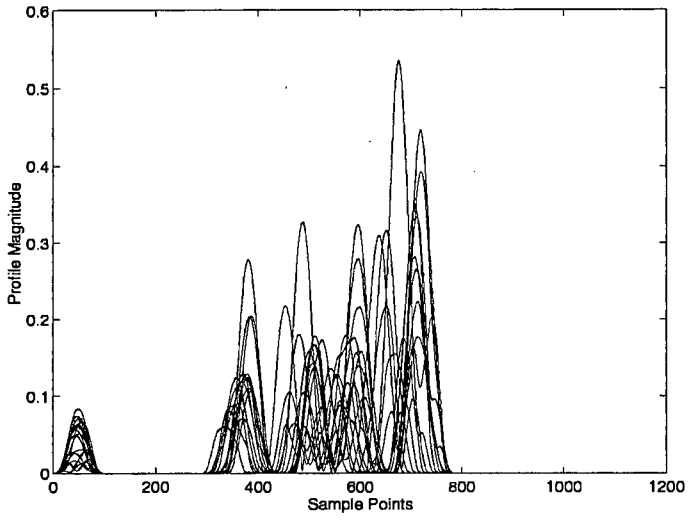


Figure 4.6: Profiles Constituting Tanker Training Set in the Aspect Angle Range of 0 to 30 Degrees. SNR = $\infty$.

**Training and Testing with the LVQ Neural Network** Training in this section of the dissertation and ensuing sections was carried with the underlying objective of minimizing the eventual training set dimensions. The goal was to evaluate the classification performance of the neural network even with the

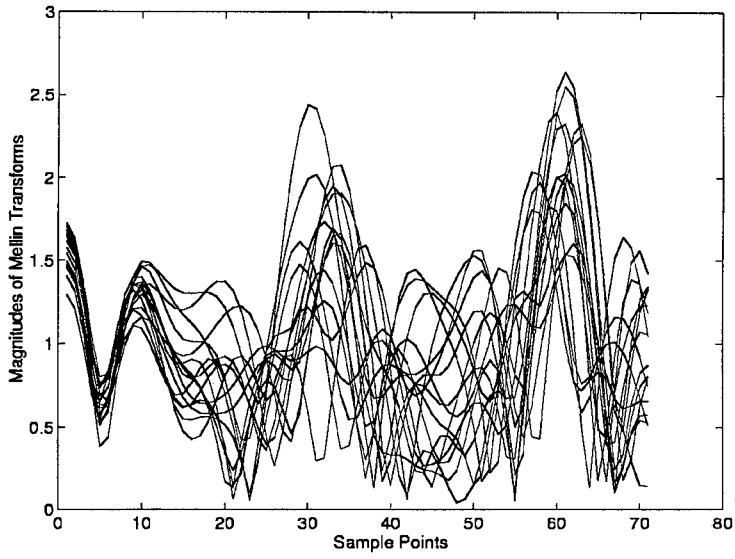


Figure 4.7: FMDMTs Constituting Tanker Training Set in the Aspect Angle Range of 0 to 30 Degrees. SNR = $\infty$.

smallest set of training data possible. These results were more closely scrutinized than those whose training sets were large. The aspect angles thus concentrated on were 0 to 30 degrees, 0 to 52 degrees and 0 to 60 degrees. Training and testing occurred as follows :

Initially the neural network was trained with 15 samples of the input vector representing aspect angle positions of 0 to 30 degrees at 2 degree intervals for all four ships. Testing was carried out with test sets representing the position of the ship at aspect angles of :

1. 1 degree to 31 degrees at 2 degree intervals
2. 1 degree to 53 degrees at 2 degree intervals
3. 1 degree to 61 degrees at 2 degree intervals

Results for the test are depicted in Table 4.2.

Secondly, the neural network was trained with samples of the input vector covering an aspect angle range of 0 to 52 degrees at 2 degree intervals. Testing was

| Aspect Angle Range of Test Set | Tanker | Trawler | Patrol Boat | Tug | Average |
|---|---|---|---|---|---|
| **1 to 31 Degrees** | 100 | 87.50 | 62.50 | 93.75 | 85.94 |
| **1 to 53 Degrees** | 66.65 | 66.67 | 51.85 | 92.50 | 69.44 |
| **1 to 61 Degrees** | 67.74 | 64.52 | 54.84 | 87.10 | 68.55 |

Table 4.2: Recognition Percentages. Aspect Angle Range of Training Set is 0 to 30 Degrees.

| Aspect Angle Range of Test Set | Tanker | Trawler | Patrol Boat | Tug | Average |
|---|---|---|---|---|---|
| **1 to 53 Degrees** | 81.48 | 81.48 | 59.26 | 96.23 | 79.63 |
| **1 to 61 Degrees** | 80.65 | 61.29 | 48.39 | 87.10 | 69.35 |

Table 4.3: Recognition Percentages. Aspect Angle Range of Training Set is 0 to 52 Degrees.

carried out with test sets representing the position of the ships at the following aspect angles :

1. 1 to 53 degrees at 2 degree intervals
2. 1 to 61 degrees at 2 degree intervals

Table 4.3 displays the results for this test.

Thirdly, the neural network was trained with samples of the input vector covering the aspect angle range of 0 to 60 degrees at 2 degree intervals. Testing was carried out with test sets encompassing the aspect angle range of :

1. 1to 61 degrees at 2 degree intervals

Signal-to-noise ratios for both sets were once again infinite (no addition of noise). Results for the test are presented in Table 4.4.

| Aspect Angle Range of Test Set | Tanker | Trawler | Patrol Boat | Tug | Average |
|---|---|---|---|---|---|
| **1 to 61 Degrees** | 87.10 | 87.20 | 58.06 | 90.32 | 80 |

Table 4.4: Recognition Percentages. Aspect Angle Range of Training Set is 0 to 60 Degrees.

**Analysis of Results for Test One** Test One examines the effects of aspect angle variations of the ship targets on target recognition. All particulars of the test can be referenced in the first scenario of Chapter 4.

Tables 4.2, 4.3 and 4.4 reveal that recognition success decreases as the aspect angle of the test set increases. These tables also indicate that the more aspect angles included in the neural network training data, the greater the recognition success. A private conversation between the author of this dissertation and Dr. Colin Andrew of the Radar Remote Sensing Group, revealed that if an input dimension of N features is used, then approximately 10.N training examples or profiles in this case, should be used. Better methods of evaluating neural classifiers is to use the methods of N-fold cross-validation or boot-strapping. These methods allow specification of the variance of the classification accuracy, rather than simply providing a single classification accuracy with the method of dividing data into a training and a testing set. This suggests that increased dimensions of the training sets ensure greater success in recognition of targets. Minimized training data sets are always most desirable in order to attain quick convergence rates with the neural networks.

## Test Case Two

Test case two attempts to examine the suitability of the Mellin Transform as far as scale invariance is concerned, while giving attention to external factors like clutter and thermal noise. Thermal noise was added in this instance. The aspect angle ranges in degrees of the training set were :

- 0 to 30

- 0 to 52
- 0 to 60

while the aspect angles in degrees of the test set were :

- 0 to 30
- 0 to 52
- 0 to 60.

**Profiles and FMDMTs** As the discussion for the test scenarios indicates, thermal noise and clutter was added to the radar range profiles presented previously for the aspect angle ranges of 0 to 30 degrees, 0 to 52 degrees and 0 to 60 degrees. Figure 4.8 indicates a signal-to-noise ratio of $0dB$ for an aspect angle range of 0 to 30 degrees for the LVQ neural network test sets. The FMDMTs of all these profiles can be viewed in Figure 4.9 for the tanker.

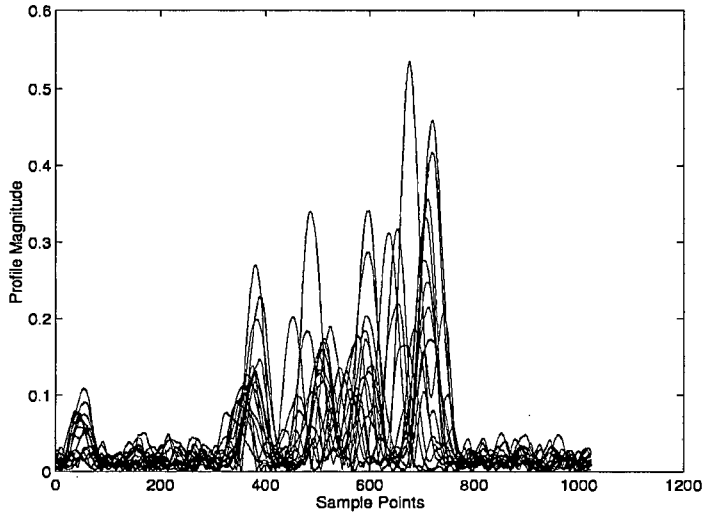


Figure 4.8: Profiles Constituting Tanker Training Set in the Aspect Angle Range of 0 to 30 Degrees. SNR = $0dB$.

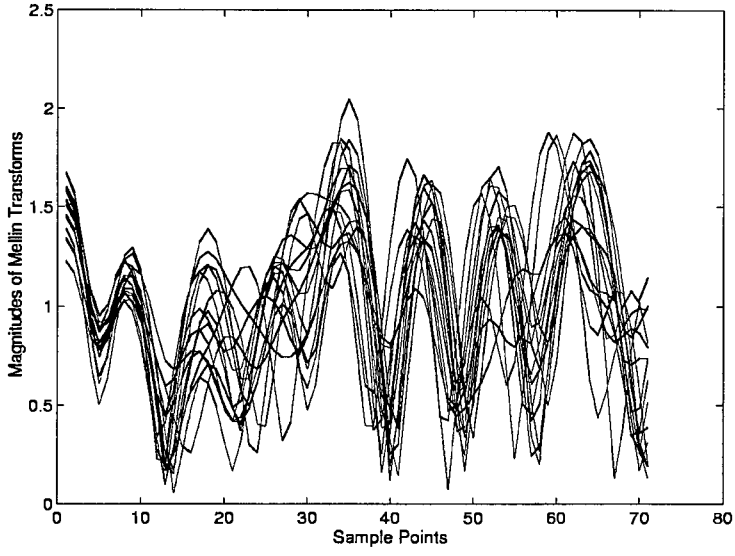


Figure 4.9: FMDMTs Constituting Tanker Training Set in the Aspect Angle Range of 0 to 30 Degrees. SNR = $0dB$.

**Training and Testing with the LVQ Neural Network** Procedural training and testing for this test case was identical to that of test scenario one, with the exception that test input vectors to the neural network were characterised by signal-to-noise ratios of infinity, $56dB$, $20dB$ and $0dB$, while training sets possessed a signal-to-noise ratio of infinity. The results of this particular test scenario are displayed in Tables 4.5, 4.6, 4.7, 4.8, 4.9 and 4.10.

| Signal-to-Noise Ratio (dB) | Tanker | Trawler | Patrol Boat | Tug | Average |
|---|---|---|---|---|---|
| $\infty$ | 100 | 87.50 | 62.50 | 93.75 | 85.94 |
| **56** | 93.75 | 87.50 | 50 | 93.25 | 81.25 |
| **20** | 100 | 87.50 | 56.25 | 93.75 | 84.40 |
| **0** | 75 | 31.25 | 62.50 | 56.25 | 56.25 |

Table 4.5: Recognition Percentages in the Presence of Noise. Aspect Angle Range of Training Set is 0 to 30 Degrees. Aspect Angle Range of Test Set is 1 to 31 Degrees.

| Signal-to-Noise Ratio (dB) | Tanker | Trawler | Patrol Boat | Tug | Average |
|---|---|---|---|---|---|
| $\infty$ | 66.65 | 66.67 | 51.58 | 92.59 | 69.44 |
| **56** | 62.96 | 70.37 | 70.37 | 48.15 | 69.44 |
| **20** | 66.67 | 55.56 | 55.55 | 88.89 | 66.67 |
| **0** | 51.85 | 14.81 | 48.15 | 62.96 | 44.44 |

Table 4.6: Recognition Percentages in the Presence of Noise. Aspect Angle Range of Training Set is 0 to 30 Degrees. Aspect Angle Range of Test Set is 1 to 53 Degrees.

| Signal-to-Noise Ratio (dB) | Tanker | Trawler | Patrol Boat | Tug | Average |
|---|---|---|---|---|---|
| $\infty$ | 67.74 | 64.52 | 54.84 | 87.10 | 68.55 |
| **56** | 51.61 | 67.74 | 58.06 | 83.87 | 65.32 |
| **20** | 54.84 | 64.52 | 51.61 | 90.32 | 65.32 |
| **0** | 61.29 | 19.35 | 48.39 | 67.74 | 49.19 |

Table 4.7: Recognition Percentages in the Presence of Noise. Aspect Angle Range of Training Set is 0 to 30 Degrees. Aspect Angle Range of Test Set is 1 to 61 Degrees.

| Signal-to-Noise Ratio (dB) | Tanker | Trawler | Patrol Boat | Tug | Average |
|---|---|---|---|---|---|
| $\infty$ | 81.48 | 81.48 | 59.26 | 96.23 | 79.63 |
| **56** | 81.48 | 74.07 | 48.15 | 92.59 | 74.07 |
| **20** | 81.49 | 74.04 | 51.85 | 92.59 | 75 |
| **0** | 51.85 | 29.63 | 81.48 | 55.56 | 54.63 |

Table 4.8: Recognition Percentages in the Presence of Noise. Aspect Angle Range of Training Set is 0 to 52 Degrees. Aspect Angle Range of Test Set is 1 to 53 Degrees.

| Signal-to-Noise Ratio (dB) | Tanker | Trawler | Patrol Boat | Tug | Average |
|---|---|---|---|---|---|
| $\infty$ | 80.65 | 61.29 | 48.39 | 87.10 | 69.35 |
| **56** | 74.19 | 77.42 | 48.39 | 90.32 | 72.58 |
| **20** | 80.65 | 70.97 | 58.06 | 80.65 | 73 |
| **0** | 64.52 | 19.35 | 45.16 | 61.29 | 47.58 |

Table 4.9: Recognition Percentages in the Presence of Noise. Aspect Angle Range of Training Set is 0 to 52 Degrees. Aspect Angle Range of Test Set is 1 to 61 Degrees.

**Analysis of Results for Test Two** Test Two was similar to the first test with the exception that the effects of thermal noise and clutter were included in the examination. Recognition percentages in Tables 4.5 to 4.10 once again convey the fact that recognition of targets by means of neural networks in conjunction with the Mellin Transform, is better, the greater the dimension of the training data set. Numerical results in Table 4.7 are poorer than those of Table 4.10 due to a smaller training set. Dimensions of the training and testing data sets correlate for test results depicted in Tables 4.5, 4.8 and 4.10 i.e. sizes of corresponding training and test sets are equal. Recognition accuracy decreases with an increase in noise content.

| Signal-to-Noise Ratio (dB) | Tanker | Trawler | Patrol Boat | Tug | Average |
|---|---|---|---|---|---|
| $\infty$ | 87.10 | 87.10 | 58.06 | 90.32 | 80 |
| **56** | 77.42 | 80.65 | 54.84 | 90.34 | 75.81 |
| **20** | 87.10 | 77.42 | 51.61 | 90 | 76.61 |
| **0** | 67.74 | 25.81 | 38.71 | 64.52 | 49.19 |

Table 4.10: Recognition Percentages in the Presence of Noise. Aspect Angle Range of Training Set is 0 to 60 Degrees. Aspect Angle Range of Test Set is 1 to 61 Degrees.

Test Case Three

Test case three attempts to determine the degree of degradation imposed by noise only on the successful recognition of classes of ships. The effect of aspect angles are excluded. Thermal noise and clutter were added. The aspect angle range in degrees of the training set was 0 to 30 at 2 degree intervals. The test set comprised of single profiles of each ship at specific aspect angles of 0 degrees, 16 degrees and 30 degrees. These angles of 0, 16 and 30 degrees were among the angles used for training the neural network. In this way, the effect of aspect angle was circumvented.

**Profiles and FMDMTs** Profiles and FMDMTs for the training set are exactly the same as those for test case 4.2.3.

**Training and Testing with the LVQ Neural Network** The training set was kept small in order that the total aspect angle variation be minimal since the effect of aspect angle in recognition was to be eliminated in this examination. Training was carried out with the set of input vectors representing the FMDMTs of each ship's profiles in the aspect angle range of 0 to 30 degrees at 2 degree intervals. Testing was carried out three times with the FMDMTs of all four ships' profiles at aspect angles of

- 0 degrees

| Signal-to-Noise Ratio (dB) | Tanker | Trawler | Patrol Boat | Tug | Average |
|---|---|---|---|---|---|
| $\infty$ | 100 | 100 | 100 | 100 | 100 |
| **20** | 100 | 100 | 100 | 100 | 100 |
| **10** | 100 | 100 | 100 | 100 | 100 |
| **0** | 100 | 100 | 93.75 | 100 | 98.40 |

Table 4.11: Recognition Percentages for Profiles Representing an Aspect Angle of 0 Degrees.

| Signal-to-Noise Ratio (dB) | Tanker | Trawler | Patrol Boat | Tug | Average |
|---|---|---|---|---|---|
| $\infty$ | 100 | 100 | 64 | 100 | 91 |
| **20** | 100 | 100 | 25 | 100 | 81.25 |
| **10** | 100 | 100 | 87.50 | 100 | 96.80 |
| **0** | 97 | 31.25 | 50 | 75 | 63.3 |

Table 4.12: Recognition Percentages for Profiles Representing an Aspect Angle of 16 Degrees.

- 16 degrees
- 30 degrees

for each of the three tests. Signal-to-noise ratios of test sets were set at infinity, $20dB$, $10dB$ and $0dB$. Outputs of the examination can be viewed in Tables 4.11, 4.12 and 4.13.

| Signal-to-Noise Ratio (dB) | Tanker | Trawler | Patrol Boat | Tug | Average |
|---|---|---|---|---|---|
| $\infty$ | 100 | 100 | 100 | 100 | 100 |
| **20** | 100 | 100 | 100 | 100 | 100 |
| **10** | 100 | 100 | 100 | 100 | 100 |
| **0** | 87.50 | 0 | 81.25 | 87.50 | 64.06 |

Table 4.13: Recognition Percentages for Profiles Representing an Aspect Angle of 30 Degrees.

**Analysis of Results for Test Three** The third test examines the effect of noise and clutter only with all effects of aspect angle variation, eliminated.

Due to the fact that the classifier does not have a large data set to analyse, recognition percentages are quite good. It is nevertheless evident that the presence of noise and clutter does adversely affect recognition. The matched filter effect does however minimize this effect, as is obvious by the high recognition percentages for signal-to-noise ratios of $10dB$.

## Test Case Four

Test case four attempts to examine the effects of reduction in dimensions of training sets, as far as recognition is concerned. The angles between profiles of the training set were increased from 2 degrees to 4, 8 and 16 degrees in 3 separate tests. This was only implemented for training sets while clutter, thermal noise and scintillation were excluded. The aspect angle ranges in degrees of the training set were :

- 0 to 30
- 0 to 52
- 0 to 60

while the aspect angle ranges in degrees of the test set were the same.

**Profiles and FMDMTs** Profiles were simulated in steps of 4 degrees for the aspect angle ratio of 0 to 30 degrees and are presented in Figure 4.10. The signal-to-noise ratio was infinite i.e. no noise. Profiles for this aspect angle range can be viewed in Figure 4.11 where each profile is representative of an eight degree interval in aspect angle, and Figure 4.12 where each profile is representative of a sixteen degree interval in aspect angle. FMDMTs of all these profiles are presented in Figures 4.13, 4.14 and 4.15 while profiles of the trawler, patrol boat and tug and the FMDMTs thereof can be referenced in [13].

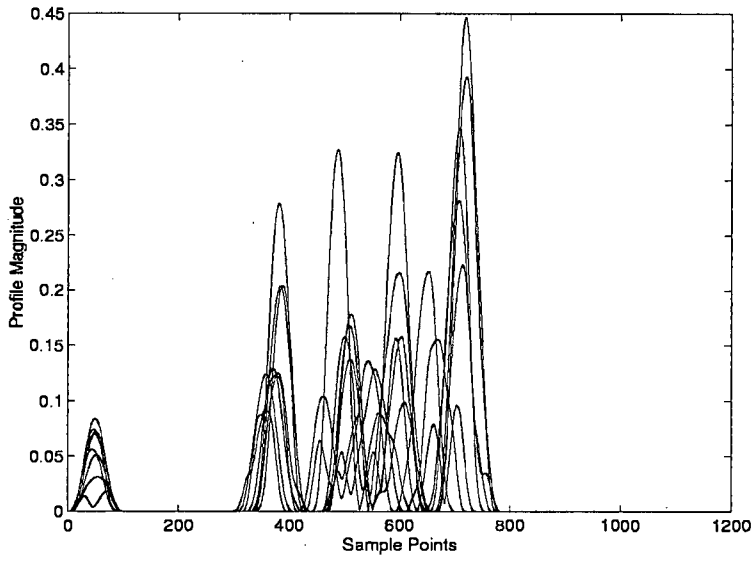


Figure 4.10: Profiles Constituting Tanker Training Set in the Aspect Angle Range of 0 to 30 Degrees. Aspect Angle Interval = 4°.

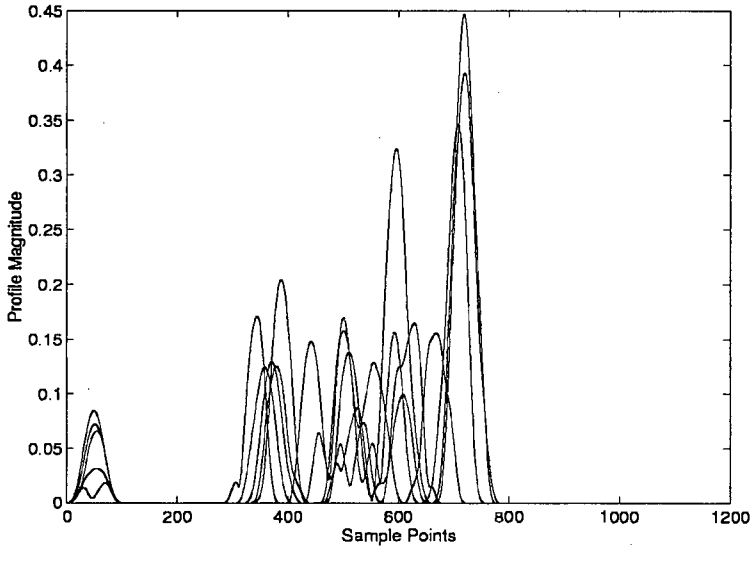


Figure 4.11: Profiles Constituting Tanker Training Set in the Aspect Angle Range of 0 to 30 Degrees. Aspect Angle Interval = 8°.

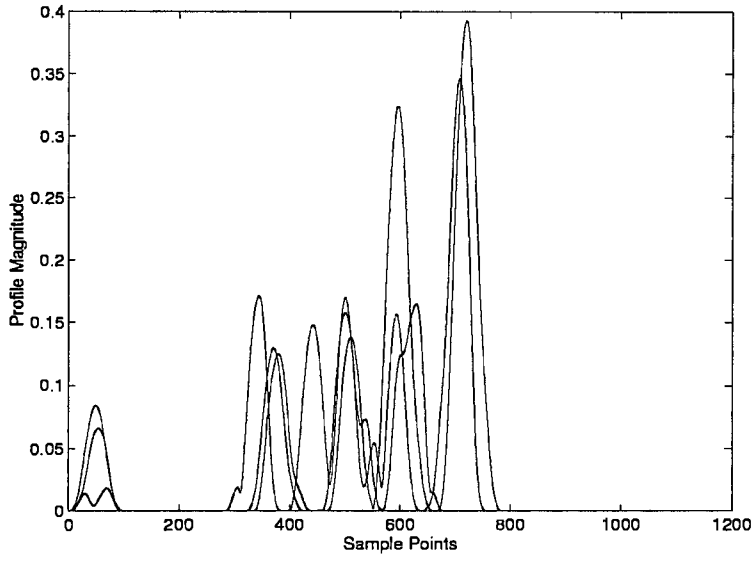


Figure 4.12: Profiles Constituting Tanker Training Set in the Aspect Angle Range of 0 to 30 Degrees. Aspect Angle Interval = 16°.

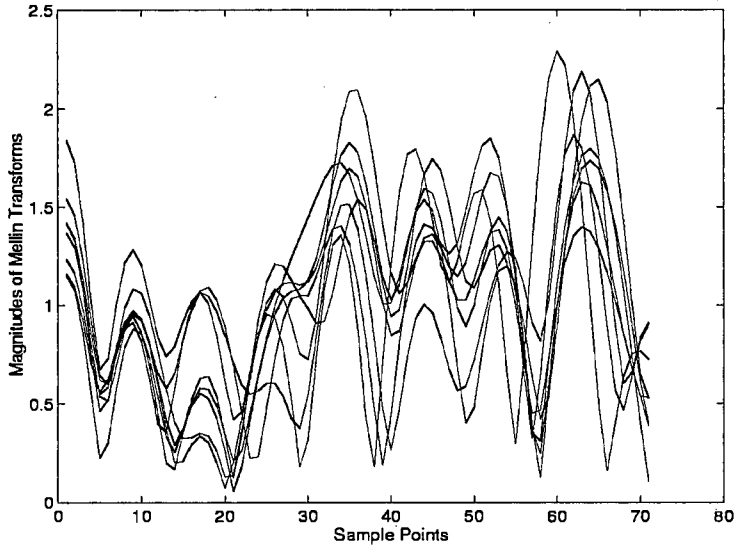


Figure 4.13: FMDMTs Constituting Tanker Training Set in the Aspect Angle Range of 0 to 30 Degrees. Aspect Angle Interval = 4°.

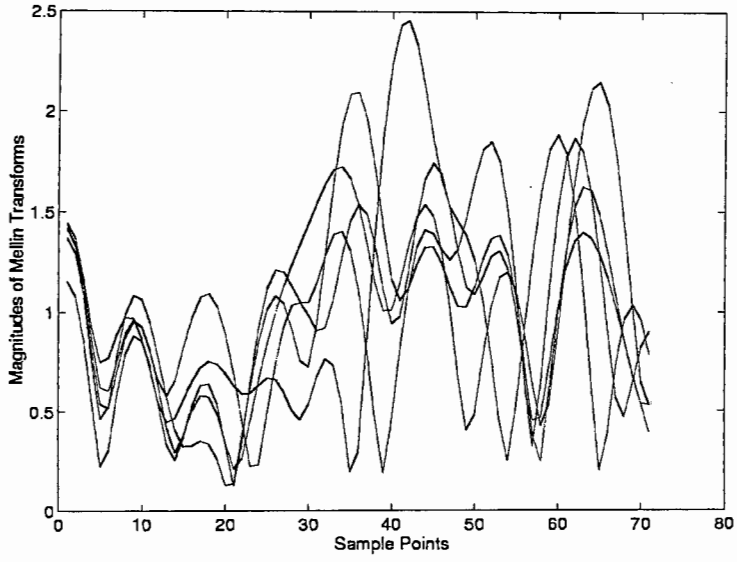


Figure 4.14: FMDMTs Constituting Tanker Training Set in the Aspect Angle Range of 0 to 30 Degrees. Aspect Angle Interval = 8°.

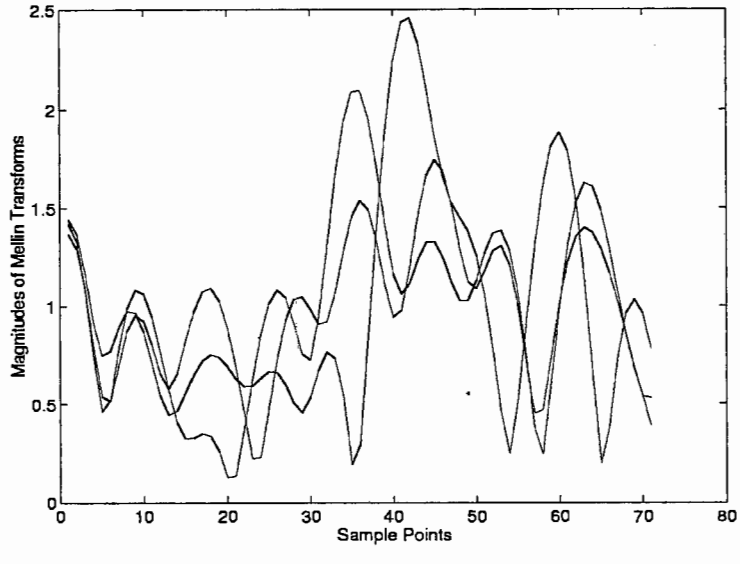


Figure 4.15: FMDMTs Constituting Tanker Training Set in the Aspect Angle Range of 0 to 30 Degrees. Aspect Angle Interval = 16°.

| Groups | Number of Codebook Vectors | Window Value 1 | Window Value 2 | Window Value 3 | Window Value 4 |
|---|---|---|---|---|---|
| **Group 1** | 9 | 0.3 | 0.2 | 0.1 | 0.05 |
| **Group 2** | 5 | 0.3 | 0.2 | 0.1 | 0.05 |
| **Group 3** | 2 | 0.3 | 0.2 | 0.1 | 0.05 |

Table 4.14: Statistics for the Three Groups of Tests

**Training and Testing with the LVQ Neural Network** This particular examination is divided into three groups. It was deemed necessary for the first group of tests that the training sets include input vectors incorporating the FMDMTs of profiles of the four ships at aspect angles of 0 to 30 degrees at 4 degree intervals. The test sets covered aspect angle ranges of :

1. 1 to 31 degrees at 2 degree intervals
2. 1 to 53 degrees at 2 degree intervals
3. 1 to 61 degrees at 2 degree intervals

Similar tests were performed for training sets in the range of 0 to 52 degrees at 2 degree intervals and 0 to 60 degrees at 2 degree intervals. Signal-to-noise ratios for all test and training sets were kept at infinity. Group two sanctioned precisely the same tests with the exception that training sets incorporated input vectors representing the positions of the ships at aspect angles of 0 to 30 degrees at 8 degree intervals, 0 to 52 degrees at 8 degree intervals and 0 to 60 degrees at 8 degree intervals. Test sets were identical to those of the first group. Training sets for the third group were identical to those of the second group with the exception that profiles were now at 16 degree intervals instead, with the consequence that the training set covering 0 to 30 degrees comprised two profiles at 0 degrees and at 16 degrees. The training set covering 0 to 52 degrees comprised three profiles while that of the third , covering 0 to 60 degrees comprised four profiles. Values for the number of codebook vectors and the *window* were as in Table 4.14:

| Aspect ∠ Range of Training Set | Aspect ∠ Range of Test Set | SNR (dB) | Tanker | Trawler | Patrol Boat | Tug | Avr. |
|---|---|---|---|---|---|---|---|
| 0-30° | 1-31° | ∞ | 93.75 | 75 | 62.5 | 100 | 82.8 |
| 0-30° | 1-53° | ∞ | 81.48 | 70.37 | 59.26 | 70.7 | 70.4 |
| 0-30° | 1-61° | ∞ | 70.97 | 74.19 | 64.52 | 58 | 66.9 |
| 0-52° | 1-53° | ∞ | 88.89 | 81.48 | 62.96 | 74 | 76.9 |
| 0-52° | 1-61° | ∞ | 70.97 | 83.87 | 61.29 | 87.1 | 75.8 |
| 0-60° | 1-61° | ∞ | 70.97 | 80.65 | 61.29 | 93.6 | 76.6 |

Table 4.15: Recognition Percentages for Aspect Angle Interval = 4 deg. for Training Set.

The number of codebook vectors obviously decreases as the dimensions of the input vectors decrease. Results of the investigation are depicted in the Tables 4.15 to 4.17.

**Analysis of Results for Test Four** The purpose of the fourth test is to examine the results attained when the training data sets for the neural network are drastically reduced in dimension. Profiles are selected at aspect angles greater than 2 degrees apart.

Recognition percentages in Tables 4.15 to 4.17 indicate that recognition success does indeed decrease as the dimension of the training data sets decrease. The decrease depicted in Tables 4.15, 4.16 and 4.17 is however not substantial, thus showing recognition is still feasible. This is the case for all results depicted in this section. Based on the results, the neural network attains good recognition success even when the training sets are such that profiles 16 degrees apart in aspect angle are selected to train the neural network.

| Aspect ∠ Range of Training Set | Aspect ∠ Range of Test Set | SNR (dB) | Tanker | Trawler | Patrol Boat | Tug | Avr. |
|---|---|---|---|---|---|---|---|
| 0-30° | 1-31° | ∞ | 93.75 | 81.25 | 56.3 | 93.8 | 81.2 |
| 0-30° | 1-53° | ∞ | 81.48 | 66.67 | 29.63 | 81.5 | 64.8 |
| 0-30° | 1-61° | ∞ | 70.97 | 70.97 | 32.26 | 74.2 | 62.1 |
| 0-52° | 1-53° | ∞ | 81.48 | 70.37 | 55.56 | 85.2 | 73.1 |
| 0-52° | 1-61° | ∞ | 77.42 | 80.65 | 45.16 | 74.2 | 69.4 |
| 0-60° | 1-61° | ∞ | 83.87 | 93.55 | 22.58 | 96.8 | 74.2 |

Table 4.16: Recognition Percentages for Aspect Angle Interval = 8 deg. for Training Set.

| Aspect ∠ Range of Training Set | Aspect ∠ Range of Test Set | SNR (dB) | Tanker | Trawler | Patrol Boat | Tug | Avr. |
|---|---|---|---|---|---|---|---|
| 0-30° | 1-31° | ∞ | 81.25 | 93.75 | 31.3 | 87.5 | 73.4 |
| 0-30° | 1-53° | ∞ | 74.07 | 81.48 | 29.63 | 62.7 | 62 |
| 0-30° | 1-61° | ∞ | 70.97 | 80.65 | 32.26 | 64.5 | 62.1 |
| 0-52° | 1-53° | ∞ | 81.48 | 85.19 | 40.74 | 51.9 | 64.8 |
| 0-52° | 1-61° | ∞ | 77.42 | 80.65 | 32.26 | 74.2 | 66.1 |
| 0-60° | 1-61° | ∞ | 77.42 | 80.65 | 32.26 | 67.7 | 64.5 |

Table 4.17: Recognition Percentages for Aspect Angle Interval = 16 deg. for Training Set.

Test Case Five

Test case five attempted to investigate the different categories of a single vessel by extracting different classes pertaining to a single ship. All aspect angles in the range of 0 to 360 degrees were considered. The input information of a vessel would be divided into different classes, the number of which, would have to be determined by the test results. Thermal noise, clutter and scintillation were excluded. The aspect angle ranges in degrees of the training sets for the neural network, were

- 0 to 72
- 0 to 80
- 0 to 90
- 180 to 210

The last aspect angle range is the same as 0 to 30 degrees, with the exception that the ship faces the radar in the opposite direction. Aspect angle ranges of the test sets were the same as those for the training sets.

The expected outcome of testing is that recognition would be feasible in the 180 to 240 degree zone and the 180 to 120 degree zone and that recognition would be equal to that of the 0 to 60 and 0 to 300 degree zones due to :

The magnitude of the time-domain representation of the range profile of a ship is :

$$f(t)$$

while that of the ship facing the opposite direction is :

$$f(-t-T)$$

i.e. the profile reversed with time shift $T$. Provided the profile magnitudes are real, which they are, the Fourier Transform thereof is always even i.e. :

$$F(\omega) = F(-\omega)$$

The Fourier Analysis rule of *Reciprocal Scaling* is [8]:

$$f(\alpha t) \longleftrightarrow \frac{1}{|\alpha|} F(\frac{\omega}{\alpha})$$

According to this rule, the following can be stated :

$$\begin{aligned} f(-t) &\longleftrightarrow \frac{1}{|-1|} F(-\omega) \\ f(-t) &\longleftrightarrow F(-\omega) \end{aligned}$$

but :

$$f(t) \longleftrightarrow F(\omega)$$

The magnitudes of profiles of ship targets are real and therefore the magnitude of the Fourier Transforms of $f(t)$ and $f(-t)$ are equal. The profile of a ship facing in the opposite direction is also characterized by a time shift which relates to a phase shift in the Fourier domain but is eradicated when the magnitude of the Fourier Transform is taken i.e. :

$$f(-t-T) \longleftrightarrow F(-\omega)e^{-j\omega T}$$

$e^{-j\omega T}$ is a phase term which drops away when the magnitude of the Fourier Transform is taken. The magnitude of the Fourier Transform of the ship facing the radar head-on is therefore equal to the magnitude of the Fourier Transform of the same ship facing the radar in the opposite direction. The FMDMT of these Fourier Transforms are thus identical.

**Profiles and FMDMTs** Profiles of the simulated tanker are presented in Figures 4.16 and 4.17 for the aspect angle ranges of 0 to 90 degrees and negative 0 to 30 degrees (180 to 210 degrees). FMDMTs of these profiles are displayed in Figures 4.18 and 4.19 for the tanker. Corresponding figures for the trawler, patrol boat and tug can be viewed in [13].

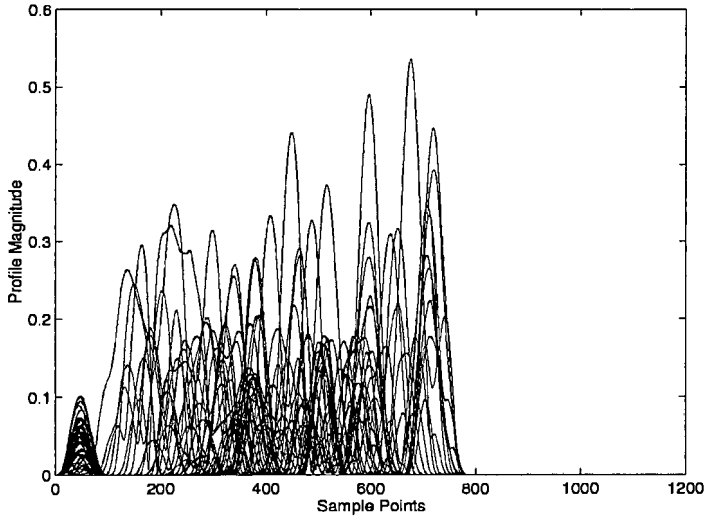


Figure 4.16: Profiles Constituting Tanker Training Set in the Aspect Angle Range of 0 to 90 Degrees.

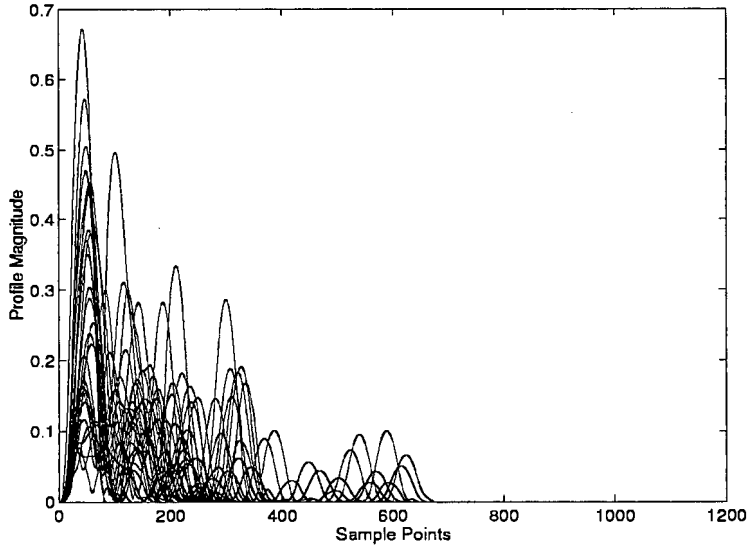


Figure 4.17: Profiles Constituting Tanker Training Set in the Aspect Angle Range of 180 to 210 Degrees.

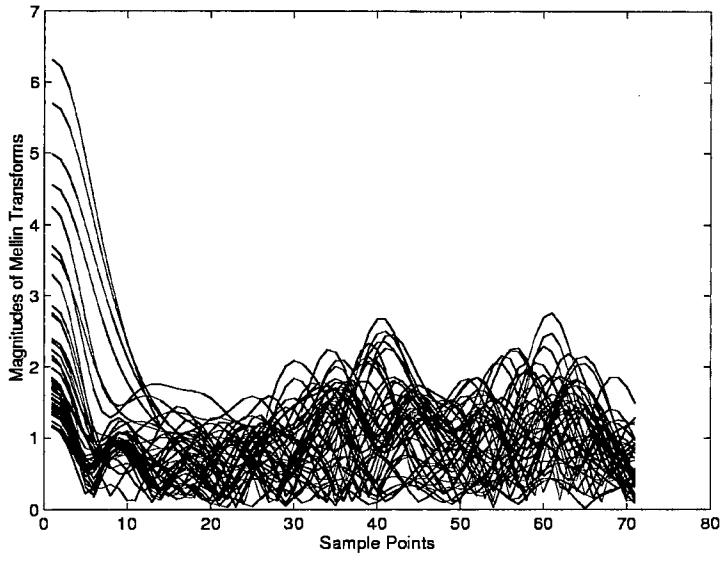


Figure 4.18: FMDMTs Constituting Tanker Training Set in the Aspect Angle Range of 0 to 90 Degrees.

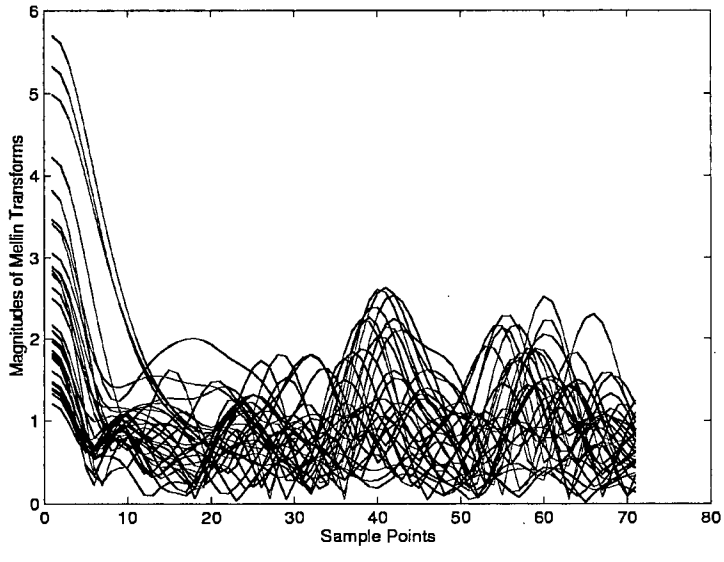


Figure 4.19: FMDMTs Constituting Tanker Training Set in the Aspect Angle Range of 180 to 210 Degrees.

| Aspect ∠ Range of Training Set | Aspect ∠ Range of Test Set | SNR (dB) | Tanker | Trawler | Patrol Boat | Tug | Average |
|---|---|---|---|---|---|---|---|
| 0-90° | 1-71° | ∞ | 63.89 | 75 | 58.33 | 91.67 | 72.22 |
| 0-90° | 1-81° | ∞ | 56.1 | 65.85 | 46.34 | 95.12 | 66.46 |
| 0-90° | 1-91° | ∞ | 63.04 | 65.22 | 36.96 | 97.83 | 65.7 |
| 0-30° | 1-71° | ∞ | 66.67 | 66.67 | 58.33 | 50 | 60.42 |
| 0-30° | 1-81° | ∞ | 48.78 | 51.22 | 73.17 | 46.34 | 54.88 |
| 0-30° | 1-91° | ∞ | 52.17 | 56.52 | 73.91 | 36.96 | 54.89 |
| 0-30° | 91-121° | ∞ | 93.75 | 93.75 | 56.25 | 100 | 85.94 |

Table 4.18: Recognition Percentages.

**Training and Testing with the LVQ Neural Network** Tests were carried out for aspect angle ranges of 0 to 72 degrees, 0 to 80 degrees and 0 to 90 degrees. Finally, a test set was included, covering the aspect angle range of 181 degrees to 211 degrees with profiles at 2 degree intervals. This means that the ships were positioned at aspect angles of 1 to 31 degrees except that they were reversed in direction of motion with the stern facing the radar while in all other examinations, the bow faced the radar. The training set for this particular test covered the aspect angle range of 0 to 30 degrees at 2 degree intervals. Primarily, the objective of the examination was to determine if recognition for a ship would differ radically if orientation of the vessel varied by 180 degrees in the test sets while utilizing precisely the same input vectors for training the neural network. Out puts of the test are displayed in Table 4.18 where training sets included the profiles of vessels from the aspect angle range of 0 to 30 degrees and 0 to 90 degrees.

**Analysis of Results for Test Five** Test five considers recognition of ship targets in the large aspect angle ranges and recognition when ships are faced in the opposite direction to the radar than for previous tests.

Table 4.18, rows one to three, present results that substantiate the feasibility of recognition, even when the ship's aspect angle is as large as 80 or even 90 degrees. Rows four to six once again possess results to suggest and corroborate that recognition success does abate as the dimensions of the training set for the neural network decreases. The number of profiles are less than those in the 0 to 90 degree aspect angle range.

Finally, the success attained in recognition as depicted by row 8, shows the feasibility of ship target recognition at an aspect angle of 180 to 210 degrees. The ship's orientation in this range is such that the opposite end of the ship faces the radar as opposed to the 0 to 30 degree aspect angle range where the ship faced the radar head-on.

Test Case Six Test case six examines the effects of scintillation on the performance of the Mellin Transform for ship target recognition. Scintillation was included in the simulations while thermal noise and clutter were excluded. The aspect angle ranges of the training sets in degrees were:

- 0 to 30
- 0 to 52
- 0 to 60

The aspect angle ranges of the test sets were exactly the same with the exception that specific aspect angles were also tested. These were angles of 0 degrees, 16 degrees and 30 degrees.

**Profiles and FMDMTs** Implementation of scintillation in the simulated radar range profiles of the tanker is displayed in Figures 4.20 and 4.21 for the 0 to 30 degree aspect angle range.

FMDMTs of these profiles constituting the test input signals to the neural network, are presented in the Figures 4.22 and 4.23.

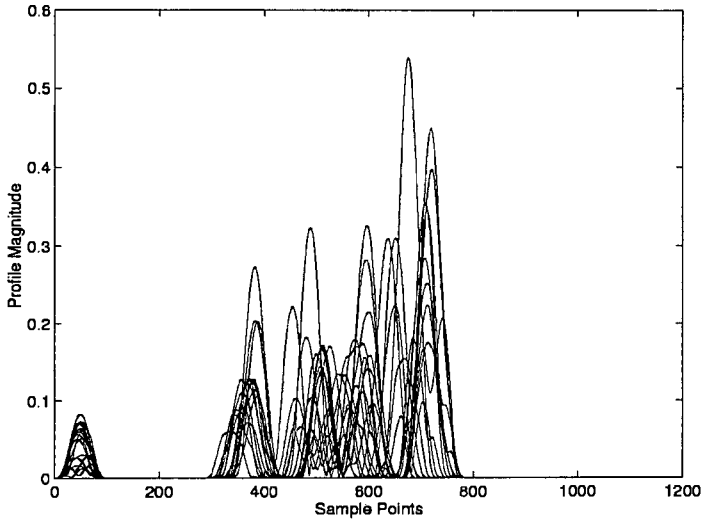


Figure 4.20: Profiles Constituting Tanker Training Set in the Aspect Angle Range of 0 to 30 Degrees. Scintillation = 10%.

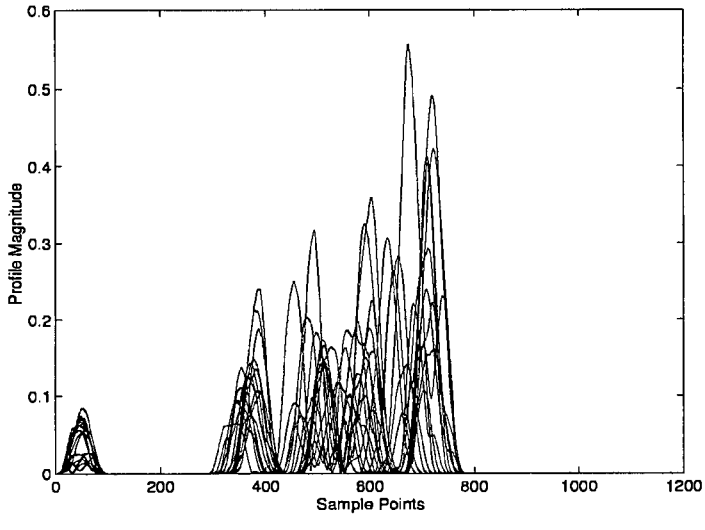


Figure 4.21: Profiles Constituting Tanker Training Set in the Aspect Angle Range of 0 to 30 Degrees. Scintillation = 100%.

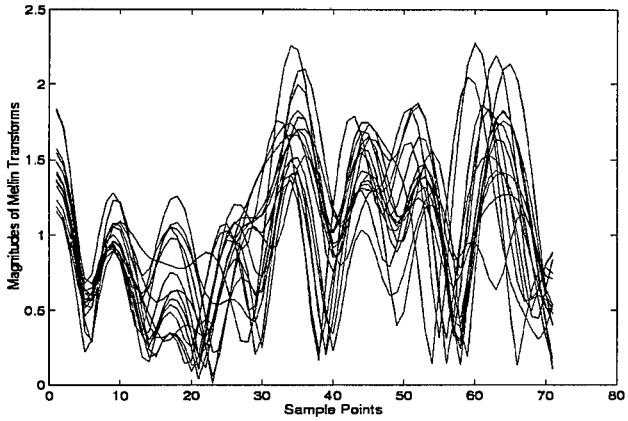


Figure 4.22: FMDMTs Constituting Tanker Training Set in the Aspect Angle Range of 0 to 30 Degrees. Scintillation = 10%.

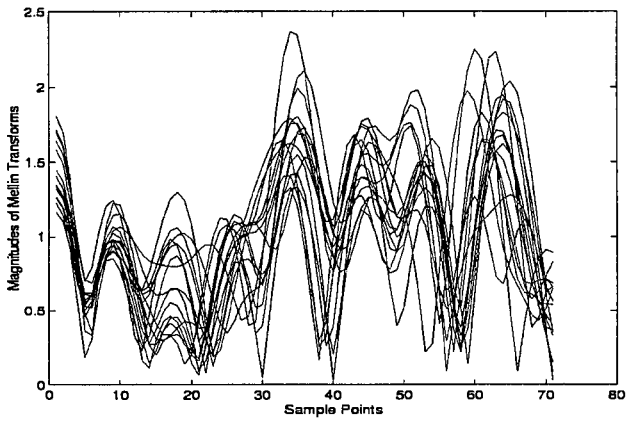


Figure 4.23: FMDMTs Constituting Tanker Training Set in the Aspect Angle Range of 0 to 30 Degrees. Scintillation = 100%.

| Scintillation Percentage | Tanker | Trawler | Patrol Boat | Tug | Total Average |
|---|---|---|---|---|---|
| 10 | 93.75 | 93.75 | 81.25 | 93.25 | 92.19 |
| 40 | 93.75 | 93.75 | 68.75 | 93.75 | 87.50 |
| 80 | 100 | 100 | 61.50 | 93.75 | 89.06 |
| 100 | 93.75 | 93.75 | 68.75 | 78.50 | 85.94 |

Table 4.19: Recognition Percentages for a Test Set of 1 to 31 degrees and a Training Set of 0 to 30 degrees

| Scintillation Percentage | Tanker | Trawler | Patrol Boat | Tug | Total Average |
|---|---|---|---|---|---|
| 10 | 62.96 | 77.78 | 51.85 | 85.19 | 69.44 |
| 40 | 66.67 | 77.78 | 55.56 | 88.89 | 72.22 |
| 80 | 62.96 | 74.07 | 55.56 | 92.59 | 71.30 |
| 100 | 70.37 | 74.07 | 55 | 92.59 | 73.15 |

Table 4.20: Recognition Percentages for a Test Set of 1 to 53 degrees and a Training Set of 0 to 30 degrees

**Training and Testing with the LVQ Neural Network** The outcome of the two tests carried out in examination scenario six is displayed in Tables 4.19, 4.20, 4.21, 4.22, 4.23, 4.24, 4.25, 4.26 and 4.27.

**Analysis of Results for Test Six** Tables 4.19 to 4.24 indicate that the effects of scintillation on recognition are insignificant and are adequately handled by the neural network. The recognition percentages of Tables 4.25 to 4.27 reveal a very minimal effect, if any, on recognition of ship targets by the neural network in

| Scintillation Percentage | Tanker | Trawler | Patrol Boat | Tug | Total Average |
|---|---|---|---|---|---|
| 10 | 58.06 | 77.42 | 51.61 | 83.87 | 67.74 |
| 40 | 61.29 | 67.74 | 61.29 | 90.32 | 70.16 |
| 80 | 51.61 | 70.97 | 61.29 | 83.87 | 66.94 |
| 100 | 61.29 | 70.97 | 54.84 | 87.10 | 68.55 |

Table 4.21: Recognition Percentages for a Test Set of 1 to 61 degrees and a Training Set of 0 to 30 degrees

| Scintillation Percentage | Tanker | Trawler | Patrol Boat | Tug | Total Average |
|---|---|---|---|---|---|
| 10 | 85.19 | 81.48 | 51.85 | 92.59 | 77.26 |
| 40 | 81.48 | 81.48 | 55.56 | 96.30 | 78.70 |
| 80 | 85.19 | 85.19 | 51.85 | 96.30 | 79.63 |
| 100 | 88.89 | 81.48 | 55.56 | 92.59 | 79.63 |

Table 4.22: Recognition Percentages for a Test Set of 1 to 53 degrees and a Training Set of 0 to 52 degrees

| Scintillation Percentage | Tanker | Trawler | Patrol Boat | Tug | Total Average |
|---|---|---|---|---|---|
| 10 | 74.19 | 77.42 | 45.16 | 90.32 | 71.77 |
| 40 | 77.42 | 77.42 | 45.16 | 90.32 | 72.58 |
| 80 | 64.52 | 77.42 | 48.39 | 90.32 | 70.16 |
| 100 | 70.97 | 83.87 | 48.39 | 90.32 | 73.39 |

Table 4.23: Recognition Percentages for a Test Set of 1 to 61 degrees and a Training Set of 0 to 52 degrees

| Scintillation Percentage | Tanker | Trawler | Patrol Boat | Tug | Total Average |
|---|---|---|---|---|---|
| 10 | 80.65 | 77.42 | 41.94 | 90.32 | 72.58 |
| 40 | 70.97 | 87.10 | 48.39 | 93.55 | 75 |
| 80 | 70.97 | 80.65 | 45.16 | 83.87 | 70.16 |
| 100 | 74.19 | 83.87 | 45.16 | 83.87 | 71.77 |

Table 4.24: Recognition Percentages for a Test Set of 1 to 61 degrees and a Training Set of 0 to 60 degrees

| Scintillation Percentage | Tanker | Trawler | Patrol Boat | Tug | Total Average |
|---|---|---|---|---|---|
| 10 | 100 | 100 | 100 | 100 | 100 |
| 40 | 100 | 100 | 100 | 100 | 100 |
| 80 | 100 | 100 | 100 | 100 | 100 |
| 100 | 100 | 100 | 100 | 100 | 100 |

Table 4.25: Recognition Percentages for a Test Profile at 0 degrees and a Training Set of 0 to 30 degrees

| Scintillation Percentage | Tanker | Trawler | Patrol Boat | Tug | Total Average |
|---|---|---|---|---|---|
| 10 | 100 | 100 | 100 | 100 | 100 |
| 40 | 100 | 100 | 100 | 100 | 100 |
| 80 | 100 | 100 | 100 | 100 | 100 |
| 100 | 100 | 100 | 43.75 | 100 | 85.93 |

Table 4.26: Recognition Percentages for a Test Profile at 16 degrees and a Training Set of 0 to 30 degrees

| Scintillation Percentage | Tanker | Trawler | Patrol Boat | Tug | Total Average |
|---|---|---|---|---|---|
| 10 | 100 | 100 | 100 | 100 | 100 |
| 40 | 100 | 100 | 100 | 100 | 100 |
| 80 | 100 | 100 | 100 | 100 | 100 |
| 100 | 100 | 100 | 100 | 100 | 100 |

Table 4.27: Recognition Percentages for a Test Profile at 30 degrees and a Training Set of 0 to 30 degrees

conjunction with the Mellin Transform.

# Chapter 5

# Recognition Results of Tests on Real Data

The goal of the following sections includes the corroboration of test results of the preceding chapter which focussed all attention on the simulations in the dissertation. Emphasis is placed on the acquisition of radar range profiles of the Outeniqua and the SAS Protea, while the aspects of signal processing and data processing of this data in the form of the Modified Direct Mellin Transform for recognition, are explained.

Recognition results of the Learning Vector Quantization neural network for the real data acquired, is presented in this chapter, as are the steps carried out to perform recognition by means of the MDMT.

## 5.1 The Acquisition of Radar Range Profiles

Scans of the SAS Protea and the Outeniqua were acquired by means of the search radar at the Institute for Maritime Technology (IMT) in Simon's Town. Each vessel was steered through a 360 degree full circle in the line of sight of the Raytheon search radar at IMT, while scans were recorded. Data for the

| File Header |
|---|
| Scan1 Header |
| Scan1 Index |
| Scan1 Data |
| More Scans |
| Scan N Header |
| Scan N Index |
| Scan N Data |

Table 5.1: Format of Captured Radar Data of Ship Profiles

downrange profiles of the vessels were stored for each scan in the format in Table 5.1.

Code presented in [13] was written in the C language for extraction of the radar data in such a form that permitted the required data processing for the dissertation to be implemented. The data processing referred to in this instance, includes the extraction of the cleanest profile in a single scan. and the implementation of the Fourier transform and the MDMT. The vessels lay at different aspect angles between 0 and 360 degrees for each scan.

## 5.2 Extraction of Clean Profiles

Extraction of clean profiles for each scan representing the position of the ship at a specific aspect angle, is the subject of this section. Only one profile is required since the individual pulses are well-correlated. Many profiles in a single scan are corrupted or spoilt due to clutter, thermal noise and interference from other search radars in the vicinity of the ships. A profile occurs in each azimuth bin of a sinogragh, corresponding to a single echo. Two methods were proposed and will be explained in detail, although implementation of the first method to be discussed, was omitted in the dissertation. Code for the discussed extraction methods, is presented in [13].

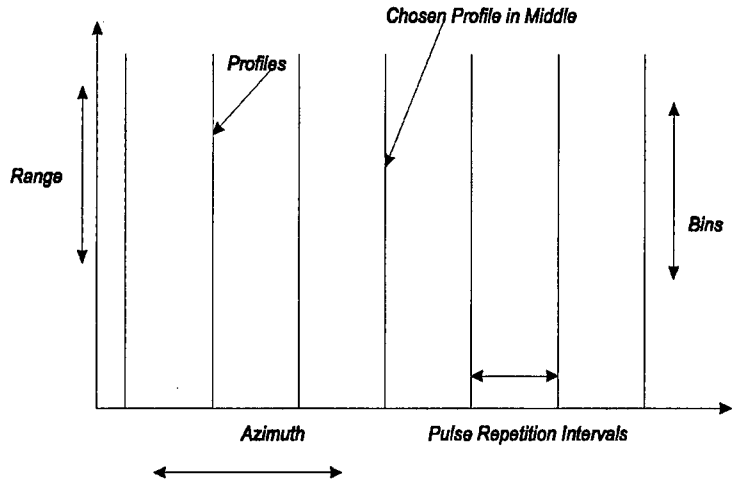


Figure 5.1: Illustration of Method of Compound Identification.

### 5.2.1 Method 1 : Compound Identification

This particular method was proposed in [12] and is explained in this section. It is referred to as *Compound Identification.*

Several profiles of a particular scan are fed into the classifier which reaches an identification on the basis of averaging the single identification for the selected profiles. A number of bins on each side of that particular profile, two in this case, are selected on each side of that profile. The profile referred to, is the one situated in the approximate centre of echoes from the ship. This means that the profile is in the centremost azimuth bin of all the azimuth bins containing the echo of the target. The transmitted pulse in this instance, should be directly in line with the ship. Should this profile possess the greatest average energy due to the presence of clutter, averaging of the other profiles will eliminate the effects of this on classification. This method is illustrated by Figure 5.1.

### 5.2.2 Method 2 : Successive Elimination

*Successive Elimination* was proposed and implemented by the author of this dissertation and is explained below.

The profile with the highest mean value is located in its azimuth bin in a single scan. Values for the mean energy value are then calculated for a profile on each side of the selected profile and the difference calculated between these and that of the chosen profile. If the difference is large, it is very probable that the chosen profile possesses a great deal of noise energy due to clutter or direct interference of other radars. The difference values are thus subject to a variable threshold. Threshold values are chosen after close scrutinization of the scans and the profiles in all the range bins. It becomes evident that the energy difference is not great for echoes of the target in neighbouring range bins. Huge differences are usually present when one of the profiles is characterised by a significant degree of noise power. The threshold value can thus be kept relatively low. If a noisy profile is encountered, the mean energy level of the azimuth bin is set to zero and a new profile with the highest mean energy is searched for.

## 5.3 Preparation of Acquired Data

In order to present a comparison of the recognition results for the SAS Protea and the Outeniqua, certain differences concerning the data for the two ships, had to be tended to. These differences will be indicated and solutions to eliminating them, provided.

During acquisition of the radar data for the two vessels at IMT, the search radar recorded scans of the SAS Protea at aspect angles 2.4 degrees apart while scans for the Outeniqua were recorded at about 1.58 degree intervals in aspect angle. The classifier was trained with every second profile for the SAS Protea while every third profile was used for the Outeniqua in order to establish similarity as far as aspect angle variations are concerned.

Echoes for the downrange profiles of the SAS Protea were sampled at a frequency of 50 MHz while data for the Outeniqua was sampled at 25 MHz. It is imperative that the sets of data for the two vessels possess the same frequency content in order for any comparison of results to be made. The subject of discussion in this instance, relates to the number of points selected for the Fast Fourier Transform (FFT) of data. In order to ensure equality of frequency content for the data of the two vessels, the following should be true for the SAS Protea as regards frequency content of the Fourier Transform of a range profile :

- Sample frequency of 50 MHz.
- Centre frequency of DFT of range profile of 25 MHz.
- 512 Sample points for the FFT.
- The frequency interval between all samples of the DFT of a range profile, $\Delta_f$ is thus 97 kHz.

The following must be ensured for the Outeniqua :

- Sample frequency of 25 MHz.
- Centre frequency of DFT of range profile of 12.5 MHz.
- 256 Sample points for the FFT.
- The frequency interval between all samples of the DFT of a range profile, $\Delta_f$ is thus 97 kHz.

In the event that data processing does not take these points into consideration, one is interpolating the data for the Outeniqua, thus introducing frequency components that are not even present in the signal. This would certainly occur if the number of sample points for the DFTs of the vessels were equal.

## 5.4 Data Processing of Acquired Data

The code for implementation of the Fast Fourier transform and the MDMT are presented in [13]. The code was written in Matlab.

## 5.5 Training and Testing with the LVQ Neural Network

The standards, objectives and test scenarios adopted in these tests were already determined in the preceding chapter. In order to compare the results of recognition for real and simulated data, similar tests were performed on the real data as was performed on the simulated data in Chapter 4.

The test scenarios and procedures thereof are similar and only vary where real data was different to the simulated data. The tests will be followed through in the following examination of test results for the data pertaining to the SAS Protea and the Outeniqua. The test scenarios adopted are similar to those used for the simulated data and can be referenced in section 4.2.3 of Chapter 4. Specific tests for the real data are outlined in the ensuing sections. As far as the simulations were concerned, the Mellin Transform range selected, ensured that 70 samples were produced for the Mellin Transforms of all profiles. Experimentation revealed that a Mellin Transform range of $100\pi$ for the real data, resulted in the greatest recognition success. Variation of the Mellin Transform range to $200\pi$ in order to produce a greater number of Mellin Transform samples, did not improve recognition by a significant margin. Ninety Mellin Transform samples were produced for the range of $200\pi$. The objective of doing so, was to increase the Hamming distance between training data sets for the neural network.

Analysis for the results of these tests will be presented in this section.

### 5.5.1 Test Case One

Since thermal noise, clutter and scintillation cannot be removed when capturing real data, the following test case will encompass the objectives and procedures adopted in Chapter 4 for the first two test scenarios. In this particular instance, the aspect angle ranges chosen for training the neural network, were 0 to 30 degrees, 0 to 60 degrees, 0 to 80 and 0 to 90 degrees instead of those chosen for simulated data in these test scenarios of Chapter 4.

#### Profiles and FMDMTs

All radar range profiles of the SAS Protea and Outeniqua are accompanied by appropriate explanations in [13] while several important examples are provided in this particular chapter.

Downrange radar profiles of the Outeniqua and SAS Protea are presented in Figures 5.2 and 5.3. These figures were attained after signal and data processing were performed in order to minimize the presence of thermal noise, clutter and scintillation. Interference was very dominant in most scans of the two vessels due to other radars in the vicinity of the search radar used to capture the data. The profiles feature scans of both ships at aspect angles in the range of 0 to 30 degrees. All profiles for a single vessel in a particular aspect angle range are superimposed in the presented figures below. One must bear in mind that the sampling frequency for the Protea is double that of the Outeniqua. Figures 5.4 and 5.5 incorporate the FMDMTs of these profiles for the SAS Protea and Outeniqua for the mentioned aspect angle range. Each FMDMT for each profile was then normalized by the mean for each specific aspect angle range for both vessels. Normalized FMDMTs of the vessels are displayed in Figures 5.6 and 5.7.

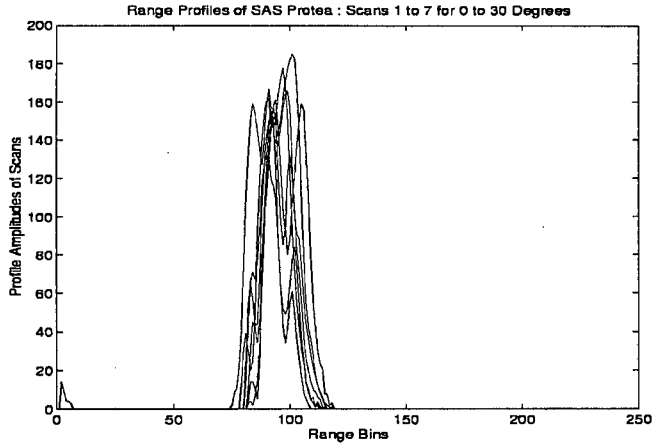


Figure 5.2: Radar Range Profiles for SAS Protea in Aspect Angle Range 0 to 30 Degrees. Sampling Frequency = 2 x Outeniqua Sampling Frequency.

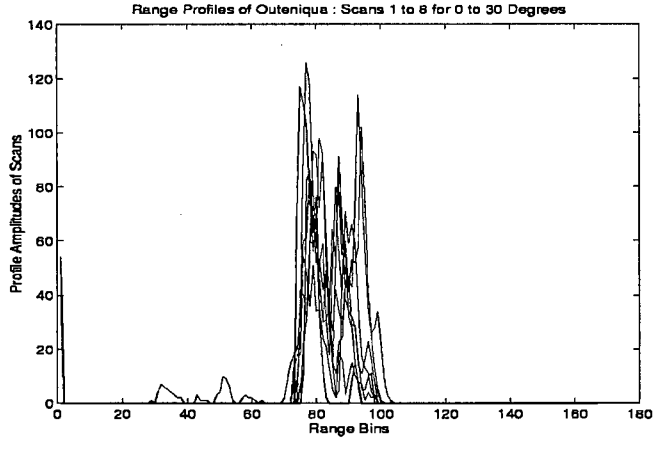


Figure 5.3: Radar Range Profiles for Outeniqua in Aspect Angle Range 0 to 30 Degrees.

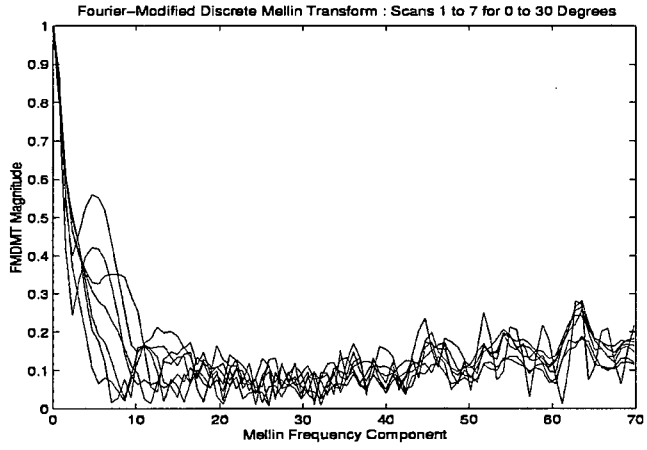


Figure 5.4: FMDMTs for SAS Protea in Aspect Angle Range 0 to 30 Degrees.

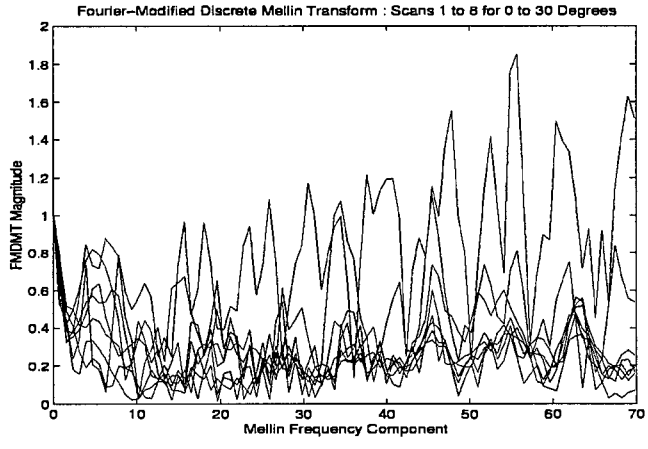


Figure 5.5: FMDMTs for Outeniqua in Aspect Angle Range 0 to 30 Degrees.

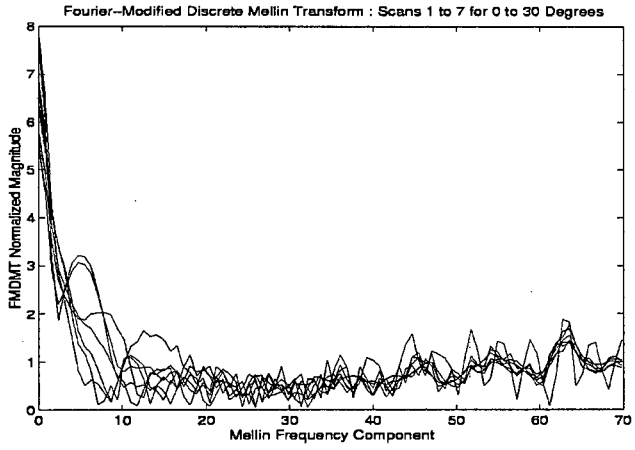


Figure 5.6: Normalized FMDMTs for SAS Protea in Aspect Angle Range 0 to 30 Degrees.

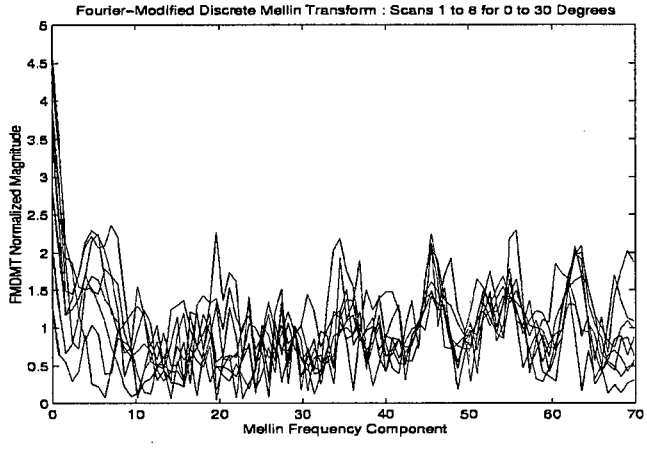


Figure 5.7: Normalized FMDMTs for Outeniqua in Aspect Angle Range 0 to 30 Degrees.

| Aspect Angle Range of Test Set | Protea | Outeniqua | Average |
|---|---|---|---|
| **1 to 31 Degrees** | 100 | 71.43 | 85.71 |
| **1 to 61 Degrees** | 92.31 | 64.29 | 77.78 |
| **1 to 81 Degrees** | 93.75 | 52.94 | 72.73 |
| **1 to 91 Degrees** | 94.12 | 52.63 | 72.22 |

Table 5.2: Recognition Percentages. Aspect Angle Range of Training Set is 0 to 30 Degrees.

| Aspect Angle Range of Test Set | Protea | Outeniqua | Average |
|---|---|---|---|
| **1 to 31 Degrees** | 100 | 100 | 100 |
| **1 to 61 Degrees** | 92.31 | 92.86 | 92.59 |
| **1 to 81 Degrees** | 100 | 76.47 | 87.88 |
| **1 to 91 Degrees** | 100 | 68.42 | 83.33 |

Table 5.3: Recognition Percentages. Aspect Angle Range of Training Set is 0 to 60 Degrees.

### Classification Results

The LVQ neural network was trained with seven codebook vectors, 675 training iterations for LVQ1 and 1000 training iterations for LVQ3. Three cycles of LVQ3 were implemented. Epsilon was 0.1. Classification results are presented in Tables 5.2, 5.3 and 5.4 :

| Aspect Angle Range of Test Set | Protea | Outeniqua | Average |
|---|---|---|---|
| **1 to 31 Degrees** | 100 | 100 | 100 |
| **1 to 61 Degrees** | 100 | 85.71 | 92.59 |
| **1 to 81 Degrees** | 100 | 76.47 | 87.88 |
| **1 to 91 Degrees** | 94.12 | 63.16 | 77.78 |

Table 5.4: Recognition Percentages. Aspect Angle Range of Training Set is 0 to 80 Degrees.

### Analysis of Results for Test One

Test one merely investigates the effect of aspect angle variations on recognition. Tables 5.2 and 5.4 present results that once again illustrate the decrease in recognition success with an increase in aspect angle of the ship target. The decrease however, is not substantial at all and in particular, it is evident that recognition is adequate even in the 0 to 90 degree aspect angle range. Recognition for the SAS Protea is more successful as depicted in Tables 5.2 and 5.4.

Recognition percentages increase as the aspect angle of the training set increases. The improvement in recognition percentages as the aspect angle range of the training sets increases from 0 to 30 degrees to 0 to 60 degrees is substantial. Recognition percentages for aspect angle ranges of 0 to 60 degrees and 0 to 80 degrees are very similar, indicating that the Mellin Transform is not very successful in the 60 to 80 degree range as far as eliminating scaling of the independent variable.

## 5.5.2 Test Case Two

The following test incorporates the objectives and procedures adopted in the fourth and fifth test scenarios of Chapter 4. The fourth scenario emphasizes the minimisation of the dimensions of training sets, on which this particular test also concentrates. The fifth scenario, on the other hand, concentrates on large aspect angle ranges such as 0 to 80 degrees and 0 to 90 degrees which have already been considered in the previous test in this section. This particular test is similar to the fifth scenario in that it examines recognition when the target is facing in the opposite direction to that of all other tests, i.e. orientated at 180 degrees from all other orientations in all other tests. The objective of such an examination serves the purpose of determining if the same recognition is possible if the ship target is orientated in any position as in this particular extreme case where the resulting profile of the ship will essentially be flipped around by 180 with respect to the independent variable. Such a test could establish if recognition is not only possible in the 0 to 90 degree range or the 270 to 360 degree range but that it

is also possible in the 90 to 180 degree range or the 180 to 270 degree range. In doing so, corroboration of the fact that recognition success is equally successful whether the bow or the stern of the ship target is facing the radar, shall be established.

### Profiles and FMDMTs

The profiles and FMDMTs of profiles used for this test, are presented and accompanied by explanations in [13].

The SAS Protea and Outeniqua rotated through 360 degrees in the line of sight of the search radar while data was captured by the author of this dissertation at IMT. Radar profiles of both vessels are displayed in Figures 5.8 and 5.9 for each position occupied by the ships in the aspect angle range of 180 degrees to 240 degrees. Once again the profiles for each ship are superimposed for this aspect angle range. The profiles constitute the images of the vessels as they occupied positions in this aspect angle range at 4.2 degree intervals while they rotated. FMDMTs of these profiles are presented in Figures 5.10 and 5.11 while the normalized FMDMTs of these profiles are displayed in Figures 5.12 and 5.13.

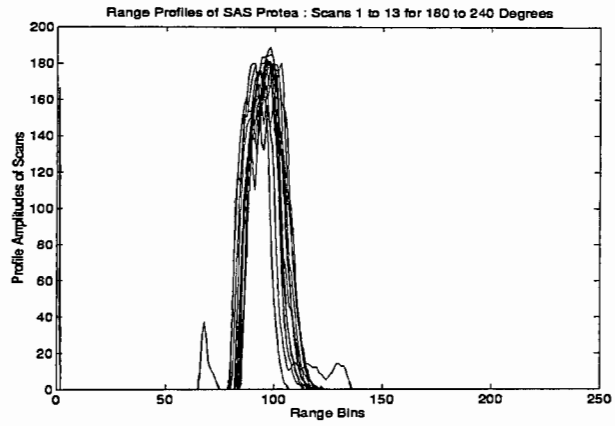


Figure 5.8: Radar Range Profiles for SAS Protea in Aspect Angle Range 180 to 240 Degrees. Sampling Frequency = 2 x Outeniqua Sampling Frequency.

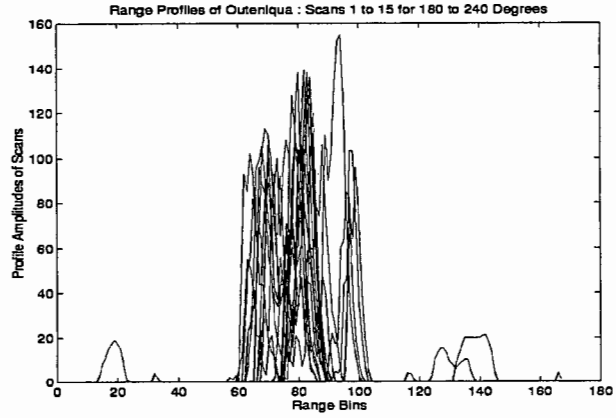


Figure 5.9: Radar Range Profiles for Outeniqua in Aspect Angle Range 180 to 240 Degrees.

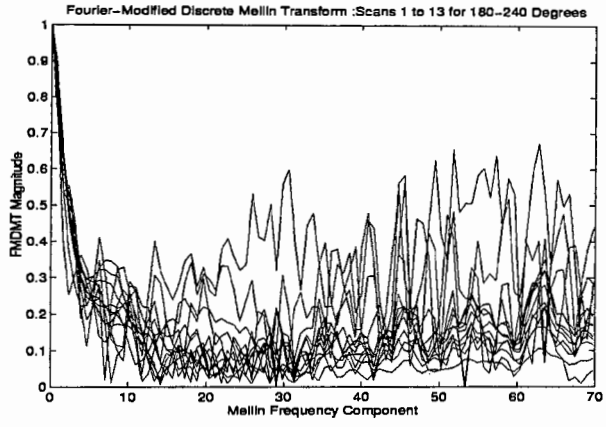


Figure 5.10: FMDMTs for SAS Protea in Aspect Angle Range 180 to 240 Degrees.

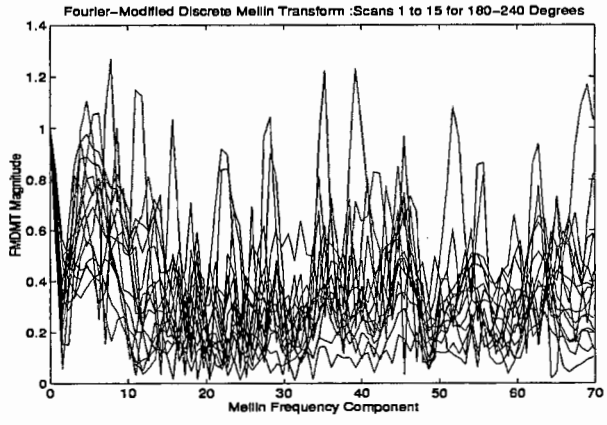


Figure 5.11: FMDMTs for Outeniqua in Aspect Angle Range 180 to 240 Degrees.

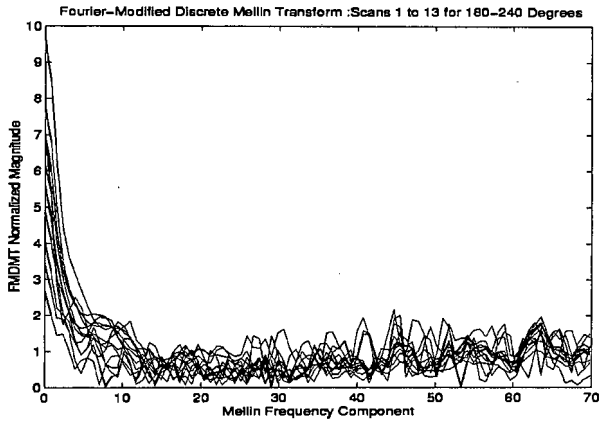


Figure 5.12: Normalized FMDMTs for SAS Protea in Aspect Angle Range 180 to 240 Degrees.

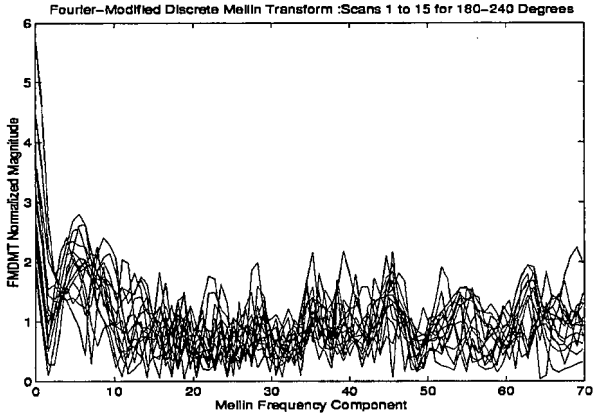


Figure 5.13: Normalized FMDMTs for Outeniqua in Aspect Angle Range 180 to 240 Degrees.

| Aspect Angle Range of Test Set | Protea | Outeniqua | Average |
|---|---|---|---|
| **1 to 61 Degrees** | 100 | 85.71 | 92.59 |
| **1 to 81 Degrees** | 100 | 70.59 | 84.85 |
| **1 to 91 Degrees** | 100 | 63.16 | 80.56 |

Table 5.5: Recognition Percentages. Aspect Angle Range of Training Set is 0 to 60 Degrees. Aspect Angle Interval = 9.6 Degrees.

| Aspect Angle Range of Test Set | Protea | Outeniqua | Average |
|---|---|---|---|
| **1 to 61 Degrees** | 92.31 | 78.57 | 85.19 |
| **1 to 81 Degrees** | 93.75 | 58.82 | 75.76 |
| **1 to 91 Degrees** | 94.12 | 52.63 | 72.22 |

Table 5.6: Recognition Percentages. Aspect Angle Range of Training Set is 0 to 60 Degrees. Aspect Angle Interval = 19.2 Degrees.

### Classification Results

The LVQ neural network was trained with thirteen codebook vectors, 585 training iterations for LVQ1 and 1000 training iterations for LVQ3. Three cycles of LVQ3 were implemented. Epsilon was 0.1. Recognition results are as in Tables 5.5 to 5.13 :

Finally, Table 5.14 will indicate that recognition is still possible when the target is turned through 180 degrees so that the back of the ship faces the radar at -0 degree aspect angle (180 degree aspect angle). All preceding examinations were carried out with the ship targets facing the radar such that the bow was closest

| Aspect Angle Range of Test Set | Protea | Outeniqua | Average |
|---|---|---|---|
| **1 to 61 Degrees** | 100 | 35.71 | 66.67 |
| **1 to 81 Degrees** | 100 | 29.41 | 63.64 |
| **1 to 91 Degrees** | 94.12 | 26.32 | 58.33 |

Table 5.7: Recognition Percentages. Aspect Angle Range of Training Set is 0 to 60 Degrees. Aspect Angle Interval = 28.8 Degrees.

| Aspect Angle Range of Test Set | Protea | Outeniqua | Average |
|---|---|---|---|
| **1 to 61 Degrees** | 92.31 | 85.71 | 88.89 |
| **1 to 81 Degrees** | 93.75 | 64.71 | 78.79 |
| **1 to 91 Degrees** | 94.12 | 57.89 | 75 |

Table 5.8: Recognition Percentages. Aspect Angle Range of Training Set is 0 to 80 Degrees. Aspect Angle Interval = 9.6 Degrees.

| Aspect Angle Range of Test Set | Protea | Outeniqua | Average |
|---|---|---|---|
| **1 to 61 Degrees** | 92.31 | 78.57 | 85.19 |
| **1 to 81 Degrees** | 93.75 | 70.59 | 81.82 |
| **1 to 91 Degrees** | 94.12 | 63.16 | 77.78 |

Table 5.9: Recognition Percentages. Aspect Angle Range of Training Set is 0 to 80 Degrees. Aspect Angle Interval = 19.2 Degrees.

| Aspect Angle Range of Test Set | Protea | Outeniqua | Average |
|---|---|---|---|
| **1 to 61 Degrees** | 100 | 35.71 | 66.67 |
| **1 to 81 Degrees** | 100 | 29.41 | 63.64 |
| **1 to 91 Degrees** | 94.12 | 26.32 | 58.33 |

Table 5.10: Recognition Percentages. Aspect Angle Range of Training Set is 0 to 80 Degrees. Aspect Angle Interval = 28.8 Degrees.

| Aspect Angle Range of Test Set | Protea | Outeniqua | Average |
|---|---|---|---|
| **1 to 61 Degrees** | 100 | 85.71 | 92.59 |
| **1 to 81 Degrees** | 100 | 70.59 | 84.85 |
| **1 to 91 Degrees** | 100 | 63.16 | 80.56 |

Table 5.11: Recognition Percentages. Aspect Angle Range of Training Set is 0 to 90 Degrees. Aspect Angle Interval = 9.6 Degrees.

| Aspect Angle Range of Test Set | Protea | Outeniqua | Average |
|---|---|---|---|
| **1 to 61 Degrees** | 92.31 | 64.29 | 77.78 |
| **1 to 81 Degrees** | 93.75 | 52.94 | 72.73 |
| **1 to 91 Degrees** | 94.12 | 47.37 | 69.44 |

Table 5.12: Recognition Percentages. Aspect Angle Range of Training Set is 0 to 90 Degrees. Aspect Angle Interval = 19.2 Degrees.

| Aspect Angle Range of Test Set | Protea | Outeniqua | Average |
|---|---|---|---|
| **1 to 61 Degrees** | 100 | 35.71 | 66.67 |
| **1 to 81 Degrees** | 100 | 29.41 | 63.64 |
| **1 to 91 Degrees** | 100 | 26.32 | 61.11 |

Table 5.13: Recognition Percentages. Aspect Angle Range of Training Set is 0 to 90 Degrees. Aspect Angle Interval = 28.8 Degrees.

to the transmitted pulses of the search radar. Results of this test are in Table 5.14.

Test scenario six of Chapter 4 was not repeated with the real data, since it is not possible to apply scintillation in an uncontrolled environment. Scintillation is an aspect well accounted for in nature and has firmly established its presence as far as the real data for the SAS Protea and Outeniqua is concerned.

### Analysis of Results for Test Two

Examination of the results in Tables 5.5 to 5.13 will indicate that recognition success does diminish with a decrease in the dimensions of the training data sets, a corroboration of the facts stated for the previous simulation tests. Degradation

| Aspect Angle Range of Test Set | Protea | Outeniqua | Average |
|---|---|---|---|
| **181 to 211 Degrees** | 84.62 | 100 | 92.59 |

Table 5.14: Recognition Percentages. Aspect Angle Range of Training Set is 0 to 60 Degrees. Aspect Angle Interval = 4.8 Degrees.

in recognition is however minimal. Feasibility of recognition while the ship faces in the opposite direction to previous tests, is made clear by the results presented in Table 5.14 for the SAS Protea and Outeniqua.

# Chapter 6

# Conclusions and Recommendations

In this dissertation, the results of an experimental study aimed at ship target recognition are presented. The dissertation is both theoretical and practical. Emphasis is placed on the functionality of the Mellin Transform and its implications in such a study. Bearing this in mind, the findings of this mathematical examination of the Mellin Transform are applied to simulated data in order to determine the outcome as far as recognition of ship targets is concerned. In executing this mathematical study, it was hoped that all shortcomings of these types of studies would be overcome. Conclusions will be drawn from all results of examinations where the mathematical theories and outcomes of the Mellin Transform were applied to simulated data and a good set of real ship data, thus contributing to the practical characteristics of the dissertation. Recommendations for future work will also be drawn.

The following conclusions may be drawn:

## 6.1 Specifics of the Mellin Transform

Investigation of the scale and translation invariant properties of the Mellin Transform in a mathematical sense, produced significant findings regarding the implementation of the algorithm for its use in ship target recognition.

Mathematical research shows that successful operation of the Mellin Transform in the realms of scale and translation invariance is only possible if the function on which the Mellin Transform is being implemented is non-linearly scaled. All points constituting the function must be scaled by a common factor as far as the independent variable is concerned. It is for this particular reason that the Mellin Transform should only be applied to one side of a real and even Fourier Transform of a range profile of a ship target.

As far as previous mentioned studies concerned [12], these points were not addressed appropriately, thus leading to the shortcomings encountered with the simulators developed for this type of study.

## 6.2 Simulator Characteristics

The fundamentals of a simulator were written by Rolf Lengenfelder and adapted and modified by the author of this dissertation for the purposes of fulfilling the objectives of this dissertation as far as adding thermal noise and clutter, adding scintillation, adding implementation of Fourier Transforms and adding implementation of the Fourier Modified Direct Mellin Transforms are concerned. It provided a valuable source of data within a controlled environment for thorough testing and analysis of the approaches adopted in this dissertation. The simulator successfully overcame the shortcomings mentioned above and produced almost realistic profiles of ship targets at all aspect angles. Signal processing in the form of the matched filter added to the realistic character of the simulator.

Flexibility is a key characteristic of the simulator, providing the ability to easily change the aspect angle of the target, the length of the target, the amount of thermal noise generated in the receiver, the amount of clutter received and the amount of scintillation estimated. These characteristics afforded a very successful examination of the conditions in reality and provided insight as to what the recognition results would most probably be when authentic ship data would be analysed.

## 6.3 Simulations and Recognition

Simulated tests reveal that recognition of ship targets becomes less successful as the aspect angle of the target increases. Examination results do however indicate that recognition is adequately successful even in the large ranges of target aspect angles like 0 to 80 and 0 to 90 degrees. Recognition, although characterised by less reasonable accuracies, is also theoretically feasible in the larger ranges of aspect angle like 180 to 210 degrees, as was illustrated by simulated results. It is therefore valid to state that recognition of ship targets is acquired over the complete range of aspect angles from 0 to 360 degrees. The effects of thermal noise, clutter and scintillation produced in the controlled simulator environment, were found to be minimal. Good signal processing by use of the matched filter ensured a good peak SNR of the incoming signal.

Experimental results on simulated data also indicate that recognition percentages do indeed deteriorate as the number of profiles considered for the training sets for the neural network decreases. Recognition is nevertheless successful even when profiles considered for the test sets were 16 degrees apart in aspect angle and limited to the 0 to 30 degree aspect angle range. It is therefore possible to attain quick conversion with neural networks by using small data sets for training while still attaining good recognition results.

## 6.4 Real Data

Analysis of the sinograms of the SAS Protea and the Outeniqua acquired from the Institute for Maritime Technology in Simon's Town, reveal that the data is fairly clean. Apart from the presence of sea clutter and interference from other radars in the harbour, it is evident that the data was acquired on a calm day when the ocean was fairly unperturbed. Sinograms depicting the location of the ships at most aspect angles in the entire aspect angle range of 0 to 360 degrees were successfully attained by the author of the thesis in Simon's Town. This provided a substantial database for the studies adopted in this dissertation.

## 6.5 Data Extraction Tools

Magnitude fluctuations in the real data were found to be relatively pronounced due to the small wavelength and low resolution of the radar. These fluctuations would contribute negatively to recognition of the targets in the dissertation. This is due to the fact that data processing in the form of the Fourier and Mellin Transforms is unidimensional in that it tends to independent variable fluctuations and not dependent variable fluctuations.

The adverse effects of these magnitude fluctuations can be dealt with by two methods mentioned in the dissertation, these being *Compound Identification* and *Successive Elimination* as explained in detail in Chapter 5. Disclosure of a shortcoming of the dissertation in this section, lies in the fact that *Compound Identification* is discussed but not implemented due to the shortage of time. Tools written in Matlab by the author of the dissertation were found to be successful in implementing the method of *Successive Elimination.* Success is attributed to the fact that magnitude thresholds for implementing this method are adjustable in the written software and can be varied according to the data acquired.

## 6.6 Real Data and Recognition

Recognition results for real data corroborate the recognition results for the simulations. It was once again found that recognition success decreases with an increase in aspect angle of the ship target. It was however found, as it was with the simulations, that recognition results are accurate adequately even in large aspect angle ranges of 0 to 90 degrees. Successful recognition was also found possible in the 180 to 240 degree aspect angle range, thus emphasizing the fact that recognition of ship targets is feasible in the entire aspect angle range of the target, as was pointed out by examinations pertaining to the simulated ship data.

Although it was found that recognition percentages decrease as the number of profiles considered for the training sets of the neural network decrease, it is obvious that adequate recognition accuracies are attained even when the dimensions of the training data sets are small.

## 6.7 Formulated Regions of Recognition

Interpretation of recognition results for simulations leads to the conclusion that there are eight predominant recognition regions or zones in the Cartesian coordinate system. The different zones of recognition are presented in Figure 6.1. Reference to the Cartesian coordinate system in this dissertation, includes only the $x$ and $y$ axes. The positive y-axis is the 0 degree aspect angle reference while the positive x-axis is the 90 degree aspect angle reference. Recognition accuracies of close to 70 percent and above are attained for ship targets which lie in the 0 to 60 degree aspect angle range (Zone 1). Recognition percentages close to 60 percent and below, are attained for the aspect angle range 0 to 90 degrees (Zone 5). In the former situation, recognition percentages are very similar but definitely above 70 percent, while percentages for the second case are close and the disparity from those of the former region is distinct and is approximately 10 percent. Regions that correspond to zone one are the 180 to 120 degree zone (Zone

2) and the 180 to 240 degree zone (Zone 3). Another region likened to these is the 0 to 300 degree zone (Zone 4). Recognition percentages will be identical for all four zones. recognition percentages will be identical for all other remaining zones. Although recognition accuracies are quite low in the remaining regions, it is however evident that recognition is indeed feasible in the entire aspect angle range of the ship target from 0 to 360 degrees.

As far as real ship data is concerned, tests reveal that recognition accuracies for ships lying in the 0 to 60 degree aspect angle zone, are very similar. Recognition becomes noticeably worse from 80 degrees onwards. The disparity between recognition percentages in the 0 to 60 degree range and between those of 80 degrees onwards is greater than the ten percent mentioned above for simulated data. Results for the Outeniqua indicate that it is accurate enough to adopt the conclusions for simulated data as far as recognition regions are concerned. These conclusions for the simulated data can be referenced in Section 6.3.

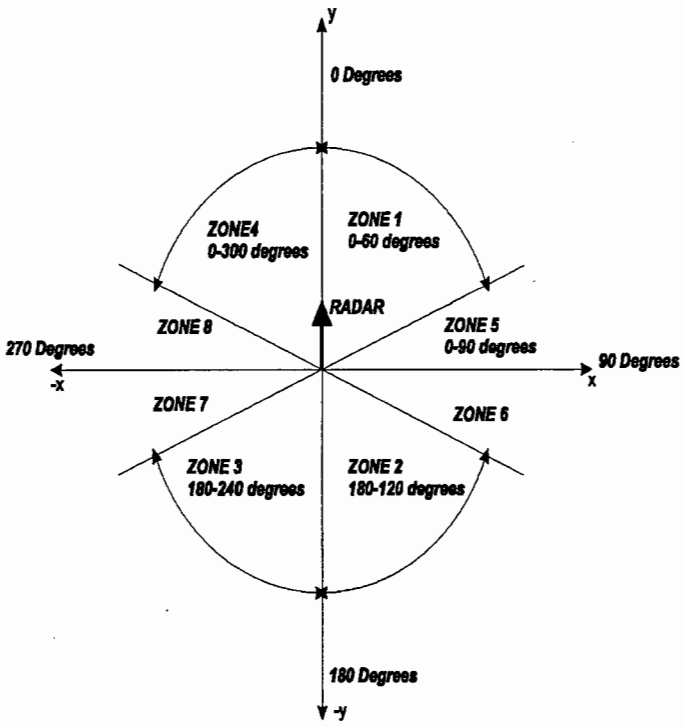


Figure 6.1: Recognition Zones.

## 6.8 Recommendations

Based on the findings and conclusions of the dissertation, the following recommendations are made.

### 6.8.1 Software

- The recognizer developed in the dissertation which incorporates the data extraction tools used to eradicate traces of clutter and interference from other radars, and the implementation of the FMDMT should be written as a single executable in C or C++.
- The threshold for eliminating clutter and interference should be scrutinized and possible values identified. Another method for implementing *Successive Elimination* could be devised.
- Rigorous examinations concerning recognition of ship targets should be carried out with the implementation of both the method of *Successive Elimination* and *Compound Identification* in order to determine which is most successful..
- The simulator which was developed in Mathcad should be written in C or C++ for a much faster and elegant implementation.

### 6.8.2 Mellin Transform

- The Mellin Transform should be investigated further so as to gain insight on the effect of the number of Mellin Transform samples on the recognition accuracies attainable.
- A limit should be identified as to how many FMDMT samples are necessary until further improvement in recognition success is unattainable.

### 6.8.3 Authentic Ship Data

- Larger sets of data for a larger range of ships should be acquired with exactly the same procedures and methods used in this dissertation. The motivation for this is to establish a means of corroborating all facts and conclusions reached in this particular dissertation, especially as far as examination of formulated recognition zones are concerned. Another motivational factor for this is to afford implementation of cross validation an input dimensions of 10.N as indicated in section 4.2.3 of Chapter 4.

- The sampling frequency should be constant for all vessels so that the frequency content for all acquired profiles is such that they are comparable.

- An investigation should be carried out concerning the normalization of FMDMTs. Recognition accuracies vary and in some cases improve when the FMDMTs of ship profiles are normalised as opposed to when they are utilised as is.

# Bibliography


[1] J. Bernard L. Lewis, Frank F. Kretschmer and W. W. Shelton. *Aspects of Radar Signal Processing.* Artech House, Norwood, MA 02062, 1986.

[2] M. B. Charles E. Cook. *Radar Signals.* Artech House, Norwood, MA 02062, 1993.

[3] C. E. C. David K. Barton and P. Hamilton. *Radar Evaluation Handbook.* Artech House, Norwood, MA 02062, 1991.

[4] M. Inggs and A. Robinson. Neural Approaches to Ship Target Recognition. In *IEEE International Radar Conference*, pages 386–391. IEEE, March 1995.

[5] T. Kohonen. The Self-Organizing Map. *IEEE Proceedings*, 78(9):1464–1478, September 1990.

[6] R. Lengenfelder and H. Gunputh. User manual for Sarsim II. Technical report, University of Cape Town, October 1997.

[7] W. Morchin. *Radar Engineer's Sourcebook.* Artech House, Norwood, MA 02062, 1993.

[8] N. Morrison. *Introduction to Fourier Analysis.* Department of Mathematics, University of Cape Town, Rondebosch, Cape Town, 1993.

[9] V. Nebabin. *Methods and Techniques of Radar Recognition.* Artech House, Norwood, MA 02062, 1995.

[10] F. Oberhettinger. *Tables of Mellin Transforms.* Springer-Verlag, Berlin, Heidelberg, New York, 1974.

[11] A. V. Oppenheim and R. W. Schafer. *Discrete-Time Signal Processing.* Prentice-Hall International, Inc., Englewood Cliffs, New Jersey, 1989.

[12] A. Robinson. Study of the Use of Neural Networks for Automatic Target Recognition. Technical report, University of Cape Town, November 1993.

[13] H. Serretta. Implementation of the Mellin Transform in Conjunction with Neural Networks for Ship Target Recognition. Technical report, University of Cape Town, March 1998.

[14] M. Skolnik. *Radar Handbook.* McGraw-Hill, Inc., New York, St. Louis, San Francisco, Aukland, Sydney., 1990.

[15] I. H. Sneddon. *The Use of Integral Transforms.* McGraw-Hill, Inc., New York, St. Louis, San Francisco, Aukland, Sydney., 1972.

[16] G. W. Stimson. *Introduction to Airborne Radar.* Hughes Aircraft Co., El Segundo, California, 1983.

[17] F. G. Stremler. *Communication Systems.* Addison-Wesley, Reading, Massachusetts, Menlo Park, California and New York, 1990.

[18] D. Widder. *An Introduction to Transform Theory.* Academic Press, New York and London, 1971.

[19] K. B. Wolf. *Integral Transforms in Science and Engineering.* Plenum Press, New York and London, 1972.

[20] P. E. Zwicke and J. Imre Kiss. A New Implementation of the Mellin Transform and its Application to Radar Classification of Ships. *IEEE Transactions on Pattern Analysis and Machine Intelligence*, 16(12):245–251, December 1994.

# Appendix A

# Mathcad Simulations

This appendix contains simulations implemented with Mathcad so as to demonstrate the functionality of the Mellin Transform. The first simulation relates to the functionality of the Mellin Transform in its simple form, while the second relates to the Mellin Transform of both sides of an even and real magnitude of a Fourier Transform.

## The Principle Behind the Mellin Transform

The profiles are represented in this case by two data samples, $g_k$ and $h_k$..

$N := 10$ $\quad j := \sqrt{-1}$

Note : first element arbitary, last element must be zero.

$g := (0\ \ 0\ \ 0\ \ 0\ \ 10\ \ 0\ \ 0\ \ 0\ \ 0\ \ 0\ \ 0)^T$

$h := (0\ \ 0\ \ 0\ \ 0\ \ 0\ \ 0\ \ 0\ \ 10\ \ 10\ \ 0\ \ 0)^T$

$k := 0 .. N - 1$

$\Delta_k := g_k - g_{k+1}$ $\quad G(\omega) := \sum_{k=1}^{N-1} (\cos(\omega \cdot \ln(k)) - j \cdot \sin(\omega \cdot \ln(k))) \cdot \Delta_k$

$\Gamma_k := h_k - h_{k+1}$ $\quad H(\omega) := \sum_{k=1}^{N-1} (\cos(\omega \cdot \ln(k)) - j \cdot \sin(\omega \cdot \ln(k))) \cdot \Gamma_k$

$\omega := 0 .. 50$

Modified Direct Mellin transform :

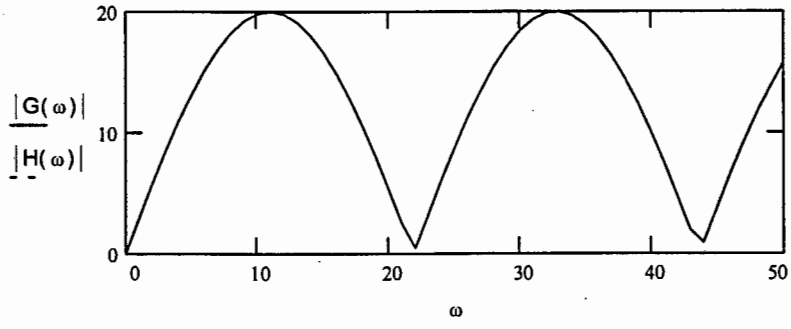


The $\Delta_k$ for $g_k$ and $h_k$ are constant throughout. $\Delta_k$ has a non-zero value for $g_k$ at elements 3 and 4 while$\Gamma_k$ has non-zero value for elements 6 and 8 for $h_k$

When $\omega=1$ the following is true:

$$G(s) = e^{j\ln 3}(-10) + e^{j\ln 4}(10)$$

$$\begin{aligned} H(s) &= e^{j\ln 6}(-10) + e^{j\ln 8}(10) \\ &= e^{j\ln 2}[e^{j\ln 3}(-10) + e^{j\ln 4}(10)] \end{aligned}$$

When the magnitudes, $|G(s)|$ and $|H(s)|$ are calculated, they produce the same resultants since the magnitude of $e^{j\ln 2} = 1$. The Direct Mellin Transforms are thus equal. The linear expansion simply introduced a rotation of the vectors before being added. This was a linear rotation and does thus not affect the resultant at all. This is the principle behind the Mellin Transform, provided the data points move in a linear fashion.

## RESULTS OF MELLIN TRANSFORM ON TWO-SIDED FOURIER TRANSFORM

The two functions in this case, are the same as those produced in the previous simulation. The only difference is that the mirror image of both is created and a zero included at the end of the profiles for the Mellin Transform. This simulation indicates the results produced when a Mellin transform of a two-sided Fourier Transform is carried out.
The simulations are carried out for ships at zero degrees and 45 degrees aspect angle.
Results indicate that the Mellin Transform of the two functions do not correspond to one another as closely as they did before when the Mellin Transform of a single-sided Fourier Transform was taken.
This method was the method utilised in the previous thesis that dealt with the same topic.
Results are generally better for Mellin Transforms of single-sided Fourier Transforms.

$t := 0 .. 2550$

$A_t := 0$

$blk1 := 0 .. 30$

$A_{blk1} := 10$

$blk2 := 200 .. 230$

$A_{blk2} := 10$

$blk3 := 400 .. 430$

$A_{blk3} := 10$

$blk4 := 600 .. 630$

$A_{blk4} := 10$

Profile for 0 degrees

$me := \overrightarrow{|rnorm(2551, 0, 0.00000001)|}$

$FUNC1 := A + me$

$B_t := 0$

$alk1 := 0 .. 21$

$B_{alk1} := 10$

$alk2 := 141 .. 163$

$B_{alk2} := 10$

$alk3 := 283 .. 304$

$B_{alk3} := 10$

$alk4 := 424 .. 445$

$B_{alk4} := 10$

Profile for 45 degrees

$you := \overrightarrow{|rnorm(2551, 0, 0.00000001)|}$

$FUNC2 := B + you$

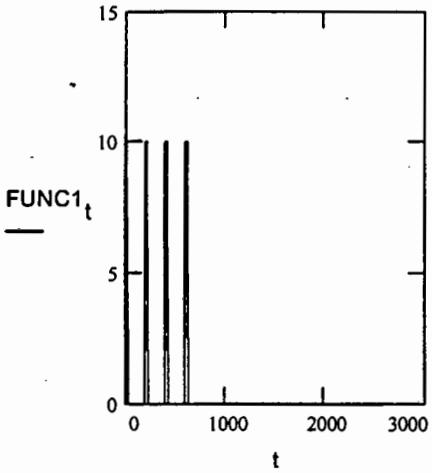


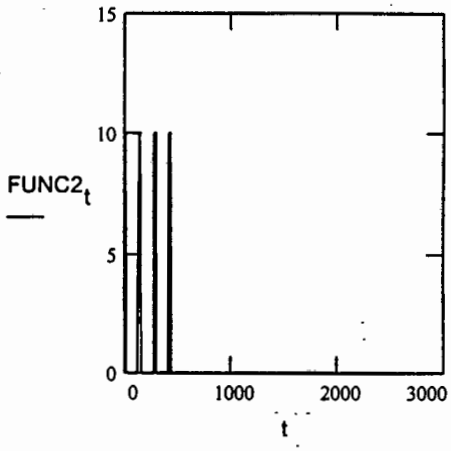


$c := 0 .. 2550$

$W_{c+1} := A_c$

$e := 1 .. 2551$

$G_e := W_{2552-e}$

$f := 2552 .. 5102$

$W_f := G_{f-2551}$

$W_{5103} := 0$

$d := 0 .. 2550$

$X_{d+1} := B_d$

$H_e := X_{2552-e}$

$X_f := H_{f-2551}$

$X_{5103} := 0$

The double-sided Fourier transforms are as follows:

The compression could be viewed as an expansion in the time domain.

$run1 := 0 .. 5103$

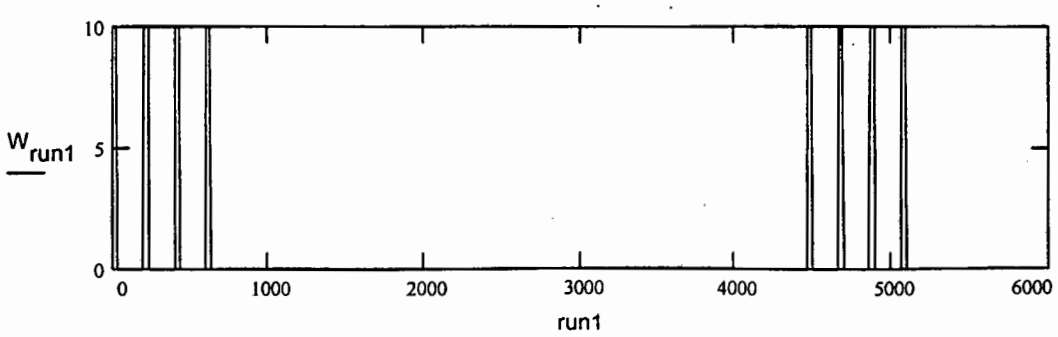

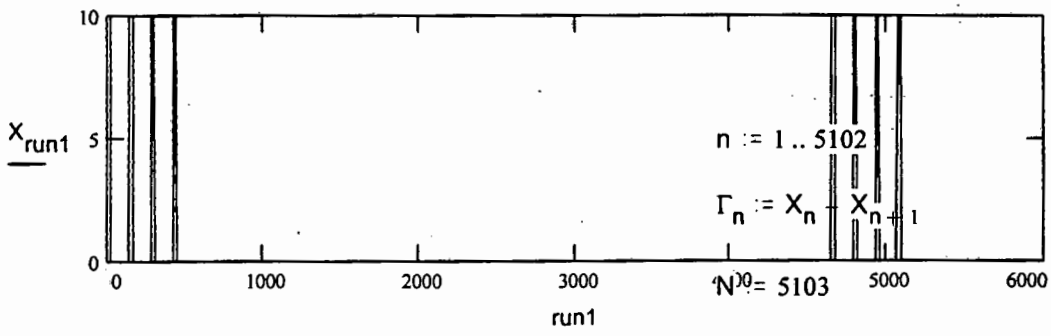


$m := 1 .. 5102$

$\Delta_m := W_m - W_{m+1}$

$N := 5103$

$j := \sqrt{-1}$

$$P(s) := \sum_{m=1}^{N-1} (\cos(s \cdot (\ln(m))) - j \cdot \sin(s \cdot (\ln(m)))) \cdot \Delta_m$$

$$Q(s) := \sum_{n=1}^{N-1} (\cos(s \cdot (\ln(n))) - j \cdot \sin(s \cdot (\ln(n)))) \cdot \Gamma_n$$

Modified Mellin transforms over 40 components from ω=120 to ω=160

$s := 120 .. 160$

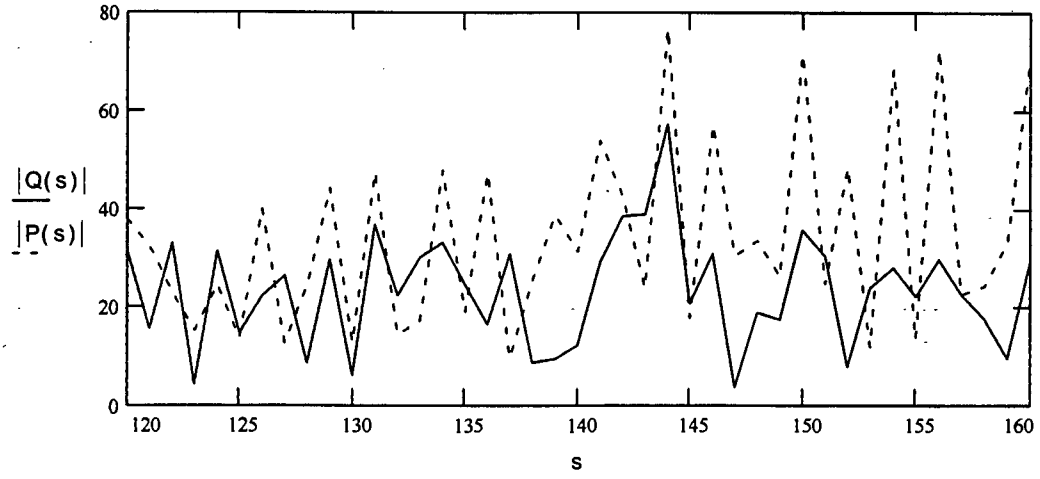


$r := 120 .. 160$

$K_r := |P(r)|$

$p := mean(K)$

$MELLK := \frac{K}{p}$

$J_r := |Q(r)|$

$q := mean(J)$

$MELLJ := \frac{J}{q}$

The Mellin transforms are divided by their mean:

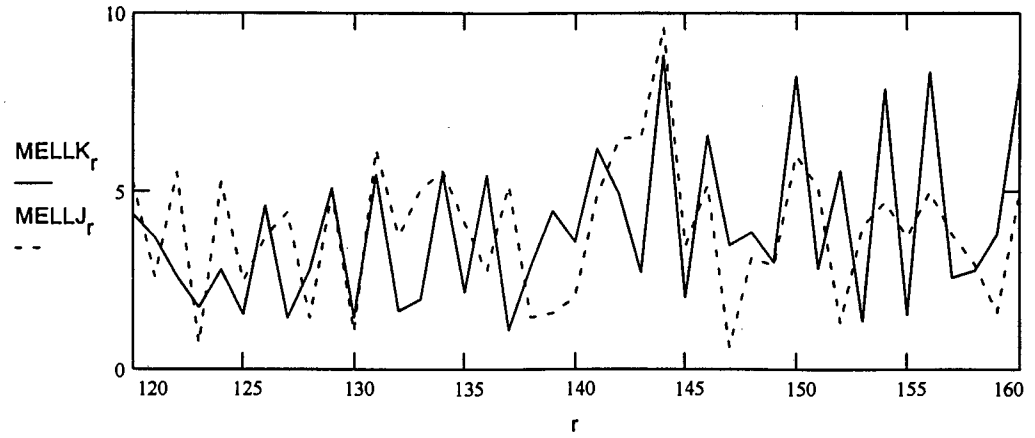

## A.1 Non-Linear Scaling of a Function with Multiple Features

This particular section deals with the product of the Mellin Transform of features which undergo non-linear scaling.

The function $FUNC1$, in the preceding demonstration, is again comprised of a set of Rect functions, all of the same width as before. $FUNC2$ consists of the same Rect functions shifted left by a factor of $\alpha = \sqrt{2}$. Although the function as a whole looks linearly compressed, the individual Rect functions have not been scaled linearly i.e. the points *within* the Rect functions were not subject to linear feature migration to the left as were the Rect functions themselves. The implications are easily explained with the aid of Figure A.1.

Examination of Figure A.1 reveals that the Mellin Transform of the relevant function $g_k$ is :

$$\begin{aligned} g^*(\omega) &= \sum_{k=1}^{N-1} e^{-j\omega \ln k} \Delta_k \\ &= e^{-j\omega \ln k_a} \Delta_k + e^{-j\omega \ln k_b} \Delta_k + .... \end{aligned} \tag{A.1}$$

The Mellin Transform for $h_k$ is:

$$h^*(\omega) = e^{-j\omega \ln(k_a * \alpha)} \Delta_k + e^{-j\omega \ln(k_b * \beta)} \Delta_k + .... \tag{A.2}$$

It must also be noted that the distance between $k_a$ and $k_b$ in Figure A.1 remained constant.

Equation A.2 reveals that a constant scale factor of $\alpha$ cannot be removed from the phase component or that the corresponding vectors for $g_k$ and $h_k$ due to the corresponding $\Delta_k$ as illustrated in Figures 2.6 and 2.7, do not possess common phase angles in their polar plot representations. The Mellin Transforms of the two different functions, $g_k$ and $h_k$ are consequently not equal. It is also evident

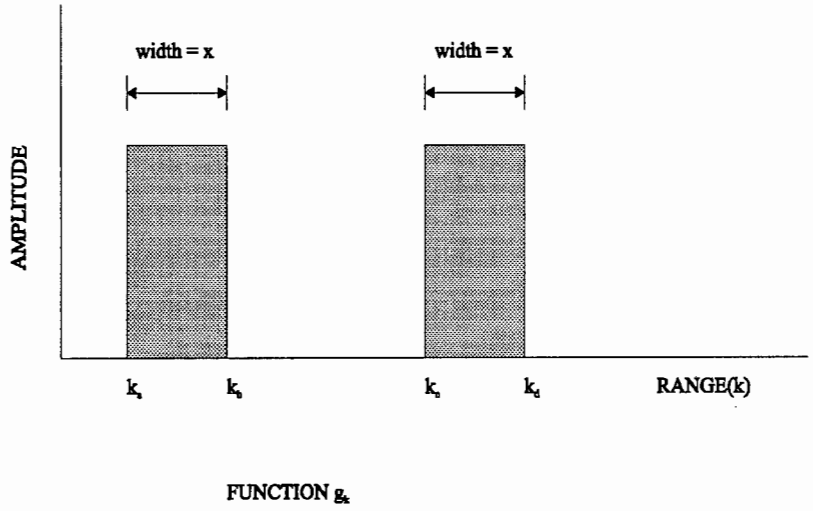


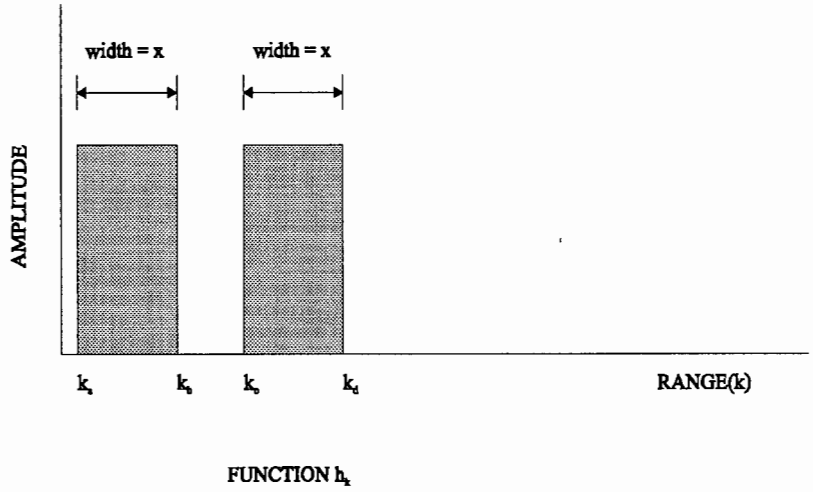


Figure A.1: Non-Linear Range Migration of Function $g_k$.

from this explanation that the desired outcome of the Mellin Transform relies on the fact that the number of $\Delta_k$'s remain constant from function to function i.e. a function possesses the same number of features as its linearly scaled counterpart.

## A.2 The Mellin Transform of a Two-sided Fourier Transform

The following section outlines the negative effects of taking the Mellin Transform of a double-sided Fourier Transform. Mathematical demonstrations are provided in order to make the explanation clearer.

A radar down-range profile of a ship target is positive and real in the time domain. The magnitude of the Fourier Transform is therefore even, the real part is even and the imaginary part is odd i.e. the magnitude of the Fourier Transform on the left side of origin is a mirror image of the section on the right-hand side. The explanation is acquired from [11]. This means the function is conjugate-symmetric. The magnitude of the Fast Fourier Transform (FFT) of a real and even function is often calculated and plotted as in Figure A.3 instead of the exact representation in Figure A.2.

Figures A.2 and A.3 are regarded as double-sided Fourier Transforms in this dissertation. If the origin is placed as in Figure A.3 and is referenced as $k = 1$ in Equation 2.14 and all N points of the FFT are used, the Mellin Transforms of this FFT and its linearly scaled counterpart in Figure A.4 will not be alike in magnitude along the entire Mellin Transform spectrum.

Computation of the Mellin Transform for this double-sided Fourier transform is not possible according to the theory of the Mellin Transform, and is explained by means of Figure A.5.

The FFT in Figure A.5, for the purpose of explanation, could be that of a range profile of a target which has been subject to linear compression by a factor $\alpha$. Part $A$ is the mirror image of part $B$. Linear migration for both components

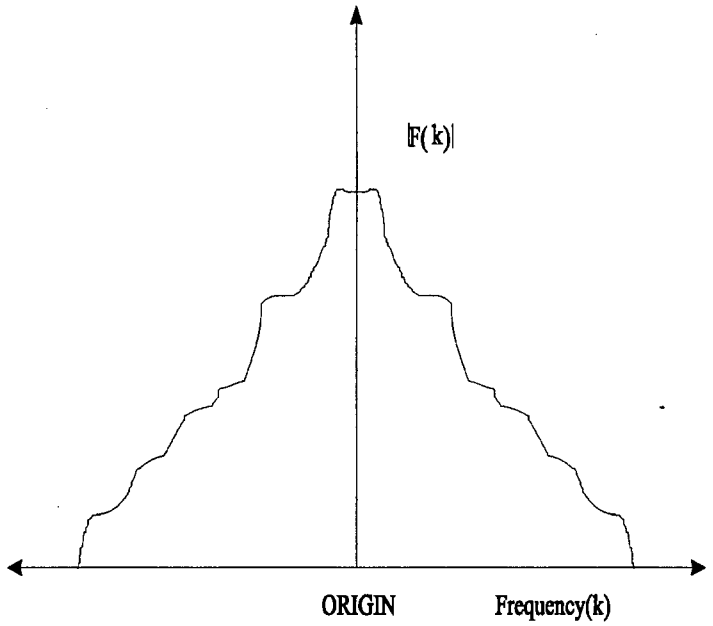


Figure A.2: Magnitude Plot of FFT of Real and Positive Function $f(nT)$. (True Representation).

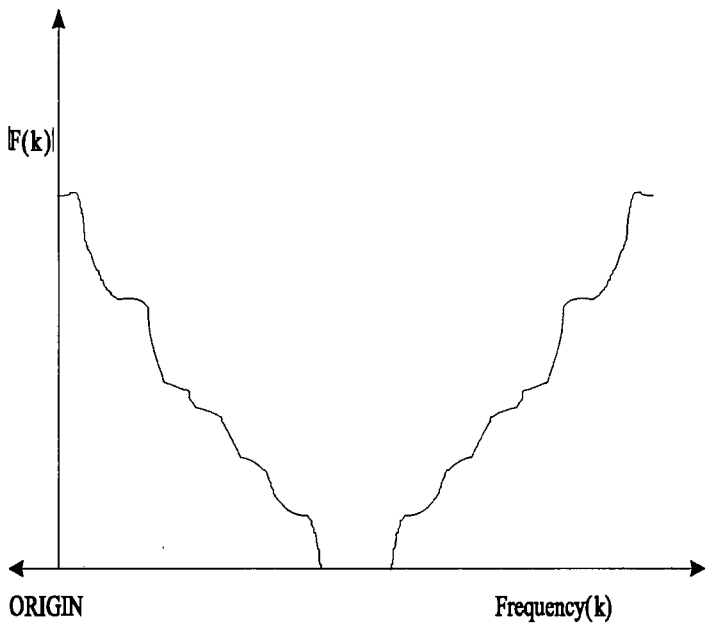


Figure A.3: Magnitude Plot of FFT of Real and Positive Function $f(nT)$. (Common Representation).

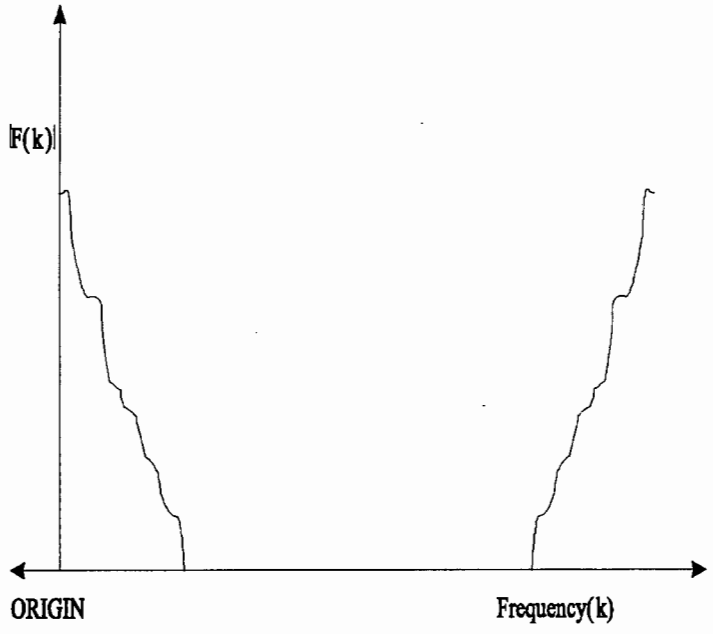


Figure A.4: Magnitude Plot of FFT of Real and Positive Function $f(nT)$. (True Representation of Linearly Scaled FFT).

occurs away from the centre point $c$, such that $A$ is linearly compressed towards origin by a factor of $\alpha$ while $B$ is compressed by a factor of $\alpha$ towards the $N_{th}$ point of the FFT, indicated by the $e$. The FFT as a whole, does not undergo linear migration in one direction i.e. towards origin. Mathematical proof of the Mellin Transform as displayed in Equation 2.16, indicates that scaling of the function should occur in a single direction from or to a single reference point, by the factor $\alpha$. The single reference point occurs at $k = 1$ in Figure A.5. In Figure A.5 :

$$\frac{a}{b} = \alpha \tag{A.3}$$

It is desired that :

$$\frac{n}{p} = \alpha \tag{A.4}$$

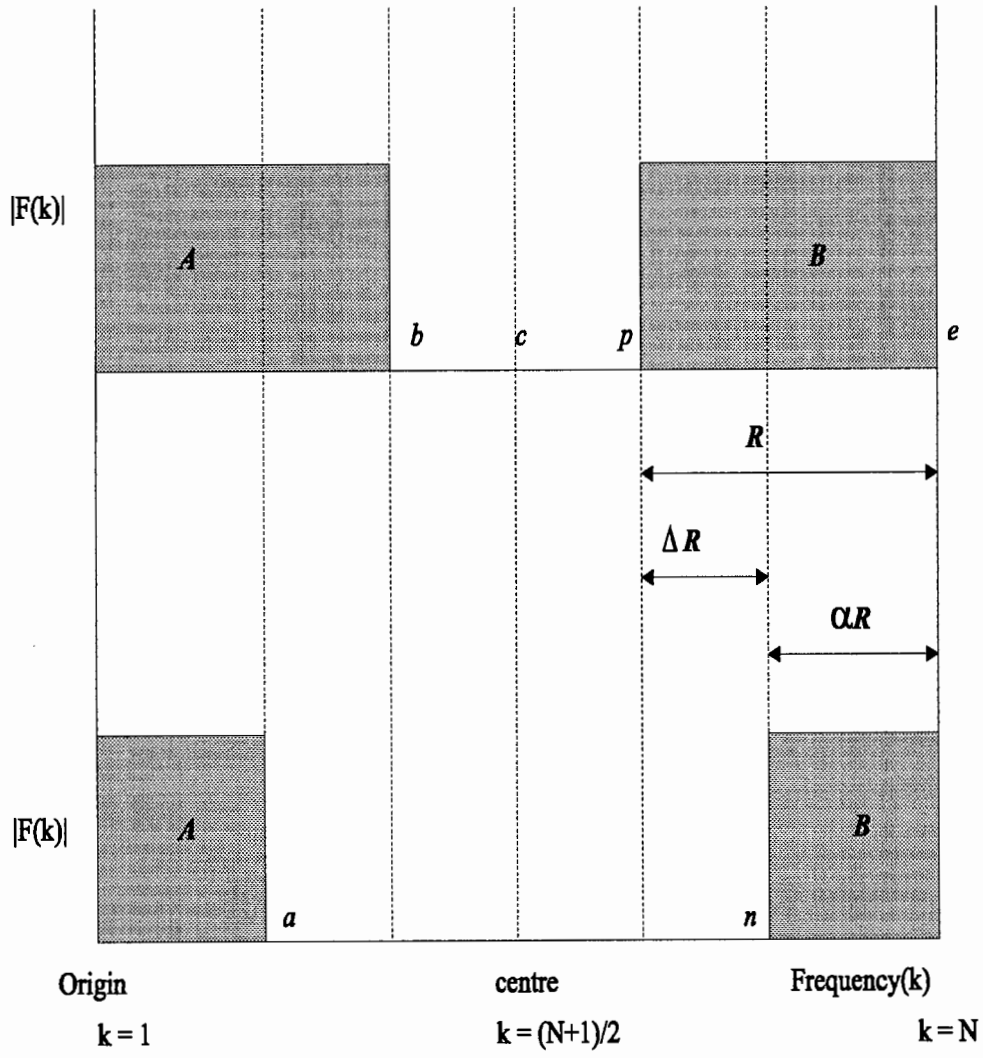


Figure A.5: Linear Scaling of Double-Sided FFT.

in order for Equation 2.16 to be implemented with the desired effect that the common factor of $\alpha$ be removed. The following mathematics will indicate that Equation A.4 is inaccurate and that the scaling factor of $\alpha$ cannot be removed from Equation 2.16. If $n$ is the new position of the edge of the FFT in Figure A.5 , then:

$$\begin{aligned} n &= p + \Delta R \\ &= p + R(1-\alpha) \end{aligned} \tag{A.5}$$

where $\alpha$ is a compression factor and $\alpha < 1$. The new position of part $B$ $(n)$, with respect to the old part $(p)$ is given by :

$$\frac{n}{p} = K - \alpha(\frac{e-p}{p}) \tag{A.6}$$

where $K$ is a constant and $e$ is the end of the Fourier transform. It should be noted that $p$ is variable and could represent all points along part $B$. $n$ Is also variable. The migration factor is not constant. The Mellin Transform of the double-sided FFT can be expressed as follows :

$$\sum_{k=1}^{\frac{N-1}{2}} e^{-j\omega \ln k}\Delta_k + \sum_{\frac{N+1}{2}}^{N-1} e^{-j\omega \ln k}\Delta_k \tag{A.7}$$

where the term on the right side of the expression is termed by the author of this particular dissertation as the 'Error Term'. Since the constant factor of $e^{j\omega \ln \alpha}$ cannot be eliminated from this term as every point in the FFT migrates, the result of the Mellin Transform applied in this event will not be equal that of the uncompressed FFT of Figure A.5. The right side of Equation A.7 is described by :

$$\sum_{\frac{N+1}{2}}^{N-1} e^{-j\omega \ln k}\Delta_k \tag{A.8}$$

for the right region of the uppermost FFT of Figure A.5, and is described by :

$$\sum_{\frac{N+1}{2}}^{N-1} e^{-j\omega(\ln k + \ln(K - \alpha(\frac{e-p}{p}))} \Delta_k \tag{A.9}$$

for the right side of the FFT on the bottom of Figure A.5. It is obvious that by Equation A.9, a constant or common migration factor cannot be eliminated from the phase portion. The outputs of these two equations are unequal in all instances. The magnitudes of the Mellin Transforms of the uppermost and bottom FFTs of Figure A.5 are characterised by dissimilarity.

## A.3 The Effect of Thermal Noise and Clutter

A simulated Fourier Transform of a noise-polluted function is presented in this particular section, and can be referenced for evaluation of the Mellin Transform under these conditions. The simulation with accompanying explanation, is provided below.

This simulation emphasizes the fact that the zero frequency component of the Fourier Tranform is considerably greater than the entire range of components in the rest of the simulated Fourier Transform. Reference to Equation 2.15 in paragraph 2.4.1 will indicate that $\Delta_{k1}$ is substantially large in this case and is ultimately dominant compared to all other $\Delta_k$. Equation 2.15, as indicated in Figures 2.6 and 2.7 is described by the addition of vectors at different phase angles on a polar plot. For $k = 1$ in Equation 2.15 a sizable $\Delta_{k1}$is produced in this particular simulation. The vector created is that of $\Delta_{k1}$ which is far greater in magnitude than all other vectors calculated from all other $\Delta_k$. The resultant magnitude at each individual Mellin frequency component of $\omega$ will be principally dominated by $|\Delta_{k1}|$ . As $\omega$ increases from zero, these vectors all rotate at different rates according to their $k$ positions in the Fourier Transform. The magnitude of the Mellin Transform thereof will therefore be centered about the value of the DC component's magnitude and will fluctuate in a minor way about

this value due to the smaller $\Delta_k$ values which rotate with the DC vector and cause the resultant to fluctuate inconsiderably. The conclusion can be drawn from this evaluation that the Mellin Transform is strongly dependent on the prominent features of the Fourier Transform and that fluctuations due to noise will be inconsiderable or slight in comparison with results produced due to the prominent features. As indicated previously in this particular section, the Fourier Transform of white noise is a dirac delta or infinitely large impulse at origin. In a situation where noise is not dominant enough in the time domain to produce a dirac in the frequency domain, the fluctuations in the Mellin Transform due to this noise are minor due to the dominance of larger more consistent features in the Fourier Transform.

**The Effect of Noise with Respect to the Mellin Transform**

Two functions have been created in order to simulate the effect of DC-biased white noise. These functions are supposed to replicate the Fourier Transforms of this noise which comprises of a dirac (infinite impulse) at origin and noisy components at higher frequencies. These functions are plotted below as g and h once again. This is what occurs in theory. The Fourier Transform of a profile is utilised. The Mellin Transform thereof is calculated. The aim of this simulation is to determine what would occur to the Mellin Transform of a profile if considerably polluted with noise.
Each sample is represented by 128 points. The first point (dirac) is a large in comparison with the other data points and occurs at origin. The magnitude of this dirac is one. The two profiles have roughly the same values. This is what is expected with the Fourier Transform of noise - the dirac dominates while all other components are small in relation.
This simulation merely describes the principle operation of the Mellin Transform on noise. For the specific purpose of explanation, the noise is not realistic.

$a := 0 .. 127$ $\quad\quad$ $j := \sqrt{-1}$

$noise1 := \overrightarrow{|rnorm(128,0,0.1)|}$ $\quad\quad$ $noise2 := \overrightarrow{|rnorm(128,0,0.1)|}$

The arrow indicates that the magnitude of each element of the vector is calculated. This is done to mimick the effects of noise in a profile which never has values below zero.

$e := noise1$ $\quad\quad$ $f := noise2$

$e_0 := 1$ $\quad\quad$ $f_0 := 1$

$g_{a+1} := e_a$ $\quad\quad$ $h_{a+1} := f_a$

$g_{128} := 0$ $\quad\quad$ $h_{128} := 0$

$k := 1 .. 127$ $\quad\quad$ $N := 128$

Application of the Modified Direct Mellin transform:

$$\Delta_k := g_k - g_{k+1} \qquad G(\omega) := \sum_{k=1}^{N-1} (\cos(\omega \cdot \ln(k)) - j \cdot \sin(\omega \cdot \ln(k))) \cdot \Delta_k$$

$$\Gamma_k := h_k - h_{k+1} \qquad H(\omega) := \sum_{k=1}^{N-1} (\cos(\omega \cdot \ln(k)) - j \cdot \sin(\omega \cdot \ln(k))) \cdot \Gamma_k$$

The function g is as follows:

$r := 0..100$

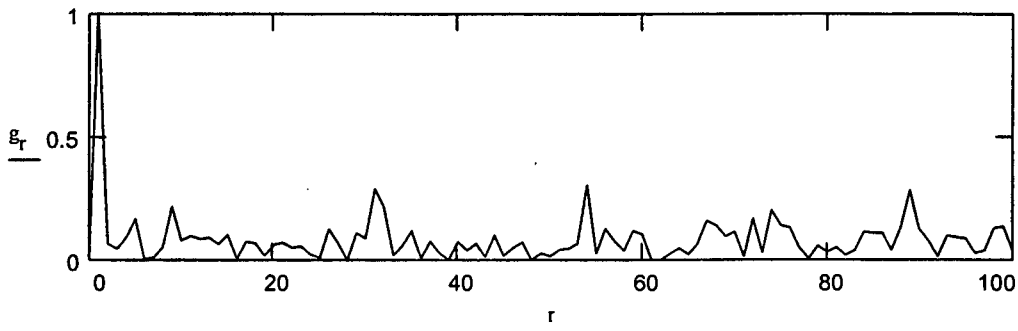


The function h is as follows:

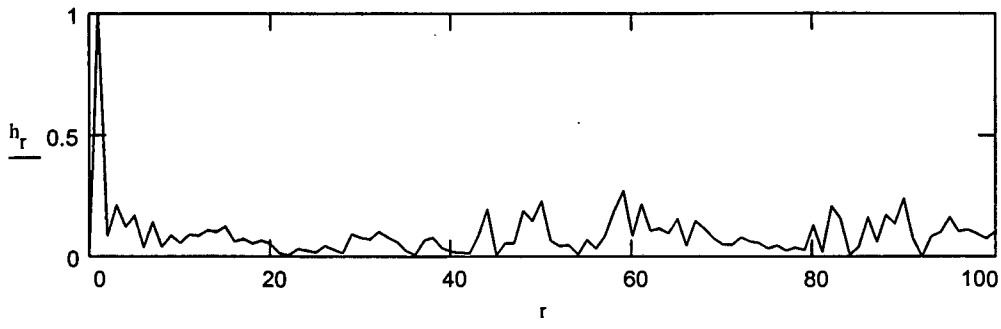

$\omega := 0..100$

Modified Direct Mellin transform :

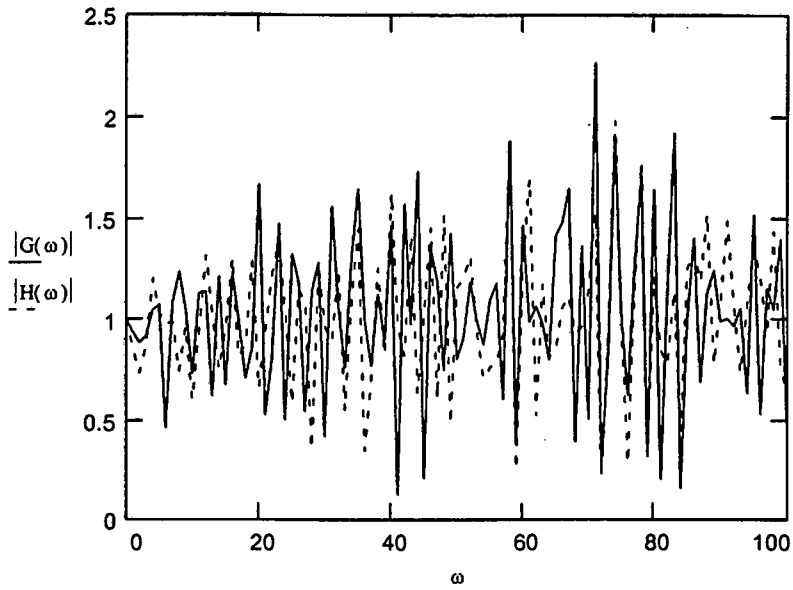


## EXPLANATION OF MELLIN TRANSFORM ON THIS FOURIER TRANSFORM OF NOISE

The Mellin Transform for this type of Fourier transform (g), is as follows:

$$e^{j.\omega.\ln(1).}(\Delta_{k1}) + e^{j.\omega.\ln(2).}(\Delta_{k2}) + .....$$

where $\Delta_{k1}$ is the size of the dirac since $\Delta_k = g_k - g_{k+1} = g_1 - g_2 = 1$- ( very small value). $\Delta_{k2}$ Is a very small value too, depending on the magnitude of the noise at k=2. Therefore, a large vector is added to many small noise vectors in the equation above, at different phases, the dominating vector being the dirac. As far as magnitude is concerned, the Mellin Transform should have a magnitude locus of one and vary about this point due to the presence of random noise vectors which are small in this case compared to the dirac. This is usually the case with noise that is above the origin.

# Appendix B

# Learning Vector Quantization Algorithms

This appendix contains a summary of the Learning Vector Quantization algorithms used in the neural network for recognition in this particular dissertation.

## B.1 Learning Vector Quantization

Learning Vector Quantization is an implementation of the concept discussed in the opening paragraphs of this chapter. The so-called cells or representative vectors ($m_i(t)$) are known as codebook vectors. Learning Vector Quantization refers to the entire process of finding the best-matching $m_i(t)$ for each $x(t)$, where $x(t)$ is the input vector. The closest $m_c$ is found for each $x$ such that the error or disparity is minimal :

$$E = \int \| x - m_c \|^r \, p(x)dx \tag{B.1}$$

where $dx$ is the volume differential in the $x$ space and $c$ is the index of the best-matching codebook vector. i.e :

$$\| x - m_c \| = \min_i \{ \| x - m_i \| \} \tag{B.2}$$

The solution of Equation B.2 depends on iterative approximation.

The codebook vectors or cells ($m_i(t)$) develop into feature-sensitive detectors for a particular class of functions. The cells operate independently and associate themselves with the different domains of the input functions, according to their inital random spacial positions at $t = 0$, i.e. all positions of these cells are initially described by $m_i(0)$. The core and principal characteristic of Learning Vector Quantization is captured in the understanding that the algorithm attempts to reduce the Euclidian distances between $x$ and $m_i$.

Learning is a stochastic process and formations of accurate feature-sensitive spatial maps depends on the implementation of these algorithms with sufficient steps or iterations. The Learning Vector Quantization methods applied in this dissertation fine-tune the feature-sensitive maps created by self-organization.

## B.2 The Algorithms Encompassing LVQ Methods

The following section provides detailed insight into the specifics of the LVQ algorithms used for recognition. Mathematical definitions and explanations will accompany the theory. This brings the rest of the data used in this dissertation into perspective as far as processing thereof is concerned for the operations and functionality of the neural network. Data is comparable to the variables used in the ensuing explanations.

### B.2.1 Learning Vector Quantization One (LVQ1)

One should assume a random selection of a number of cells or reference vectors (codebook vectors) $m_i(t)$, placed into the input space so as to approximate

domains of the discrete vector $x$. The domains of $x$ are discrete with time.

For every $t$ the closest-matching $m_i$ ($m_c$) is found such that the Euclidean distance between $x$ and $m$ is minimal i.e.:

$$c = \arg\min_i \{\| x - m_i \|\} \tag{B.3}$$

In order to acquire a solution to Equation B.3, the following learning process is implemented with reference to these LVQ-specific equations :

$$m_c(t+1) = m_c(t) + \alpha(t)[x(t) - m_c(t)] \tag{B.4}$$

if $x$ and $m_c$ belong to the same class,

$$m_c(t+1) = m_c(t) - \alpha(t)[x(t) - m_c(t)] \tag{B.5}$$

if $x$ and $m_c$ belong to different classes, and

$$m_i(t+1) = m_i(t) \tag{B.6}$$

for $i \neq c$ i.e.all other $m_i$ remain intact.

Reference to the explanations provided with Equations B.4, B.5 and B.6, indicate that $\alpha(t)$ is greater than zero and smaller than one. $\alpha(t)$ Should decrease as the number of training iterations increase.

### B.2.2 Learning Vector Quantization Two (LVQ2)

LVQ 2 incorporates a similar learning process to that applied in LVQ1. The disparity emanates from the fact that two nearest neighbours to $x$ ($m_i$ and $m_j$) are updated simultaneously. $m_j$ Is a member cell of a class dissimilar to that of the input vector $x$ while $m_i$ belongs to the same class as the input vector. $x$

Falls into a zone (*window*) considered the midplane of all $m_i$ and $m_j$. LVQ2 is described by the following algorithm :

$$m_i(t+1) = m_i(t) - \alpha(t)[x(t) - m_i(t)] \tag{B.7}$$

where $m_i$ and $x$ are of unlike classes and,

$$m_i(t+1) = m_j(t) + \alpha(t)[x(t) - m_j(t)] \tag{B.8}$$

where $m_j$ and $x$ belong to equivalent classes.

### B.2.3 Learning Vector Quantization Three (LVQ3)

The consequences of shifting all $m_i$ away from $x$ were not considered in the LVQ2 algorithms. LVQ3 takes this migration into consideration. Characteristics of the algorithms are thus described as follows :

$$m_i(t+1) = m_i(t) - \alpha(t)[x(t) - m_i(t)] \tag{B.9}$$

and,

$$m_j(t+1) = m_j(t) + \alpha(t)[x(t) - m_j(t)] \tag{B.10}$$

where $m_i$ and $m_j$ are the closest codebook vectors to $x$ such that $m_i$ and $x$ belong to different classes and $m_j$ belongs to the same class as $x$. $m_i$ Must however conform to approximations of other classes incorporated in the learning process simultaneously. In the instance that $m_i$ and $m_j$ fall into the same class as $x$, the following is applied :

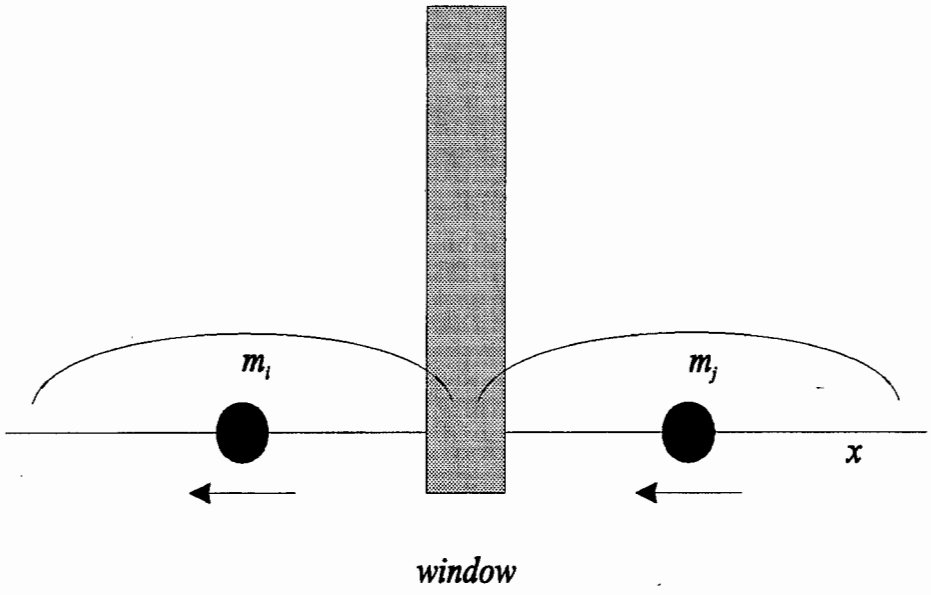


Figure B.1: Window Referred to in the LVQ3 Algorithm.

$$m_k(t+1) = m_k(t) + \epsilon\alpha(t)[x(t) - m_k(t)] \tag{B.11}$$

for $k \in \{i, j\}$. $x$ Still falls in the *window* mentioned in paragraph B.2.2. Values for $\epsilon$ thus depend on the size of the so-called *window*. The *window* described in paragraphs B.2.2 and B.2.3 is presented in Figure B.1 below.